Annu. Rev. Nucl. Part. Sci. 1996. 46:395–469

NONLEPTONIC DECAYS AND LIFETIMES OF CHARM AND BEAUTY PARTICLES

Thomas E. Browder
University of Hawaii at Manoa, Honolulu, Hawaii 96822

Klaus Honscheid
Ohio State University, Columbus, Ohio 43210

Daniele Pedrini
Istituto Nazionale di Fisica Nucleare—Sezione di Milano, I-20133 Milan, Italy

KEY WORDS: bottom decays, charm decays, heavy flavor, hadronic decays

ABSTRACT

We review recent experimental results on lifetimes and on hadronic decays of hadrons that contain c and b quarks. The theoretical implications of these results are also considered. An understanding of hadronic decays of heavy quarks is required to interpret the charge-parity–violating asymmetries in B decays that will be observed in experiments planned for the near future.

CONTENTS

0163-8998/96/1201-0395$08.00

1. INTRODUCTION

Heavy-flavor physics began in 1974 with the discovery of the J/ψ meson (1), a narrow resonance at a mass of 3.1 GeV. The J/ψ was quickly identified as a bound state of a charm and anti-charm quark, a previously unobserved quark flavor with a mass around 1.5 GeV.

Charm was not only the first heavy-flavor quark, it was also the first quark whose existence was predicted before its discovery. In 1970, Glashow et al introduced the GIM mechanism and postulated a new type of quark in order to explain the absence of flavor-changing neutral currents in kaon decay (2).

In 1977, the second heavy flavor, the bottom (or b) quark with a mass of $m_b \sim 5$ GeV/c^2 and a charge of $-1/3$, was observed at Fermilab in forms of bound states with the Υ family (3).

The recent observation of the top quark by the CDF and D0 collaborations (4) completes the three quark families of the standard model:

$$\begin{pmatrix} u \\ d \end{pmatrix} \begin{pmatrix} c \\ s \end{pmatrix} \begin{pmatrix} t \\ b \end{pmatrix}.$$

The six quarks are divided naturally into heavy and light flavors. The c, b, and t quarks are called heavy because their masses are larger than the QCD scale, Λ, while the masses of the u, d, and s quarks are lighter.

Weak decays of heavy quarks test the standard model and can be used to determine its parameters, including the weak mixing angles of the Cabibbo-Kobayashi-Maskawa (CKM) matrix (5). In addition, the study of heavy-quark decay provides important insight into the least well understood sector of the strong interaction: the nonperturbative regime, which describes the formation of hadrons from quarks.

In the standard model, the charm (bottom) quark decays through the weak-charged current into a light quark with a charge of $-1/3$ ($+2/3$), i.e. an s (c) or d (u) quark. The coupling is proportional to the element V_{Qq} of the CKM mixing matrix, where Q denotes a heavy quark, either c or b. In charm decays, the CKM matrix can be approximated by a 2×2 rotation matrix with one real angle, the Cabibbo angle $\theta_c \sim 14^\circ$. In this approximation, $c \to Ws$ transitions, proportional to $\cos\theta_c$, are favored with respect to $c \to Wd$ transitions, proportional to $\sin\theta_c$. These two types of transitions are called Cabibbo-favored and Cabibbo-suppressed, respectively.

The lowest order decay diagrams for charm (bottom) mesons are shown in Figure 1. The spectator diagram (Figure 1*a* and *b*), in which the light antiquark does not take part in the weak interaction, is thought to be dominant. Similar to muon decay, the decay rate for this diagram is proportional to m_Q^5. In the external spectator diagram (Figure 1*a*), color is automatically conserved, while the internal spectator amplitude (Figure 1*b*) is color suppressed since the color of the quarks from the virtual W must match the color of the quarks from the parent meson. In the naive-quark model, the color-matching factor ξ has a value of $1/N_c = 1/3$, so that the decay rate should be reduced by a factor $1/18$ [$= (1/3)^2 \times (1/\sqrt{2})^2$ for the π^0 wave function] for a decay such as $B^0 \to D^0\pi^0$.

The exchange and annihilation diagrams (Figure 1*c* and *d*) are helicity suppressed. This suppression can be somewhat mitigated by the emission of soft gluons. There is also a further reduction in the amplitude, which is proportional to the magnitude of the wavefunction at the origin.

In addition, there are small contributions from the penguin diagram and the box diagrams, which are responsible for $B^0 - \overline{B^0}$ mixing. These are shown in Figure 1*e* and *f*, respectively. Because of the GIM mechanism, these diagrams are highly suppressed in charm decay.

Decays of heavy baryons containing charm or bottom quarks are more complex. The annihilation amplitude is absent, but the exchange diagram is no longer helicity-suppressed. The dominant hadronic decay mechanisms for charm (bottom) baryons are shown in Figure 2. The external spectator decay mechanism is shown in Figure 2*a* while the diagrams for the internal spectator contributions are shown in Figure 2*b* and *c*. Figure 2*d* shows the

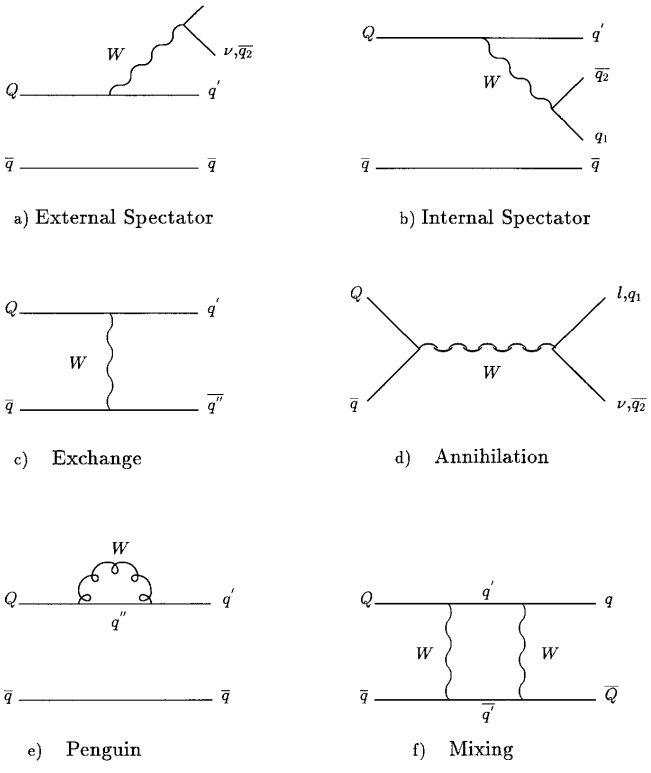

Figure 1 Decay diagrams for *c*- and *b*-mesons.

W-exchange mechanism. The contribution of diagrams other than the external spectator diagram is expected to be significant for decays of baryons with heavy quarks.

Decay modes can be subdivided into three categories according to the final state particles produced. These are leptonic, semileptonic, and hadronic decays. The first can only proceed by the annihilation diagram, while semileptonic decays occur by the spectator diagram. Hadronic decays may proceed via all the decay mechanisms. In contrast to semileptonic and purely leptonic transitions, hadronic decays involve an intricate interplay of quark rearrangement due to soft and hard gluon exchanges. In addition, the hadrons in the final state can rescatter into one another. For example, a D^0 can decay directly into $\overline{K^0}\pi^0$ or rescatter via the intermediate state $K^-\pi^+$, since $K^-\pi^+ \rightarrow \overline{K^0}\pi^0$ is an allowed strong interaction. These processes are referred to generically as final-state interactions (FSI).

Although readily accommodated in the standard model by a complex phase in the CKM matrix, charge-parity (CP) violation remains one of the least understood phenomena in physics. So far, it has only been observed in the decays of kaons. While the results from the kaon sector are consistent with the standard model, the complications introduced by strong interaction effects make it nearly impossible to ascertain whether the complex CKM phase is the sole source for the observed asymmetries. If the standard model is correct, large CP asymmetries are expected in hadronic B decays to CP eigenstates. Efforts are now underway at every major high-energy physics laboratory to observe these CP-violating effects in the B sector.

Data samples at least one order of magnitude larger than those available at present are required to observe CP asymmetries in the B meson system and to provide fundamental consistency checks of the standard model. This is the justification for the construction of high-luminosity e^+e^- storage rings in the United States at SLAC (PEP II/BABAR) and Cornell (CESR PHASE III/CLEO III) and in Japan (KEK-B/BELLE), as well as for the dedicated fixed-target experiment at the HERA ring at DESY. Hadron-collider experiments dedicated to the study of CP violation have also been proposed at Fermilab and at CERN. In addition, these new machines will produce large samples of charm mesons and baryons, which can also be studied in detail.

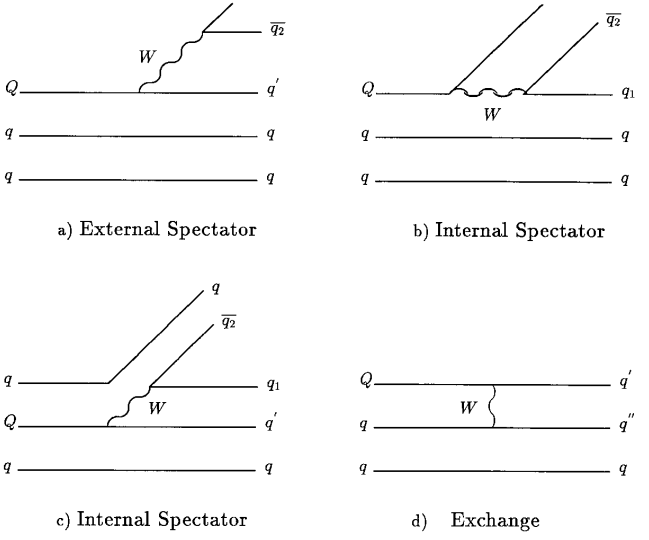

Figure 2 Hadronic decay mechanisms for *c*- and *b*-baryons.

Table 1 Charm event samples of e^+e^- colliding beam experiments

Experiment	$\sqrt{s}$	Charm events[a]
Mark III	3.77 GeV	28,000 $D^\circ D^\circ$
		20,000 D^+D^-
	4.14 GeV	3000 $D_s\overline{D}_s$
BES	4.03 GeV	6000 $D_s\overline{D}_s$
CLEO II	$\sim$ 10.5 GeV	4×10^6 $c\bar{c}$
ARGUS	$\sim$ 10.5 GeV	0.7×10^6 $c\bar{c}$
LEP	91 GeV	220,000 $c\bar{c}$ per experiment
SLD	91 GeV	14,000 $c\bar{c}$

[a]Number produced.

In order to extract information about the weak phase from the asymmetries that will be observed by these experiments in the near future, an understanding of the interplay between the weak and strong interaction responsible for hadronic decays and of the lifetimes of particles containing heavy quarks is needed. In this review, we describe recent experimental results on lifetimes and decays of mesons and baryons containing heavy quarks, and we report on the progress in interpreting these results.

Semileptonic and leptonic decays of charm and bottom hadrons have been reviewed elsewhere (6, 7). More detailed reviews of B decays are also available (8).

2. EXPERIMENTAL STUDY OF CHARM AND BOTTOM DECAY

For many years after the discovery of the charm quark in fixed-target and e^+e^- collisions, e^+e^- colliders provided most of the results in the study of charmed hadrons. In the mid-1980s, however, the introduction of silicon vertex detectors made fixed-target experiments competitive once again (9). Fermilab fixed-target experiments now dominate several areas of charm physics, including lifetime measurements and rare-decay searches.

Table 1 gives the sizes of charm data samples from e^+e^- colliding-beam experiments (6). The major advantage offered by e^+e^- annihilation is that the fraction of hadronic events containing heavy quarks is relatively large and, hence, backgrounds are small. In fixed-target experiments, the production cross section is larger but the fraction of hadronic events that contains charm particles is much smaller. The charm hadroproduction cross section is on the order of 20 μb (for an incident proton momentum of $\sim$ 400 GeV/c), but charm events represent only about 10^{-3} of the total cross section (6). Photoproduction has a smaller charm cross section but a larger fraction of charm produced.

Table 2 gives the number of reconstructed charm decays for several fixed-target experiments. The current data samples contain $\mathcal{O}(10^5)$ reconstructed charm decays. Samples with $\mathcal{O}(10^6)$ reconstructed events are expected during the next few years from Fermilab experiments E781 (SELEX) and E831 (FOCUS), as well as in e^+e^- annihilation from CLEO III at CESR.

2.1 e^+e^- *Experiments Near Threshold*

Most of the current knowledge of the decays of B mesons is based on analyses of data collected by experiments at CESR and DORIS. These experiments record data at the $\Upsilon(4S)$ resonance, which is the lowest lying $b\bar{b}$ resonance above the threshold for $B\bar{B}$ pair production. The $\Upsilon(4S)$ resonance decays exclusively to $B\bar{B}$, as there is not sufficient energy to produce additional particles. The B mesons are produced nearly at rest, and the average momentum is about 330 MeV; thus, the average decay length is approximately 30 μm.

In recent years, advances in detector technology, in particular the introduction of high-resolution silicon vertex detectors, have allowed experiments at high-energy colliders (i.e. LEP, SLC, and the TEVATRON) to observe decay vertices of b quarks. This has led to precise lifetime measurements, as well as to the direct observation of time-dependent $B-\bar{B}$ mixing and to the discovery of new b-flavored hadrons.

The first fully reconstructed B mesons were reported in 1983 by the CLEO I collaboration. Since then, the CLEO 1.5 experiment has collected a sample with an integrated luminosity of 212 pb^{-1}, the ARGUS experiment has collected 246 pb^{-1}, and to date the CLEO II experiment has collected about 4fb^{-1}, of which up to 3fb^{-1} have been used to obtain the results described in this review.

For quantitative studies of B decays, the initial composition of the data sample must be known. The ratio of the production of neutral and charged B mesons in

Table 2 Fully reconstructed charm events samples of fixed-target experiment

Experiment	Beam/target	Fully reconstructed charm decays
FNAL E691	γ Be 170 GeV	10,000
FNAL E687	γ Be 220 GeV	100,000
CERN WA75	π^- N 350 GeV	350
CERN NA32 (ACCMOR)	K^- and π^- N 200 GeV	1300
CERN WA82	π^- N 340 GeV	3000
FNAL E653	π^- N 600 GeV	1000
FNAL E769	π^- N 250 GeV	4000
FNAL E791	π^- N 500 GeV	200,000
EXCHARM	n N 40 GeV	
CERN WA89	Σ^- N 330 GeV	

$\Upsilon(4S)$ decay is, therefore, an important parameter for these experiments. The ratio is denoted f_+/f_0 and is measured (10) to be

$$\frac{f_+}{f_0} = \frac{\mathcal{B}(\Upsilon(4S) \to B^+B^-)}{\mathcal{B}(\Upsilon(4S) \to B^0\bar{B}^0)} = 1.13 \pm 0.14 \pm 0.13 \pm 0.06.$$

The third error is due to the uncertainty in the ratio of B^0 and B^+ lifetimes. This result is consistent with equal production of B^+B^- and $B^0\bar{B}^0$ pairs, and unless explicitly stated otherwise, we assume that $f_+/f_0 = 1$. The assumption of equal production of the charged and neutral B mesons is further supported by the near equality of the observed B^- and $\bar{B}^0$ masses. Older experimental results, which assumed other values of f_+ and f_0, have been rescaled.

Two variables are used to isolate the exclusive hadronic B decay modes at CLEO and ARGUS near threshold. To determine the signal yield and display the data, the beam constrained mass is

$$M_B^2 = E_{\text{beam}}^2 - \left(\sum_i \vec{p}_i\right)^2, \qquad 1.$$

where $\vec{p}_i$ is the reconstructed momentum of the i daughter of the B candidate. An example is shown in Figure 3. The resolution in this variable is determined by the beam energy spread and is about 2.7 MeV for CLEO II, and about 4.0 MeV for ARGUS. These resolutions are a factor of ten better than the resolution in invariant mass obtained without the beam energy constraint. The measured sum of charged and neutral energies, E_{meas}, of correctly reconstructed B mesons produced at the $\Upsilon(4S)$ must also equal the beam energy, E_{beam}, to within the experimental resolution. Depending on the B decay mode, $\sigma_{\Delta E}$, the error on the energy difference $\Delta E = E_{\text{beam}} - E_{\text{meas}}$ varies between 14 and 46 MeV. Note that this resolution is usually sufficient to distinguish the correct B decay mode from a mode with one additional or one fewer pion.

2.2 *High-Energy Collider Experiments*

The four LEP experiments and SLD operate on the Z^0 resonance. At this energy, the cross section for $b\bar{b}$ production is about 6.6 nb and the signal-to-noise ratio for hadronic events is 1:5, comparable to the $\Upsilon(4S)$ resonance. Compared with e^+e^- annihilation, the $b\bar{b}$ production cross section at hadron colliders is enormous, about 50 μb at 1.8 TeV. However, a signal-to-background ratio of about 1:1000 makes it difficult to extract b quark signals and to fully reconstruct B mesons.

The kinematic constraints available on the $\Upsilon(4S)$ cannot be used on the Z^0. However, due to the large boost, the b quarks travel ≈ 2.5 mm before they decay and the decay products of the two b-hadrons are clearly separated in the detector. The large boost makes precise lifetime measurements possible.

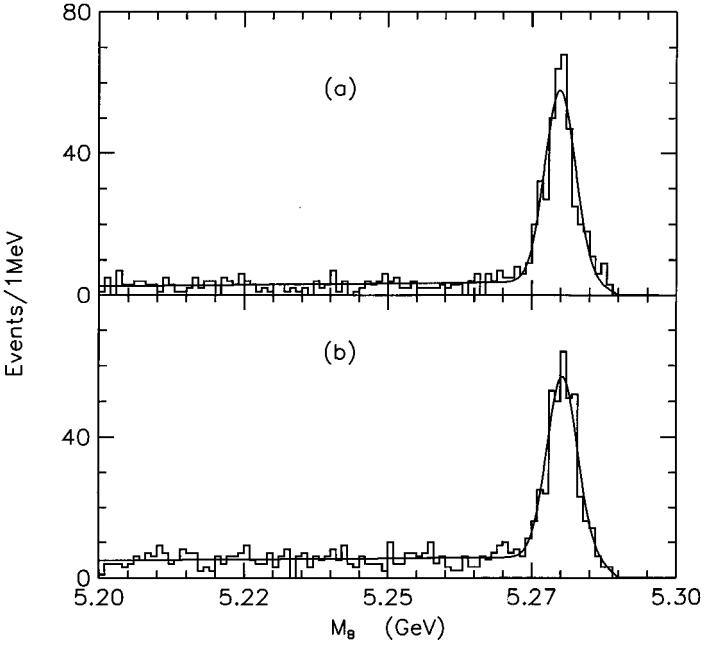

Figure 3 Beam-constrained mass distributions from CLEO II for (*a*) B^- events and (*b*) $\bar{B}^0$ events.

2.3 *Averaging Experimental Results*

To extract B meson branching fractions, the detection efficiencies are determined from a Monte Carlo simulation and the yields are corrected for the charmed meson branching fractions. In order to determine world-average branching fractions for B and D meson decays, the results from individual experiments must be normalized with respect to a common set of values for absolute branching fractions of charm mesons and baryons. The branching fractions for the D^0 and D^+ modes used to calculate the B branching fractions are given in Table 13. For the $D^0 \to K^-\pi^+$ branching fraction, we have chosen an average of values recently reported by the CLEO II, ARGUS, and ALEPH experiments (11). The value $\mathcal{B}(D^+ \to K^-\pi^+\pi^+) = 8.9 \pm 0.7\%$ is used in this review to normalize branching fractions for D^+ modes. Our value for $\mathcal{B}(D^0 \to K^-\pi^+\pi^0)$ is calculated using a recent result from CLEO II (12), $\mathcal{B}(D^0 \to K^-\pi^+\pi^0)/\mathcal{B}(D^0 \to K^-\pi^+) = (3.67 \pm 0.08 \pm 0.23)\%$, averaged with an older measurement from ARGUS (13). The branching ratios of other D^0 decay modes relative to $D^0 \to K^-\pi^+$ are taken from the PDG compilation (14). The D^+ branching ratios are also taken from the PDG compilation (14).

The CLEO II results for $D^+ \to K^-\pi^+\pi^+$, however, have been rescaled to account for the new $D^0 \to K^-\pi^+$ branching fraction. For older measurements of B decays involving D^* mesons, the branching fractions have been rescaled to account for improved measurements of the D^* branching fractions.

Branching ratios for all D_s decay modes are normalized relative to $\mathcal{B}(D_s^+ \to \phi\pi^+)$. Two model-independent measurements of the absolute branching fraction for $D_s^+ \to \phi\pi^+$ have been published by BES (15) and CLEO (16). These have been averaged to determine the value used here (see Table 14). Branching ratios involving D_s^* modes are also rescaled to account for the isospin-violating decay $D_s^* \to D_s\pi^0$ recently observed by CLEO (17).

The determination of branching fractions for B decays to charmed baryons requires knowledge of $\mathcal{B}(\Lambda_c^+ \to pK^-\pi^+)$. The uncertainty in this quantity, however, is still large, as it can only be determined by indirect and somewhat model-dependent methods. In this review, we use $\mathcal{B}(\Lambda_c^+ \to pK^-\pi^+) = 4.4 \pm 0.6\%$, determined by the particle data group (14).

Statistical errors are recalculated in the same way as the branching ratios. For results from individual experiments on B decays to final states with D mesons, two systematic errors are quoted. The second systematic error contains the contribution due to the uncertainties in the $D^0 \to K^-\pi^+$, $D^+ \to K^-\pi^+\pi^+$, or $D_s^+ \to \phi\pi^+$ branching fractions. This will allow easier rescaling at a time when these branching ratios are measured more precisely. The first systematic error includes the experimental uncertainties and, when relevant, the uncertainties in the ratios of charm branching ratios, e.g. $\Gamma(D^0 \to K^-\pi^+\pi^+\pi^-)/\Gamma(D^0 \to K^-\pi^+)$ and the error in the D^* branching fractions. For modes involving D_s^+ mesons, the first systematic error also includes the uncertainties due to the D^0 and D^+ branching ratios. For all other modes, only one systematic error is given. For world averages, the statistical and the first systematic error are combined in quadrature while the errors due to the D^0, D^+, and D_s^+ branching ratio scales are listed separately.

With the improvement in the precision of the D^0 and D^* branching fractions, these quantities are no longer the dominant source of systematic error in the study of hadronic B meson decay. The errors on the D_s^+ and Λ_c^+ branching ratios remain large.

3. LIFETIME MEASUREMENTS

3.1 *Theoretical Expectations for Lifetimes of Hadrons with Heavy Quarks*

In the naive spectator model, the external spectator amplitude is the only weak decay mechanism and, thus, the lifetimes of all mesons and baryons containing

heavy quarks should be equal. Differences in hadronic decay channels and interference between contributing amplitudes modify this simple picture and give rise to a hierarchy of lifetimes. Experimentally, we find the measured lifetimes to be significantly different. For example, the D^+ lifetime is ~ 2.5 times longer than the D^0 lifetime.

The decay width of charmed hadrons ($\Gamma_{\rm tot} = \Gamma_{\rm l} + \Gamma_{\rm sl} + \Gamma_{\rm had}$) is dominated by the hadronic component. For example, for the D^+ meson, one finds that the semileptonic component, $\Gamma_{\rm sl} = (16.3 \pm 1.8) \times 10^{10} s^{-1}$, is a small fraction of the total width $\Gamma = (94.6 \pm 1.4) \times 10^{10} s^{-1}$. The contribution from purely leptonic decays can be neglected.

Measurements of the lifetime ratio $\tau(D^+)/\tau(D^0) = 2.547 \pm 0.044$ (14) and of the inclusive semileptonic branching ratios, $D^+ \to eX = (17.2 \pm 1.9)\%$ (14) and $D^0 \to eX = (6.64 \pm 0.18 \pm 0.29)\%$ [using a recent result from CLEO (18)], show that the D^0 and D^+ semileptonic decay widths are nearly equal.

$$\frac{\Gamma(D^0 \to eX)}{\Gamma(D^+ \to eX)} = \frac{\mathcal{B}(D^0 \to eX)}{\mathcal{B}(D^+ \to eX)} \times \frac{\tau(D^+)}{\tau(D^0)} = 0.98 \pm 0.11. \qquad 2.$$

This implies that differences in the total decay widths must be due to differences in the hadronic decay amplitudes.

In the past, it was suggested that the large difference in the charm meson lifetimes was due to the presence of the exchange (annihilation) diagram for the D^0 (D_s). A more reliable explanation invokes the destructive interference of the external and internal spectator diagrams, which decrease the hadronic width of the D^+. The external and internal spectator diagrams can give the same final states only for the D^+ meson and not for the D^0 or D_s^+ mesons (see Figure 1*a* and *b*). The two diagrams will interfere destructively. This effect reduces the total width of the D^+ (see Section 7.7.2). As a consequence, we expect $\Gamma_{\rm had}(D^+) < \Gamma_{\rm had}(D^0) \sim \Gamma_{\rm had}(D_s)$, or the following hierarchy of lifetimes,

$$\tau(D^0) \sim \tau(D_s) < \tau(D^+). \qquad 3.$$

It is important to note that the difference in the hadronic decay width should be understandable at the level of two-body decays, since three-body and four-body decays are experimentally found to be dominated by quasi two-body channels.

The baryon sector is more complex. The exchange mechanism is no longer helicity suppressed and can be comparable to the spectator diagram. In addition, color suppression is operative only for particular decay channels.

There are three large effects that modify hadronic widths in charm baryon decay (19): (*a*) destructive interference between the external spectator (Figure 2*a*) and the internal spectator (Figure 2*c*) if a spectator quark is a *u*-quark (as in Λ_c and Ξ_c^+), analogous to the effect in D^+ decay; (*b*) constructive interference

between two internal spectator diagrams (Figures 2*b* and *c*) if the spectator quark is an *s*-quark (as in Ξ_c^+, Ξ_c^0, and Ω_c); and (*c*) W-exchange contributions (Figure 2*d*), which can be large if the baryon contains a *d*-quark (Λ_c and Ξ_c^0). Neglecting mass differences and Cabibbo-suppressed decays, the nonleptonic decay rates for charm baryons are qualitatively given by

$$\Gamma(\Lambda_c) = \Gamma_{\text{spec}} + \Gamma_{\text{des.int.}} + \Gamma_{\text{exch.}}$$
$$\Gamma\left(\Xi_c^+\right) = \Gamma_{\text{spec}} + \Gamma_{\text{des.int.}} + \Gamma_{\text{con.int.}}$$
$$\Gamma\left(\Xi_c^0\right) = \Gamma_{\text{spec}} + \Gamma_{\text{con.int.}} + \Gamma_{\text{exch.}}$$
$$\Gamma(\Omega_c) = \Gamma_{\text{spec}} + \Gamma_{\text{con.int.}} \qquad 4.$$

where spec is the spectator component, exch is the W-exchange component, con.int is the component from the constructive interference, and des.int is the destructive interference component. Models with different relative weights for these non–spectator effects lead to different predictions. There are two models that predict a baryon lifetime hierarchy

$$\tau(\Omega_c) \sim \tau\left(\Xi_c^0\right) < \tau\left(\Lambda_c\right) < \tau\left(\Xi_c^+\right) \qquad (19) \qquad 5.$$
$$\tau(\Omega_c) < \tau\left(\Xi_c^0\right) < \tau(\Lambda_c) \sim \tau\left(\Xi_c^+\right) \qquad (20).$$

Since the ground-state hadrons containing *b* quarks decay weakly, their lifetimes should be in the range of 0.1–2 ps. Ten years ago, before the MAC (21) and MARK II (22) collaborations presented the first measurements of the *b* lifetime, the only phenomenological guide to the strength of the coupling between the quark generations was the Cabibbo angle. If the coupling between the third and second generations ($|V_{cb}|$) had the same strength as the coupling between the second and first($|V_{cs}|$), the *b* lifetime would be about 0.1 ps. When measurements at PEP indicated lifetimes longer than 1 ps, it was deduced that the CKM matrix element $|V_{cb}|$ is very small.

As in the charm sector, we expect a lifetime hierarchy for *b*-flavored hadrons. However, since the lifetime differences are expected to scale as $1/m_Q^2$, where m_Q is the mass of the heavy quark, the variation in the *b* system should be significantly smaller, on the order of 10% or less (23). For the *b* system, we expect

$$\tau(B^-) \geq \tau(\bar{B}^0) \approx \tau(B_s) > \tau\left(\Lambda_b^0\right). \qquad 6.$$

Measurements of lifetimes for the various *b*-flavored hadrons provide a means of determining the importance of non–spectator mechanisms in the *b* sector.

3.2 *Techniques for Charm Lifetime Measurements*

The measurements of the charm hadron lifetimes are dominated by fixed-target experiments using silicon vertex detectors. The measurement of the lifetime is, in principle, very simple. One measures the decay length $L = \beta\gamma ct$ to extract the proper time t. The typical proper time for a c-hadron decay is in the range 10^{-12}–$10^{-13}s$, so that high-precision vertex detectors are necessary. The lifetimes are determined using a binned maximum likelihood fit to the distribution of reduced proper time, which is defined as $t' = t - N\sigma/\beta\gamma c$, where σ is the error on the longitudinal displacement (L) between the primary and the secondary vertex (typically about 400 μm). The value of N varies depending on the analysis (typically $N = 3$). The reduced proper time avoids the use of large corrections at short t. Corrections for acceptance and hadronic absorption at long times and resolution at short times are included in the fitting function. Events from the mass sidebands are used to model the background lifetime distribution.

This technique must be modified slightly for measurements of the short-lived charmed hyperons, for example, the Ω_c lifetime is comparable to experimental resolution (24). In E687, the fit is performed for all observed times greater than -0.05 ps to retain sufficient statistics. The effect of resolution is significant; it is included in the analysis by convoluting the exponential decay and the resolution function (25).

3.3 *Techniques for Beauty Lifetime Measurements*

The lifetime of a particle is related to its decay length L_b by

$$\tau_b = \frac{L_b}{\gamma\beta c}. \qquad 7.$$

At LEP energies, the average b momentum is about 30 GeV, which results in an average decay length of 2.5 mm for $\langle\tau_b\rangle = 1.5$ ps. Similarly, at CDF, the mean vertex displacement in the plane transverse to the beam is about 0.9 mm.

A variety of methods has been developed to measure the decay length and to determine the b lifetime. They all follow the same basic steps. A purified sample is selected and the decay length is either measured directly or determined indirectly by using the impact parameter. The resulting decay length is then corrected for the Lorentz boost. An additional correction for background contamination is applied as well.

To determine the lifetime of a specific b hadron, as in charm hadron lifetime measurements, one would like to have a sample of fully reconstructed decays. The b vertex could then be reconstructed, allowing a measurement of the decay length. The momentum of the b hadron gives the $\gamma\beta$ factor in Equation 7 without any further assumptions. The resulting proper-time distribution would

be an exponential function convoluted with a Gaussian resolution function representing the measurement errors. Although currently limited by statistics, this procedure will ultimately yield the most precise measurements of individual *b*-hadron lifetimes.

The best statistical precision in the determination of lifetimes of hadrons containing *b* quarks is currently obtained from measurements using partial reconstruction of semileptonic decays. These decays represent about 21% of the total *b* decay rate and have the advantage that both electrons and muons can be efficiently identified with low background. The purity of the sample can be enhanced by kinematical cuts that take advantage of the large mass of the *b* quark, e.g. selecting leptons with large transverse momentum with respect to the *b* direction. Event samples with purities above 90% have been obtained at LEP. However, in such semileptonic decays, the neutrino is not detected, so the *b* hadron is not completely reconstructed. One then has to rely on Monte Carlo simulations to estimate the *b* momentum and to extract the proper-time distribution from the decay-length measurements.

For inclusive lifetime measurements, the presence of a high $p_\perp$ lepton or a ψ meson is usually sufficient to demonstrate the presence of a *b* quark, while for exclusive measurements of individual *b*-hadron lifetimes, an additional decay particle has to be reconstructed in order to establish a signature characteristic for the decaying *b* hadron (Figure 4). The Λ_b lifetime, for example, is measured using a sample of events containing $\Lambda_c^+ \ell^-$ or $\Lambda \ell^-$ combinations.

In early experiments, the vertexing precision was not adequate to measure the decay length, $l = \gamma\beta c\tau$, directly. The impact parameter method shown schematically in Figure 4*a* was developed as an alternative. Because of the

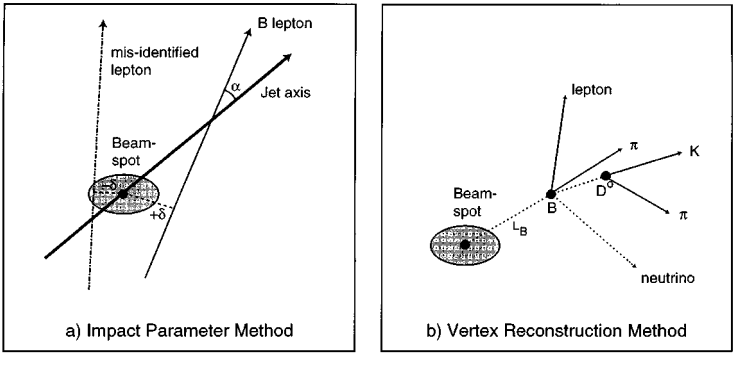

Figure 4 Lifetime measurements using the impact parameter method (*a*) and decay length method (*b*) for inclusive and exclusive *B* hadrons.

finite lifetime of the b hadron, a lepton from the semileptonic decay of the heavy quark will miss the primary vertex where the b hadron was produced. The miss distance or impact parameter, δ, is given by

$$\delta = \gamma\beta c\tau_b \sin\alpha \sin\theta, \qquad 8.$$

where α is the angle between the lepton and the b directions and θ is the polar angle. The b direction is usually approximated by the axis of the hadronic jet. A negative sign is assigned to the impact parameter if the lepton track crosses the jet axis behind the the beam spot, indicating a mismeasured lepton or a background event. The main advantage of the impact parameter method is that it is rather insensitive to the unknown boost of the parent; as $\gamma\beta$ increases with the b momentum, $\sin\alpha$ decreases approximately as $1/\gamma\beta$ for $\beta \approx 1$.

In experiments with sufficient statistics and vertex resolution, the decay length for the b hadron vertex is reconstructed by using the lepton track and the direction of the reconstructed charm meson, as shown in Figure 4*b*. The momentum of the b hadron is estimated by using the observed decay products, the missing momentum, and a correction factor determined from a Monte Carlo simulation. The proper-time distribution is then given by an exponential convoluted with a Gaussian resolution function and the momentum correction factor. A maximum likelihood fit is used to extract the lifetime (37).

To obtain the most precise value for inclusive and exclusive b lifetimes, the results of lifetime measurements from different experiments have been combined. Using the conventional approach of weighting the measurements according to their error does not take into account the underlying exponential decay-time distribution. If a measurement fluctuates low then its weight in the average will increase, leading to a bias towards low values. This is particularly relevant for low statistics measurements such as the B_s lifetime. According to a study by Forty (26), this bias can be avoided if the weight is calculated using the relative error σ_i/τ_i.[1] We find a 1–3% difference in the average lifetimes computed, with the second method giving the larger value. A slight bias of the latter method toward higher lifetime values could be avoided by taking into account asymmetric errors. This effect has been found empirically to be rather small, and we omit this additional complication in the calculation of our lifetime averages.

3.4 *Results on Lifetimes of Hadrons That Contain c Quarks*

The experimental results are summarized in Figure 5, where updated world averages for the c-hadron lifetimes are given (14, 25, 27). From these results, the full lifetime hierarchy can be studied.

[1]This procedure assumes good vertex resolution, i.e. $\sigma < \tau/10$.

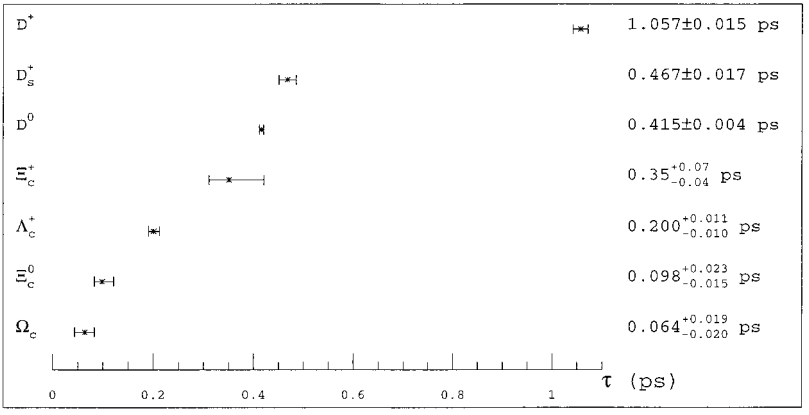

Figure 5 Summary of measurements of lifetimes of charm hadrons.

The measurements of the charm hadron lifetimes are now very precise. Systematic effects will soon become the largest component of the error for some measurements, e.g. the D^0 and D^+ lifetimes. These systematic effects are due to the uncertainty in the D momentum distribution, to the nuclear absorption of the D meson or its decay products in the target, and to the lifetime of the background. In the baryon sector the measurements are still statistics limited. There are now results for the Ω_c lifetime from E687 (25) and WA89 (27) which complete the baryon hierarchy. It is quite remarkable that the lifetime of this rare and short-lived baryon is now being measured.

The world averages for lifetime measurements are dominated by results from E687, which is the only single experiment that has measured all the charmed hadron lifetimes (28, 25). The results are internally consistent, and the ratios of lifetimes, which characterize the hierarchy, are to a large extent unbiased by systematic effects (29). For the charm mesons lifetimes, a clear pattern emerges, in agreement with the theoretical predictions

$$\tau(D^0) < \tau(D_s) < \tau(D^+). \qquad 9.$$

These meson lifetimes are now measured at the level of a few percent, probably beyond the ability to compute them. The near equality of $\tau(D_s)$ and $\tau(D^0)$ is direct evidence for the reduced weight of the non-spectator (W-exchange and W-annihilation) contribution in charm meson decays (30).

The agreement between the measurements of charm baryon lifetimes and theoretical expectations is remarkable, since, in addition to the exchange diagram, there are constructive as well as destructive contributions to the decay

rate. The experimental results lead to the following baryon lifetime hierarchy:

$$\tau(\Omega_c) \leq \tau\left(\Xi_c^0\right) < \tau(\Lambda_c) < \tau\left(\Xi_c^+\right). \quad 10.$$

Although statistically limited, the present values tend to favor the model of Guberina et al (19).

3.5 *Results on Lifetimes of Hadrons That Contain b Quarks*

Inclusive measurements of the b lifetime were important historically to establish the long b lifetime. In addition, they provided the first evidence that the coupling between the second and third quark generation is quite small. They are still needed for some electroweak studies, such as the determination of the forward-backward asymmetry in $Z \rightarrow b\bar{b}$, where the different hadrons containing b-quarks are not distinguished. For B physics, i.e. the study of B meson decays, exclusive measurements of individual b-hadron lifetimes are preferable. For example, to extract the value of the CKM matrix element $|V_{cb}|$ from measurements of semileptonic B decays, the average of the B^+ and B^0 lifetimes should be used rather than the inclusive b lifetime, which contains contributions from B_s mesons and b baryons.

The current world average for the inclusive b lifetime, which includes many measurements, is (32)

$$\langle \tau_b \rangle \; = \; 1.563 \pm 0.019 \quad \text{ps}.$$

The world average for this quantity in 1992 was (1.29 ± 0.05) ps. The substantial change in the value has been attributed to several improvements: the use of neutral energy when calculating the b jet direction, and better knowledge of the resolution function as a result of the use of silicon vertex detectors (26, 31).

Precise measurements of exclusive lifetimes for b-flavored hadrons have been carried out by CDF (33,35), by some of the LEP experiments, and by SLD (47). The most recent results and the techniques used are given in Table 3.

3.5.1 B^- AND $\bar{B}^0$ LIFETIME MEASUREMENTS The best statistical precision in the determination of exclusive lifetimes is obtained from measurements using lepton-particle correlations. For example, a sample of B^0 candidates can be obtained from events with lepton-D^{*+} correlations of the correct sign; these events originate from the decay $B^0 \rightarrow D^{*+}\ell^-\nu$, $D^{*+} \rightarrow D^0\pi^+$ and $D^0 \rightarrow K^-\pi^+$ (see Figure 4*b* for the method and Figure 6 for the CDF results). The pion from the strong decay and the lepton form a detached vertex. This information combined with the direction of the reconstructed D^0 meson determines the location of the B decay vertex. To obtain the lifetime from the decay length requires knowledge of $\gamma\beta$, which is estimated from the momenta of the observed

Table 3 Measurements of lifetimes for *b*-flavored hadrons

Particle	Method	CDF	ALEPH	OPAL	DELPHI	SLD
$\bar{B}^0$	D^{*+}	$1.57 \pm 0.08 \pm 0.07$	$1.61 \pm 0.07 \pm 0.05$	$1.53 \pm 0.12 \pm 0.08$	$1.61^{+0.14}_{-0.13} \pm 0.08$	$1.60^{+0.15}_{-0.14} \pm 0.10$
$\bar{B}^0$	excl.	$1.64 \pm 0.11 \pm 0.06$	$1.25^{+0.15}_{-0.13} \pm 0.05$			
$\bar{B}^0$	topol.				$1.63 \pm 0.14 \pm 0.13$	$1.55 \pm 0.07 \pm 0.12$
$\bar{B}^0$	$\pi\pi$		$1.49^{+0.17+0.08}_{-0.15-0.06}$			
B^-	$D^0 l^-$	$1.51 \pm 0.12 \pm 0.08$	$1.58 \pm 0.09 \pm 0.04$	$1.52 \pm 0.14 \pm 0.09$	$1.61 \pm 0.16 \pm 0.12$	$1.49^{+0.11}_{-0.11} \pm 0.05$
B^-	excl.	$1.68 \pm 0.09 \pm 0.06$	$1.58^{+0.21}_{-0.18} \pm 0.04$			
B^-	topol.				$1.72 \pm 0.08 \pm 0.06$	$1.67 \pm 0.06 \pm 0.09$
B_s^0	$D_s - l$	$1.42^{+0.27}_{-0.23} \pm 0.11$	$1.64^{+0.16}_{-0.14} \pm 0.04$	$1.54^{+0.25}_{-0.21} \pm 0.06$	$1.54^{+0.31}_{-0.27} \pm 0.06$	
B_s^0	$D_s - h$		$1.61^{+0.30+0.29}_{-0.18-0.16}$		$1.57^{+0.45+0.15}_{-0.37-0.14}$	
B_s^0	D_s incl.				$1.61^{+0.34+0.18}_{-0.29-0.13}$	
B_s^0	$\phi - l$				$1.45^{+0.20+0.32}_{-0.23-0.16}$	
B_s^0	ϕ	$1.74^{+1.08}_{-0.69} \pm 0.07$				
Λ_b	$\Lambda - l$		$1.21 \pm 0.09 \pm 0.07$	$1.16 \pm 0.11 \pm 0.06$	$1.10^{+0.16+0.05}_{-0.14-0.08}$	
Λ_b	$\Lambda_c - l$	$1.33 \pm 0.16 \pm 0.07$	$1.24^{+0.15}_{-0.14} \pm 0.05$	$1.14^{+0.22}_{-0.19} \pm 0.07$	$1.26^{+0.26+0.03}_{-0.22-0.05}$	
Λ_b	$p - l$				$1.27^{+0.35+0.08}_{-0.29-0.09}$	
Ξ_b^0	$\Xi - l$		$1.25^{+0.55}_{-0.35} \pm 0.20$		$1.5^{+0.7}_{-0.4} \pm 0.3$	

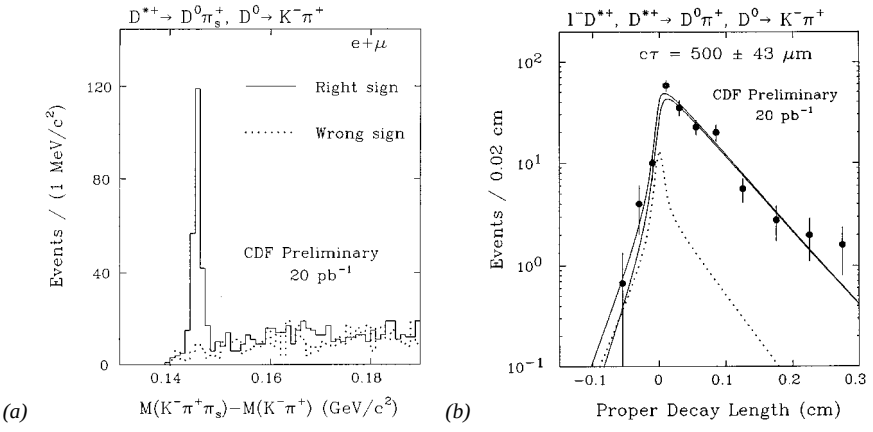

Figure 6 B^0 lifetime measurements by CDF: (*a*) effective mass and (*b*) decay length distribution for D^*-ℓ^- decays. A clear signal is present in opposite sign combinations, whereas no signal is present when same sign-charged leptons are combined with D^{*+} candidates.

decay products. Since the neutrino is not observed, a correction is made. The uncertainty in the size of this correction is included in the systematic error and is typically on the order of 3%. Another systematic problem is the contamination from decays $B^- \to D^{**}\, l^- \nu$, followed by $D^{**} \to D^{*+}\pi^-$ where the π^- from the strong decay of the D^{**} (p-wave) meson is not detected. These backgrounds will lead to a B^- meson contamination in the $\bar{B}^0$ lifetime sample. Since the branching fractions for such decays are poorly measured, this is another important systematic limitation and contributes on the order of 5% to the systematic error. Significant contributions to the systematic error also result from the uncertainty in the level of background and its lifetime distribution. More detailed discussions of exclusive lifetime measurements can be found in recent reviews by Sharma (31) and Kroll (32).

The systematic problems associated with the boost correction and the contamination from poorly measured backgrounds can be avoided by using fully reconstructed decays such as $\bar{B}^0 \to D^+\pi^-$ or $B^- \to \psi K^-$. However, since exclusive B branching ratios are small, this method has much poorer statistical precision. In hadron-collider experiments, this approach has been successfully used to determine the B^0, B^-, and B_s lifetimes from exclusive modes with ψ mesons, e.g. $B^0 \to \psi K^{*0}$, $B^- \to \psi K^-$ (34), and $B_s \to \psi\phi$ (35).

A topological vertexing method has been used by the DELPHI and SLD experiments. Candidate B^0 and B^+ mesons are distinguished on the basis of the net charge of the tracks at the decay vertex. This method has small statistical

errors; however, care must be taken to assure that systematic uncertainties from tracking and incorrect assignments of decay vertices are controlled. The neutral B lifetime that is extracted represents an average over the lifetimes over all neutral b-flavored hadrons, including B_d^0, B_s^0, and Λ_b^0. With good knowledge of the production fractions, the exclusive B^0 lifetime can be extracted. In the case of SLD, the excellent resolution of the CCD vertex detector compensates to some degree for the low statistics.

Using the procedure for averaging measurements (described in Section 3.3.1), we combine the individual B^- and $\bar{B}^0$ lifetime measurements and obtain

$$\tau_{B^-} = 1.62 \pm 0.04 \quad \text{ps}$$

$$\tau_{\bar{B}^0} = 1.57 \pm 0.04 \quad \text{ps}.$$

When averaging the results obtained by studying $D^{(*)} - \ell$ correlations, a common systematic error of 3% has been assumed.

3.5.2 B_s LIFETIME MEASUREMENTS The B_s lifetime was measured by CDF (35) and the LEP experiments using partial reconstruction of the semileptonic decay $\bar{B}_s^0 \to D_s^- \ell^+ \nu$. Candidate D_s^- mesons were reconstructed in the $\phi\pi^-$ or $K^{*0}K^-$ final states. Figure 7*a* shows the $K^-K^+\pi^+$ invariant mass spectrum obtained by ALEPH (37) for right-sign and wrong-sign $D_s\ell$ combinations. The B_s decay length was measured and converted to the B_s proper time using a B_s momentum estimator based on the reconstructed lepton and the D_s momentum, as well as on an estimated neutrino energy obtained by using a missing mass technique. The B_s lifetime was extracted from the proper-time distribution using a maximum likelihood fit. The result of such a procedure is shown in Figure 7*b*.

The uncertainty in the B_s lifetime is still dominated by the statistical error. Assuming a common systematic error of 2% (31) for the uncertainty in the vertex resolution and the neutrino energy estimate, we obtain

$$\tau_{B_s} = 1.55 \pm 0.09 \quad \text{ps}.$$

For the B_s meson, there are two weak eigenstates with different lifetimes that can be distinguished by their CP quantum number. The decay $\bar{B}_s^0 \to D_s^- \ell^+ \nu$ contains an equal mixture of the two eigenstates. An appreciable lifetime difference $\Delta\Gamma$ is expected for the B_s [O(10%)] and should be measurable at future experiments. Measurements of the B_s lifetime difference may be used to constrain $|V_{td}|/|V_{ts}|$ (49).

3.5.3 B BARYON LIFETIME MEASUREMENTS Studies of $\Lambda_c^+\ell^-$ and $\Lambda\ell^-$ correlations at LEP are used to determine the lifetime of the Λ_b^0 baryon. For example,

using the decay chain,

$$\Lambda_b \to \Lambda_c^+ \ell^- \overline{\nu},\ \Lambda_c \to \Lambda X \to p\pi^- X,$$

the $p\pi^-$ invariant mass distribution shown in Figure 8*a* was obtained by OPAL (42). Although the composition of the *b* baryon sample is not known, it is expected that the Λ_b baryon is the most copiously produced. Both impact-parameter and decay-length measurements have been used to determine τ_{Λ_b}. Since the Λ_c^+ lifetime is short, the Λ_b decay length can be estimated by using the displacement of the $\Lambda\ell^-$ vertex. The time distribution from the OPAL analysis, which uses this technique, is shown in Figure 8*b*.

A better estimate of the Λ_b^0 decay point is obtained from fully reconstructing the Λ_c^+ baryon and finding the $\Lambda_c^+\ell^-$ vertex. However, the sample sizes are somewhat small. Using this method, CDF finds $\tau_{\Lambda_b} = 1.33 \pm 0.16 \pm 0.07$ ps. Combining the results listed in Table 3, the world average Λ_b lifetime is found to be

$$\tau_{\Lambda_b} = 1.21 \pm 0.07 \quad \text{ps}.$$

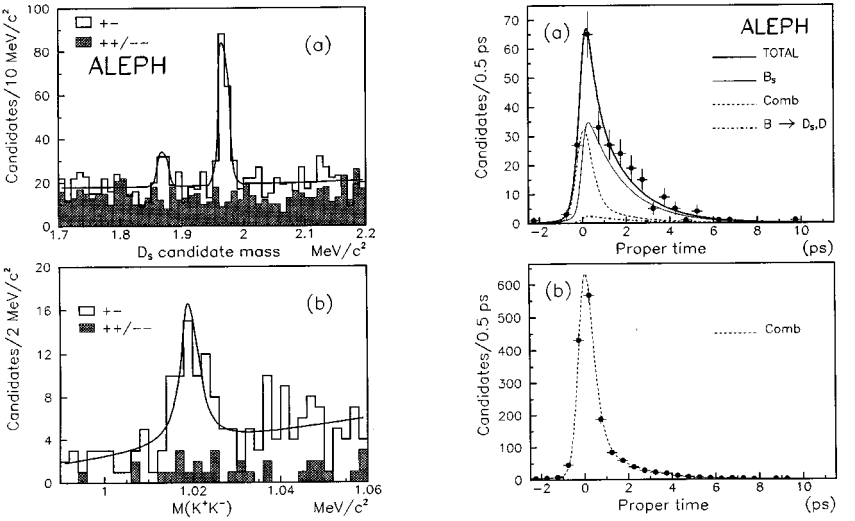

Figure 7 B_s event selection and lifetime measurement by ALEPH. (*a*) $K^-K^+\pi^+$ invariant mass distribution for right-sign $D_s^+\ell^-$ and wrong-sign (++ and $--$) combinations are shown as a shaded histogram. (*b*) K^-K^+ invariant mass distribution for right-sign and wrong-sign $D_s^+\ell^+$ combinations. (*c*) Proper-time distribution of the right-sign $D_s^+\ell^-$ sample. (*d*) Proper-time distribution of the combinatorial background.

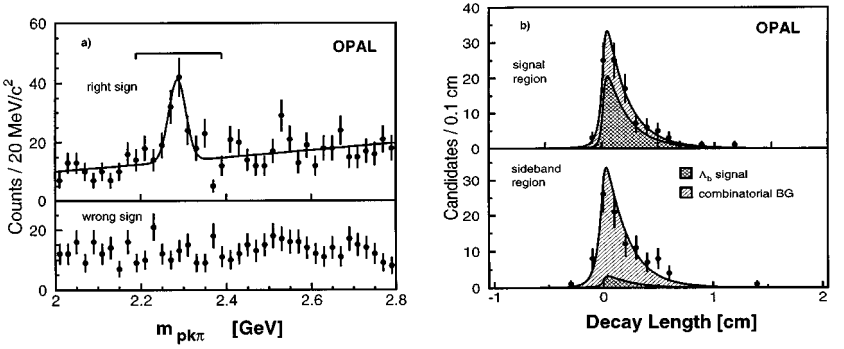

Figure 8 Λ_b lifetime measurement by OPAL. (*a*) $pk\pi^-$ invariant mass distribution for right-sign $\Lambda_c^+\ell^-$ and wrong-sign $\Lambda_c^-\ell^-$ combinations. (*b*) Decay length distribution of the right-sign and $\Lambda\ell^-$ sample. The inset shows the corresponding distribution for wrong-sign $\Lambda\ell^+$ candidates.

This confirms the original indications that the lifetime of Λ_b is very short, a fact that is difficult to accommodate theoretically.

DELPHI and ALEPH have observed small signals in $\Xi^-\ell^-$ correlations. These are expected to come from $\Xi_b^- \to \Xi_c^0\ell^-\bar{\nu}X$ and $\Xi_b^0 \to \Xi_c^+\ell^-\bar{\nu}X$ followed by $\Xi_c \to \Xi^- X'$. These samples have been used to measure the lifetime of Ξ_b^- (39, 46).

3.5.4 MEASUREMENTS OF LIFETIME RATIOS The ratio of the B^- and $\bar{B^0}$ lifetimes has been measured by a number of experiments. These measurements are performed either by using correlations between D mesons and leptons or by using exclusive final states such as $B^- \to \psi K^-$ and $B^0 \to \psi K^{*0}$. The CLEO II experiment has measured $\mathcal{B}(B^0 \to X\, l^-\nu)$ and $\mathcal{B}(B^- \to X\, l^-\nu)$ using the yield of leptons found opposite fully and partially reconstructed B decays (48). From isospin invariance, the ratio of the two branching fractions is the ratio of the lifetimes.

Table 4 Measurements of B^-/B^0 lifetime ratio

Method	CDF	ALEPH	OPAL	DELPHI	SLD
$D-l$	$0.96 \pm 0.10 \pm 0.05$	$0.98 \pm 0.08 \pm 0.02$	$0.99 \pm 0.14^{+0.05}_{-0.04}$	$1.00^{+0.17}_{-0.15} \pm 0.10$	$0.94^{+0.14}_{-0.12} \pm 0.07$
excl.	$1.02 \pm 0.09 \pm 0.15$	$1.27^{+0.23}_{-0.19} \pm 0.03$			$1.08^{+0.09}_{-0.08} \pm 0.10$
topol.				$1.06^{+0.13}_{-0.11} \pm 0.10$	
B tags (CLEO II)					$0.93 \pm 0.18 \pm 0.12$

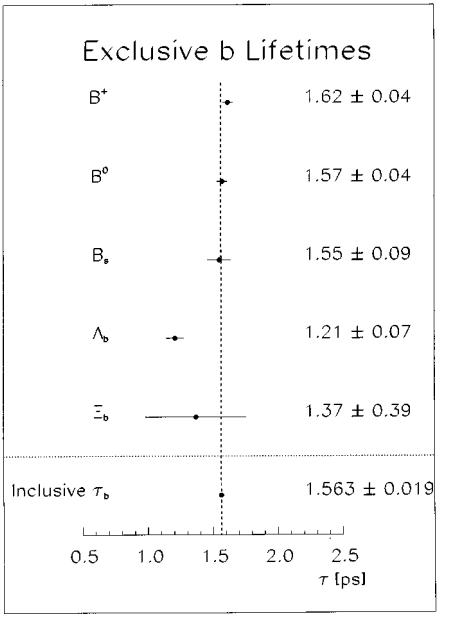

Figure 9 Summary of exclusive *b*-hadron lifetime measurements.

Averaging the results listed in Table 4, we obtain

$$\frac{\tau_{B^-}}{\tau_{\bar{B}^0}} = 1.00 \pm 0.05.$$

Note that this value is not exactly equal to the ratio of the world averages for the B^- and $\bar{B}^0$ lifetimes since the average value of $\tau_{B^-}/\tau_{\bar{B}^0}$ is calculated directly from the ratios reported by the experiments.

3.6 *Lifetime Summary*

The experimental results on lifetimes for hadrons with *c* quarks are shown in Figure 5. For the D^0 and D^+ mesons, the lifetimes measurements will soon become systematics dominated. It is clear from the observed lifetime hierarchy that non–spectator effects are important in the charm sector.

A summary of the measurements of *b* hadron lifetimes is shown in Figure 9. The pattern of measured lifetimes follows the theoretical expectations outlined above, and non–spectator effects are observed to be small. However, the Λ_b baryon lifetime is unexpectedly short. As has been noted by several authors, the observed value of the Λ_b lifetime is quite difficult to accommodate theoretically (50, 51).

Assuming that the relative production ratios of B^-, $\bar{B}^0$, B_s, Λ_b at the Z^0 are 0.39 : 0.39 : 0.12 : 0.10, the exclusive lifetime measurements can be averaged

to give $\langle \tau_{\text{excl.}} \rangle = 1.551 \pm 0.025$ ps; this is consistent with the world average for the inclusive b lifetime, $\tau_b = 1.563 \pm 0.019$ ps.

4. NONLEPTONIC DECAYS OF C-QUARK HADRONS

4.1 *Introduction*

In the past few years, there has been an impressive increase in the size of charm particle data samples.

D mesons are the only examples of heavy quark systems in which Cabibbo-flavored decays, single Cabibbo-suppressed decays, and double Cabibbo-suppressed decays (DCSD) have all been measured.

The high statistics now available allow for isospin analyses of related decay modes. The effect of elastic FSI can then be taken into account when making comparisons with model predictions. Further improvements are sophisticated amplitude analyses for three-body and four-body final states, from which the resonant substructure of multibody final states can be determined.

A systematic investigation of charm baryon decay modes has also begun. This is complementary to investigations of the meson sector. In the case of charm baryons, the W-exchange mechanism is no longer helicity-suppressed and can be studied in detail.

4.2 *Double Cabibbo-Suppressed Decays*

The decay mode $D^+ \rightarrow K^+\pi^+\pi^-$, recently measured by the E687 and E791 collaborations (52, 53), has an unambiguous interpretation as a double Cabibbo-suppressed spectator decay. The decays $D^0 \rightarrow K^+\pi^-$ and $D^0 \rightarrow K^+\pi^+\pi^-\pi^-$ may occur either by DCSD or by $D^0 - \overline{D^0}$ mixing (see Figure 1*f*). To observe these decay modes, experiments use the decay chain $D^{*+} \rightarrow D^0\pi^+$ to tag the flavor of the neutral D. The mixing and DCSD contribution can be separated by using their different decay time dependences. The DCSD component follows the usual $e^{-t/\tau}$ time evolution, while the rate for the mixing is proportional to $t^2e^{-t/\tau}$ in the limit of small mixing (54). In the standard model, $D^0 - \overline{D^0}$ mixing is expected to be small: The ratio of mixed to unmixed decays, r_m, is less than 10^{-8} (55). The best limit on r_m comes from the E691 experiment, which found $r_m < 0.0037$ (56). A measurement of the corresponding DCSD parameter, r_{DC}, expected to be on the order of $\tan^4\theta_c \sim 0.0026$, can be obtained from the time-integrated measurement of CLEO if no mixing is assumed (57). Since CLEO does not measure time evolution, their measurement is sensitive to mixing and to DCSD as well as to possible interference between the two mechanisms.

In Table 5, we summarize the status of the DCSD measurements. Since there is no Pauli interference for DCSD in D^+ decays, the ratio of a DCSD decay to

a Cabbibo-favored decay, which has destructive interference, is expected to be greater than $\tan^4\theta_c$. The rate for DCSD in D^0 decay is somewhat greater than was expected from $SU(3)$ breaking. However, the errors are still too large to draw any firm conclusions.

4.3 *Amplitude Analyses of Hadronic Charm Decays*

Dalitz plot analyses of nonleptonic decays have become an important source of information on the dynamics of charm hadron decay. Resonant substructure analyses of three-body and four-body final states of D mesons, which correctly take into account interference effects, allow for meaningful comparisons of experimental data and theoretical models.

For example, Figure 10 shows the $K^{\mp}K^{\pm}\pi^{\pm}$ invariant mass distribution and Dalitz plots for the D^+ and D_s mass region from experiment E687 (58). One notes that the $\overline{K^*}$ and ϕ bands dominate both decays. A Dalitz plot analysis shows that these modes are saturated by quasi two-body processes: $\phi\pi^+$ and $\overline{K^{*0}}(892)K^+$ for D_s^+; and $\phi\pi^+$, $\overline{K^{*0}}(892)K^+$, and $\overline{K^{*0}}(1430)K^+$ for D^+. Amplitude analyses have also been performed for several $D \to K\pi\pi$ and $D \to K\pi\pi\pi$ modes. These analyses support the hypothesis that all D and D_s nonleptonic decays are dominated by two-body modes. The one exception is the decay mode $D^+ \to K^-\pi^+\pi^+$, which cannot be fitted without including a large nonresonant three-body component (59).

It is important to study the decay $D_s \to \pi^-\pi^+\pi^+$, which is observed with a branching fraction of $0.31 \pm 0.06\%$ [the charm meson branching fractions are calculated using the procedure described by Browder & Honscheid (8) with the average branching fractions taken from Montanet et al (14)], in order to determine the importance of the W-annihilation diagram. In this decay mode, none of the initial quarks is present in the final state and the decay is Cabibbo-favored. However, a Dalitz plot analysis is crucial, as the presence of resonant submodes that contain a meson with $s\bar{s}$ quark content, such as $D_s^+ \to f_0(980)\pi^+$ [the $q\bar{q}$ assignment of the f mesons is still controversial; see e.g. (60)], occur through a spectator process rather than through W-annihilation.

Table 5 Measured decay ratios of double Cabibbo-suppressed to Cabibbo-favored D decays

Decay modes	Ratio
$\Gamma(D^+ \to K^+\pi^+\pi^-)/\Gamma(D^+ \to K^-\pi^+\pi^+)$	$0.0072 \pm 0.0023 \pm 0.0017$
$\Gamma(D^0 \to K^+\pi^-)/\Gamma(D^0 \to K^-\pi^+)$	$0.0077 \pm 0.0025 \pm 0.0025$
$\Gamma(D^0 \to K^+\pi^+\pi^-\pi^-)/\Gamma(D^0 \to K^-\pi^+\pi^+\pi^-)$	≤ 0.018 (C.L. = 90%)

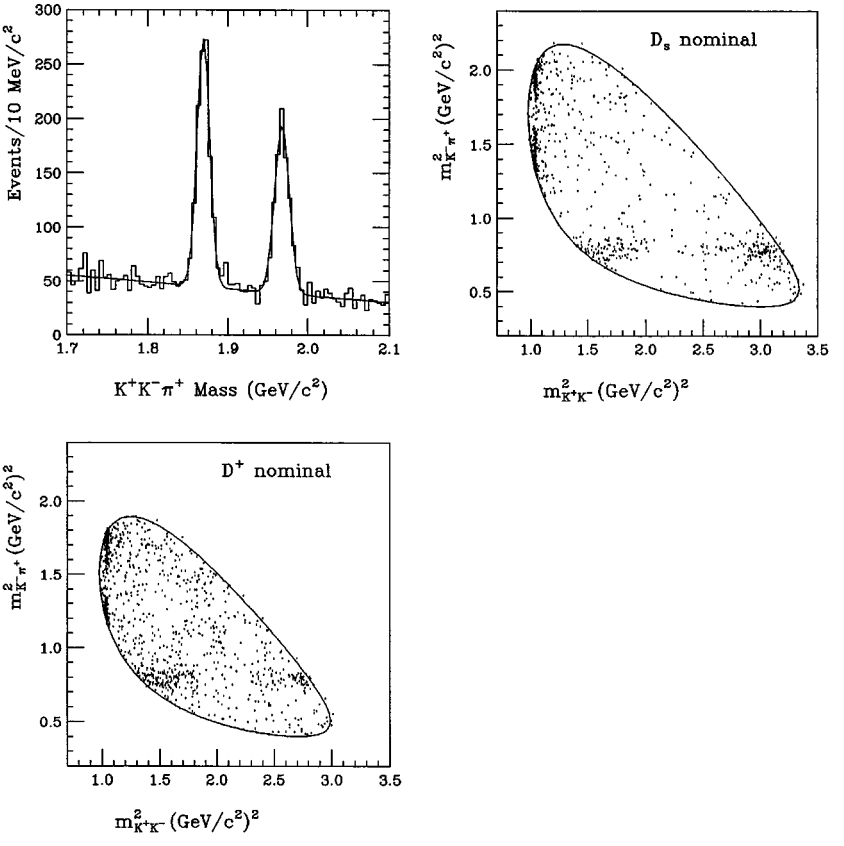

Figure 10 The $K^{\pm}K^{\mp}\pi^{\pm}$ invariant mass distribution and Dalitz plots in the D^+ and D_s mass regions (58).

Preliminary results from the E687 experiment on this decay have been presented recently (61). Their Dalitz plot analysis is appreciably different from the previously accepted scenario (14). No significant nonresonant $D_s^+ \to 3\pi$ is observed. Two new decay modes ($D_s^+ \to f_2(1270)\pi^+$ and $D_s^+ \to f_0(1300)\pi^+$) have been found. The presence of a sizeable $D_s^+ \to f_0(980)\pi^+$ component has been confirmed. The absence of the $D_s^+ \to \rho^0\pi^+$ mode is also confirmed with higher statistics. We note that all the resonant submodes observed in the $D_s^+ \to \pi^+\pi^-\pi^+$ decay have a meson with $s\bar{s}$ quark content and, thus, can be attributed to the spectator process.

The observation of a nonresonant contribution might be interpreted as evidence for W-annihilation; however, it is experimentally difficult to distinguish

this possibility from a coherent sum of wide resonances that could easily mimic a flat distribution. The observation of the decay mode $D_s^+ \to \rho^0\pi^+$ would be a clear indication of the presence of the W-annihilation mechanism. However, the absence of the $D_s^+ \to \rho^0\pi^+$ channel may have other explanations and does not preclude a significant contribution from the annihilation diagram. A sizeable branching fraction for the decay mode $D_s^+ \to \omega(980)\pi^+$ would be a strong signature for the existence of the W-annihilation diagram (62). E691 finds $D_s^+ \to \omega(980)\pi^+/D_s^+ \to \phi\pi^+ < 0.5$ (63), which is not restrictive enough to rule out this possibility. More data, therefore, are necessary to demonstrate the presence of non–spectator contributions in charm meson decay.

4.4 *Hadronic Decays of Charmed Baryons*

In the baryon sector, only charm baryons with one c-quark have been observed. Impressive progress in the study of charm baryons has been made in the last few years. The existence of the Ω_c has been established (64). Experimental sensitivity has progressed to the level that Cabibbo-suppressed decay modes of Λ_c have been observed (65, 66).

The study of charm baryons gives information complementary to that gained from the study of the charm mesons. Due to the presence of a diquark, the exchange diagram is no longer helicity-suppressed. Predictions for decay rates of charm baryons into two-body final states are now available (67).

To date, the decays $\Lambda_c^+ \to \Lambda(n\pi)^+$, $\Sigma^0(n\pi)^+$, $\Sigma^-(n\pi)^+$, $\Sigma^+(n\pi)^0$, $pK^-(n\pi)^+$, and $pK_s(n\pi)^0$ with $n \leq 3$ and including up to 1 π^0 have been reconstructed. Recently, some decay modes of Λ_c with an η meson in the final states have been observed (68); these decays are expected to proceed entirely through nonfactorizable internal W-emission and W-exchange diagrams.

The observation of certain decay modes such as $\Lambda_c^+ \to \Xi^{\star 0}K^+$ (69) or $\Lambda_c^+ \to \Sigma^+\phi$ (70) provides strong evidence for the importance of W-exchange in charm baryon decays. The simplest way, in fact, for these decays to proceed is through the W-exchange diagram, although it is hard to completely rule out contributions from FSI. Table 6 gives branching fractions for this class of Λ_c

Table 6 Decay modes of Λ_c which can occur through the W-exchange diagram

Decay mode	Branching fraction (%) (14)
$\Lambda_c \to \Delta^{++}K^-$	0.7 ± 0.4
$\Lambda_c \to \Sigma^+\phi$	0.30 ± 0.13
$\Lambda_c \to \Xi^0 K^+$	0.34 ± 0.09
$\Lambda_c \to \Xi^{*0}K^+$	0.23 ± 0.09

decay modes. Evidence for color-suppressed decay modes such as $\Lambda_c \to p\phi$ has also been found by CLEO (65).

5. INCLUSIVE *B* DECAY

5.1 *Motivation*

Because of the large mass of the *b* quark, *B* meson decays give rise to a large number of secondary decay products. For instance, CLEO finds that the charged and photon multiplicities at the $\Upsilon(4S)$ are $n_{\text{charged}} = 10.99 \pm 0.06 \pm 0.29$ and $n_\gamma = 10.00 \pm 0.53 \pm 0.50$, respectively (71, 72). The high multiplicity of final-state particles leads to a large number of possible exclusive final states. Even with a detector that has a large acceptance for both charged tracks and photons, it is difficult to reconstruct many exclusive final states because of combinatorial backgrounds. Furthermore, the detection efficiency drops for high-multiplicity final states. Thus, to get a complete picture of *B* meson decay, it is important to study inclusive decay rates.

A number of theoretical calculations of inclusive *B* decay rates have been made using the parton model. It is believed that measurements of such inclusive rates can be more reliably compared to the theoretical calculations than can measurements of exclusive decays While this is sufficient motivation for studying the inclusive rates, there is also a need for accurate measurements in order to model the decays of *B* mesons, both for high-energy collider experiments and for experiments at the $\Upsilon(4S)$. As a specific example, the inclusive rate for $B \to \psi$ has been used to determine the *B* meson production cross section at the Tevatron (73).

The branching ratios for inclusive *B* decays to particular final-state particles are determined by measuring the inclusive yields of these particles in data taken on the $\Upsilon(4S)$ resonance and subtracting the nonresonant background using data taken at energies below the $\Upsilon(4S)$ resonance. The off-resonance data are scaled to correct for the energy dependence of the continuum cross section. Results on inclusive production at the $\Upsilon(4S)$ are usually presented as a function of the variable x, which is the fraction of the maximum possible momentum carried by the particle $p_{\max} = \sqrt{E^2_{\text{beam}} - M^2}$. The endpoint for production in *B* decays is at $x = 0.5$.

The results reported by the different experiments have been rescaled to accommodate the new charm branching fraction. The world averages for inclusive $B \to$ meson decays are given (see Table 8).

5.2 *Inclusive B Decay to Mesons*

CLEO 1.5 (74) has measured the branching fractions of inclusive *B* decays to light mesons, while ARGUS (75) has determined the average multiplicities of

Table 7 Multiplicities and branching fractions of light mesons in B meson decay

Mode	CLEO 1.5 (74) (Branching ratio)	ARGUS (75) (Multiplicity)
$B/\bar{B} \to \pi^{\pm}$ (not from K_s, Λ)		$3.59 \pm 0.03 \pm 0.07$
$B/\bar{B} \to \pi^{\pm}$ (incl. K_s, Λ)		$4.11 \pm 0.03 \pm 0.08$
$B/\bar{B} \to K^{\pm}$	$0.85 \pm 0.07 \pm 0.09$	$0.78 \pm 0.02 \pm 0.03$
$\bar{B} \to K^{-}$	$0.66 \pm 0.05 \pm 0.07$	
$\bar{B} \to K^{+}$	$0.19 \pm 0.05 \pm 0.02$	
$B/\bar{B} \to K^0/\bar{K}^0$	$0.63 \pm 0.06 \pm 0.06$	$0.64 \pm 0.01 \pm 0.04$
$B/\bar{B} \to K^{*0}$		$0.146 \pm 0.016 \pm 0.020$
$B/\bar{B} \to K^{*+}$		$0.182 \pm 0.054 \pm 0.024$
$B/\bar{B} \to \rho^0$		$0.209 \pm 0.042 \pm 0.033$
$B/\bar{B} \to \omega$		< 0.41 (90% C.L.)
$B/\bar{B} \to f_0(975)$		< 0.025 (90% C.L.)
$B/\bar{B} \to \eta$	$0.176 \pm 0.011 \pm 0.0124$ (CLEO II)	
$B/\bar{B} \to \eta'$		< 0.15 (90% C.L.)
$B/\bar{B} \to \phi$	$0.023 \pm 0.006 \pm 0.005$	$0.039 \pm 0.003 \pm 0.004$

light mesons in B decay. If more than one meson of the particle type under study is produced in a $B\bar{B}$ decay, then the branching fraction and the multiplicity will differ. Unless otherwise noted, the results reported in Table 7 are averaged over B and $\bar{B}$ decay.

In the decay $b \to c \to s$, the charge of the kaon can be used to determine the flavor of the b quark. A first attempt to measure the tagging efficiency and misidentification probability for this method was made by ARGUS (75). With the large sample of reconstructed B^0 and B^+ decays from CLEO II, it should be possible to measure these quantities directly. The experiments also measure the momentum spectra for the particles listed in Table 7. These results provide important information needed to improve Monte Carlo generators and to determine tagging efficiencies for future B experiments [the importance of measurements of inclusive B decays for future experiments is discussed at length by Dunietz (76)]. The inclusive production of D^0, D^+, D_s^+, and D^{*+} mesons in B decay has been measured by ARGUS (77) and CLEO 1.5 (78). Preliminary measurements of several of these inclusive branching fractions from CLEO II have also become available (79, 80). To improve signal to background and obtain low systematic errors, only the $D^0 \to K^-\pi^+$, $D^+ \to K^-\pi^+\pi^+$, and $D_s^+ \to \phi\pi^+$ decay modes are used. The results are given in Table 8.

Analyses of the shape of the D_s momentum spectrum (Figure 11) indicates a substantial two-body component. In model-dependent fits, the ARGUS and

Table 8 Branching fractions (%) of inclusive B decays

Particle	ARGUS	CLEO 1.5	CLEO	Average
$\bar{B} \to D^0 X$	$51.6 \pm 4.0 \pm 6.6 \pm 2.1$	$61.9 \pm 3.4 \pm 3.7 \pm 2.5$	$67.1 \pm 2.2 \pm 1.5 \pm 2.7$	$64.8 \pm 2.2 \pm 2.6$
$\bar{B} \to D^- X$	$23.5 \pm 3.0 \pm 4.5 \pm 1.8$	$25.5 \pm 3.4 \pm 2.0 \pm 2.0$	$24.0 \pm 1.2 \pm 0.8 \pm 1.9$	$24.2 \pm 1.3 \pm 1.9$
$\bar{B} \to D^{*-} X$	$27.7 \pm 2.3 \pm 4.7 \pm 1.1$	$23.6 \pm 1.3 \pm 2.3 \pm 0.9$	$25.3 \pm 1.7 \pm 1.0 \pm 1.0$	$24.9 \pm 1.5 \pm 1.0$
$\bar{B} \to D^{*0} X$			$28.1 \pm 1.5 \pm 1.9 \pm 1.1$	$28.1 \pm 2.4 \pm 1.1$
$\bar{B} \to D_s^- X$	$8.1 \pm 1.1 \pm 0.9 \pm 2.0$	$8.5 \pm 1.3 \pm 2.1$	$11.8 \pm 0.4 \pm 0.9 \pm 2.9$	$10.1 \pm 0.7 \pm 2.5$
$\bar{B} \to \phi X$	$3.9 \pm 0.3 \pm 0.4$	$2.3 \pm 0.6 \pm 0.5$	$3.7 \pm 0.1 \pm 0.3$	3.6 ± 0.3
$\bar{B} \to \Psi X$	$1.25 \pm 0.19 \pm 0.26$	$1.31 \pm 0.12 \pm 0.27$	$1.12 \pm 0.04 \pm 0.06$	1.14 ± 0.07
$\bar{B} \to \Psi X$(direct)	0.95 ± 0.27		0.81 ± 0.08	0.82 ± 0.08
$\bar{B} \to \Psi' X$	$0.50 \pm 0.18 \pm 0.12$	$0.36 \pm 0.09 \pm 0.13$	$0.34 \pm 0.04 \pm 0.03$	0.35 ± 0.05
$\bar{B} \to \chi_{c1} X$	$1.23 \pm 0.41 \pm 0.29$		$0.40 \pm 0.06 \pm 0.04$	0.42 ± 0.07
$\bar{B} \to \chi_{c1} X$ (direct)			0.37 ± 0.07	0.37 ± 0.07
$\bar{B} \to \chi_{c2} X$			$0.25 \pm 0.10 \pm 0.03$	0.25 ± 0.10
$\bar{B} \to \eta_c X$			< 0.90 (90% C.L.)	< 0.90 (90% C.L.)
$\bar{B} \to \bar{p} X$	$8.2 \pm 0.5 \pm 1.2$	$8.0 \pm 0.5 \pm 0.3$		8.0 ± 0.5
$\bar{B} \to \bar{\Lambda} X$	$4.2 \pm 0.5 \pm 0.6$	$3.8 \pm 0.4 \pm 0.6$		4.0 ± 0.5
$\bar{B} \to \Xi^+ X$	< 0.51 (90% C.L.)	$0.27 \pm 0.05 \pm 0.04$		0.27 ± 0.06
$\bar{B} \to \Lambda_c^- X$	$6.8 \pm 2.7 \pm 1.4 \pm 0.9$	$6.1 \pm 1.1 \pm 0.9 \pm 0.8$		$6.3 \pm 1.3 \pm 0.9$
$\bar{B} \to \Sigma_c^0 \bar{X}$			$0.53 \pm 0.19 \pm 0.16 \pm 0.16$	$0.53 \pm 0.25 \pm 0.07$
$\bar{B} \to \Sigma_c^0 \bar{N}$			< 0.17 (90% C.L.)	< 0.17 (90% C.L.)
$\bar{B} \to \Sigma_c^{++} \bar{X}$			$0.50 \pm 0.18 \pm 0.15 \pm 0.15$	$0.50 \pm 0.23 \pm 0.07$
$\bar{B} \to \Sigma_c^{++} \bar{\Delta}^{--}$			< 0.12 (90% C.L.)	< 0.12 (90% C.L.)
$\bar{B} \to \Xi_c^+ X$			1.5 ± 0.7	1.5 ± 0.7
$\bar{B} \to \Xi_c^0 X$			2.4 ± 1.3	2.4 ± 1.3

CLEO 1.5 experiments find two-body fractions of $(58 \pm 7 \pm 9)\%$ (77) and $(56 \pm 10)\%$ (78), respectively. CLEO II finds a somewhat smaller two-body fraction, $45.7 \pm 1.9 \pm 3.7 \pm 0.6\%$; here, the last error accounts for the uncertainty due to model-dependence in the predictions for the rates of two-body modes (79). This result does not include additional uncertainty from the $D_s^+ \to \phi\pi^+$ branching fraction. Averaging the results from the three experiments, we find a two-body component of $(48.3 \pm 3.6)\%$, which leads to $\mathcal{B}[B \to D_s X \text{ (two body)}] = (4.9 \pm 1.3)\%$. It is important to determine what mechanisms are responsible for the production of the remainder, the lower momentum D_s mesons. Two possibilities are external W^- emission with $W^- \to \bar{c}s$ or $W^- \to \bar{u}d$ with $s\bar{s}$ quark popping. A limit on the latter possibility ($< 31\%$ of D_s mesons are produced by this mechanism) is obtained from the absence of wrong-sign $D_s^+ - \ell^+$ correlations.

Results on inclusive B decay to final states with ψ and ψ' mesons have been reported by CLEO 1.5, ARGUS, and CLEO II (81) and are given in Table 8. In the most recent high-statistics analysis from CLEO II, the effect of final-state radiation has been taken into account. The resulting invariant dielectron and dimuon mass distributions are shown in Figure 12. The theoretical predictions for the production of charmonium states in B decay (82, 83, 93) are discussed in Section 7.6.4.

The momentum spectrum for $B \to \psi, \psi'$ transitions has been measured (Figure 13). The two-body component due to $B \to \psi K$ and $B \to \psi K^*$ saturates the spectrum in the momentum range between 1.4 and 2.0 GeV. By subtracting the contributions from ψ's originating in ψ' and χ_c decays, CLEO and ARGUS measured the momentum distribution of the direct component shown in Figure 13*b*. The average branching ratio for direct ψ production is found to be $\mathcal{B}(B \to \psi)$, where ψ not from $\psi' = (0.82 \pm 0.08)\%$. The two-body component constitutes about 1/3 of direct ψ production. The composition of the remainder is not yet determined.

Results on inclusive $B \to \chi_c X$, $\chi_c \to \gamma\psi$ decays have been reported by ARGUS (85) and CLEO II (81, 86). ARGUS assumes there is no χ_{c2} production. CLEO II has significantly better χ_c mass resolution than ARGUS and allows for both possibilities. The branching ratio for $\chi_{c0} \to \gamma\psi$ is $(6.6 \pm 1.8) \times 10^{-3}$, so the contribution of the χ_{c0} meson to the $\psi\gamma$ final-state can be neglected. CLEO finds evidence at the 2.5 standard deviation level for a $B \to \chi_{c2}$ contribution, which would indicate either nonfactorizable contributions or higher order processes $O(\alpha_s^2)$ in $b \to c\bar{c}s$ (83).

The decay of B mesons to the lightest charmonium state, the η_c, has not yet been observed. A recent CLEO II search placed an upper limit of 0.9% on the process $B \to \eta_c X$ at the 90% confidence level (82).

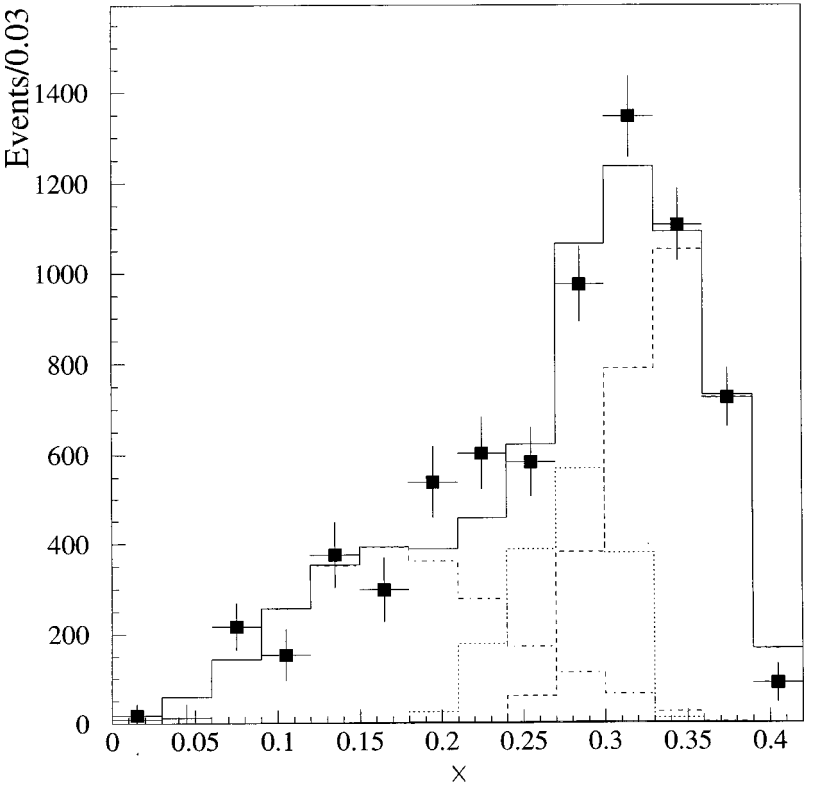

Figure 11 $B \to D_s X$ momentum spectrum in CLEO II data. (*solid histogram*) The sum of the two components; (*dotted histograms*) the two-body components from $\bar{B} \to D^{(*)} D_s^{(*)-}$ and $\bar{B} \to D^{(**)} D_s^{(*)-}$; and (*dash-dotted histogram*) the contribution of the three-body process.

By using the results in Table 8, it is possible to isolate the component of $B \to \psi$ production, which is due to production of higher charmonium states in B decay and the direct component. Similarly, the direct $B \to \chi_{c1}$ component can be determined by removing the contribution from $B \to \psi'$, $\psi' \to \chi_{c1}\gamma$. It is assumed that all ψ' mesons are directly produced.

5.3 *Inclusive B Decay to Baryons*

ARGUS (87) and CLEO 1.5 (88) have observed inclusive production of $\bar{p}$, Λ, Ξ, and the charmed Λ_c^+ baryon. Recently, CLEO II has reported the observation of $B \to \Sigma_c X$ (89), $B \to \Xi_c^0 X$, and $B \to \Xi_c^+ X$ (90). The measured branching ratios for these decays and the world averages can be found in Table 8.

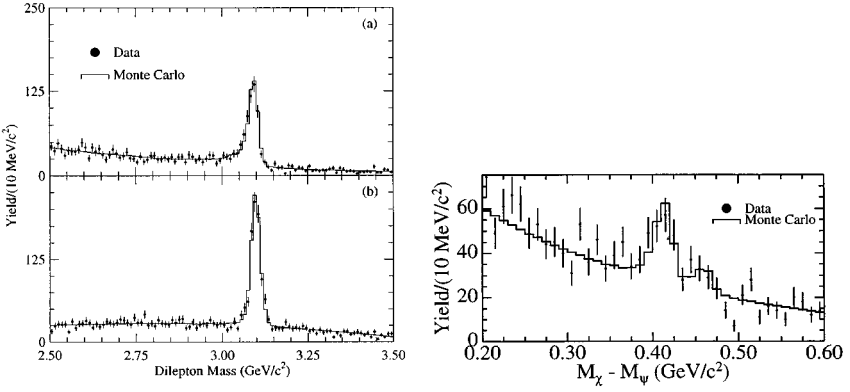

Figure 12 Invariant mass spectra for $B \to \psi$ decays from CLEO II: (*a*) $\psi \to e^+e^-$ and (*b*) $\psi \to \mu^+\mu^-$. (*c*) $\psi\gamma - \psi$ mass difference showing the χ_{c1} and χ_{c2} signals.

The momentum spectrum of $B \to \Lambda_c$ transitions has been measured by CLEO (89). The spectrum is rather soft, indicating Ξ_c production or the presence of a significant multibody component. Similarly, CLEO II has found that $B \to \Sigma_c^0 X$ and $B \to \Sigma_c^{++} X$ decays have no two-body contribution.

In addition to the inclusive branching ratios given above, the experimental data have been used in attempts to disentangle which of the baryon production mechanisms shown in Figure 14 dominates. CLEO 1.5 (88) and ARGUS (87) have investigated baryon correlations in B decay in order to elucidate the underlying decay process. We follow the notation of Crawford et al (88). Let N

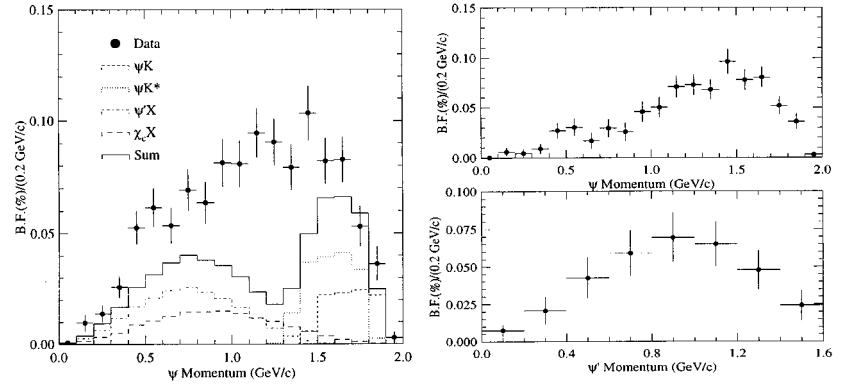

Figure 13 ψ and ψ' momentum spectra (CLEO II) from B decay. (*a*) Inclusive $B \to \psi X$ production with contributions from individual decay channels overlaid. (*b*) Direct $B \to \psi X$ production. (*c*) $B \to \psi' X$.

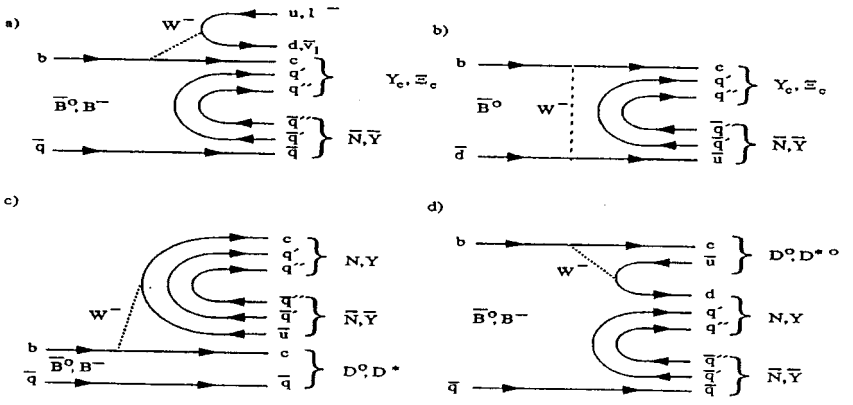

Figure 14 Decay diagrams for B meson decays to baryons: (*a*) external spectator diagram; (*b*) W exchange diagram; (*c*) external spectator diagram that produces $DN\bar{N}X$ and $DY\bar{Y}X$ final states; and (*d*) internal spectator diagram that produces $DN\bar{N}X$ and $DY\bar{Y}X$ final states.

denote baryons with $S = C = 0$ (e.g. p, n, Δ, N^*). Let Y refer to baryons with $S = -1, C = 0$ (e.g. Λ, Σ^0, Σ^+). Let Y_c refer to baryons with $S = 0, C = 1$ [e.g. Λ_c^+, $\Sigma_c^{(+,0,++)}$]. Then, the following final states can be used to distinguish possible mechanisms for baryon production in B decay (Figure 14).

1. $\bar{B} \to Y_c\bar{N}X$, $\bar{B} \to \Xi_c\bar{Y}X$ These final states are produced by the usual $b \to cW^-$ coupling in a spectator or exchange diagram in conjunction with the popping of two quark pairs from the vacuum (as shown in Figures 14*a* and *b*). It should be noted that the two mechanisms can be distinguished by examination of the Y_c momentum spectrum, since the exchange diagram will produce two-body final states (e.g. $\Lambda_c\bar{p}$ or $\Sigma_c^{++}\bar{\Delta}^{--}$).

2. $\bar{B} \to DN\bar{N}X$, $\bar{B} \to DY\bar{Y}X$ The non–charm baryon-antibaryon pair is produced from W fragmentation after hadronization with two quark-antiquark pairs popped from the vacuum (as shown in Figures 14*c* and *d*). The D meson is formed from the charm spectator quark system. If this mechanism is significant, inclusive production of charmless baryon-antibaryon pairs should be observed in B decay.

3. $\bar{B} \to Y_c\bar{Y}X$, $\bar{B} \to \Xi_c\bar{Y}_cX$ These states are produced by the internal spectator graph with $W^- \to \bar{c}s$ in conjunction with the popping of two quark-antiquark pairs.

4. $\bar{B} \to D_s^- Y_c \bar{N} X$, $\bar{B} \to D_s^- \Xi_c \bar{Y} X$ This is the same as Mechanism 1 with $W^- \to \bar{c}s$. Since the minimum mass of the final-state system is 5.2 GeV, this mechanism is highly suppressed by phase space.

The low rates for $B \to \Lambda \bar{\Lambda} X$, $\Lambda \bar{p} X$, and $D^* p \bar{p} X$ suggest that Mechanism 2 is small. The absence of a two-body component in the momentum spectra of $B \to \Lambda_c X$, $\Sigma_c X$ indicates that the W-exchange mechanism is small. Thus, it was thought reasonable to assume that $\bar{B} \to Y_c \bar{N} X$ with an external spectator $b \to cW^-$ coupling (Figure 14*a*) is the principal mechanism in B to baryon transitions (87).

If B decays to baryons are dominated by $\bar{B} \to \Lambda_c \bar{p} X$ and $\bar{B} \to \Lambda_c \bar{n} X$, then measurements of the branching fractions for $B \to \bar{p} X$, $B \to p \bar{p} X$ can be used to extract the absolute $\Lambda_c^+ \to pK^-\pi^+$ branching fraction. The CLEO 1.5 measurements give $B(\Lambda_c \to pK^-\pi^+) = 4.3 \pm 1.0 \pm 0.8\%$, which can be used to normalize all other measured Λ_c^+ branching fractions. In a similar fashion, ARGUS finds $(4.1 \pm 2.4)\%$ for this branching fraction.

An alternate explanation for the absence of a two-body component in B decays to baryons was recently proposed by Dunietz et al (91). These authors suggested that the primary mechanism in such decays is the internal W-emission process $b \to c\bar{c}s$. This might lead to two-body final states such as $\bar{B} \to \bar{\Lambda}_c \Xi_c$, which would account for the softness of the Λ_c^+ momentum spectrum. CLEO has searched for the mechanism suggested by Dunietz et al in a variety of ways. By examining Λ_c-lepton correlations, it is possible to constrain the size of the $b \to c\bar{c}s$ component in $B \to$ baryon decays. The $b \to c\bar{c}s$ component gives rise to opposite-sign $\Lambda_c^+ \ell^-$ correlations (Figure 15*b*), whereas the internal process W-emission process $b \to cu\bar{d}$ gives same-sign $\Lambda_c^+ \ell^+$ correlations (Figure 15*a*). From the ratio of same-sign to opposite-sign Λ_c-lepton yields, CLEO finds $b \to c\bar{c}s/b \to c\bar{u}d = (20 \pm 12 \pm 4)\%$ for internal W-emission processes. This shows that $b \to c\bar{c}s$, although present at a modest level, is not the dominant mechanism operating in B decays to baryons.

Since the $b \to c\bar{c}s$ mechanism is present, Ξ_c^+ and Ξ_c^0 baryons should be produced in $B \to$baryon transitions. However, Ξ_c^0 baryons can also be produced from $b \to c\bar{u}d$ transitions with $s\bar{s}$ popping. CLEO II has observed signals $B \to \Xi_c^+$ and $B \to \Xi_c^0$. The observed rates are consistent with what is expected from the measurements of Λ_c-lepton correlation and quark popping.

To verify whether the dominant mechanism for baryon production in B decays is the external spectator mechanism with $b \to c\bar{u}d$ as was previously assumed by the CLEO and ARGUS analyses, CLEO II has searched for evidence of $B \to \Lambda_c \bar{N} \ell \nu$. This should give rise to several distinctive experimental signatures: Λ-lepton correlations, Λ_c-lepton correlations, and semi-exclusive

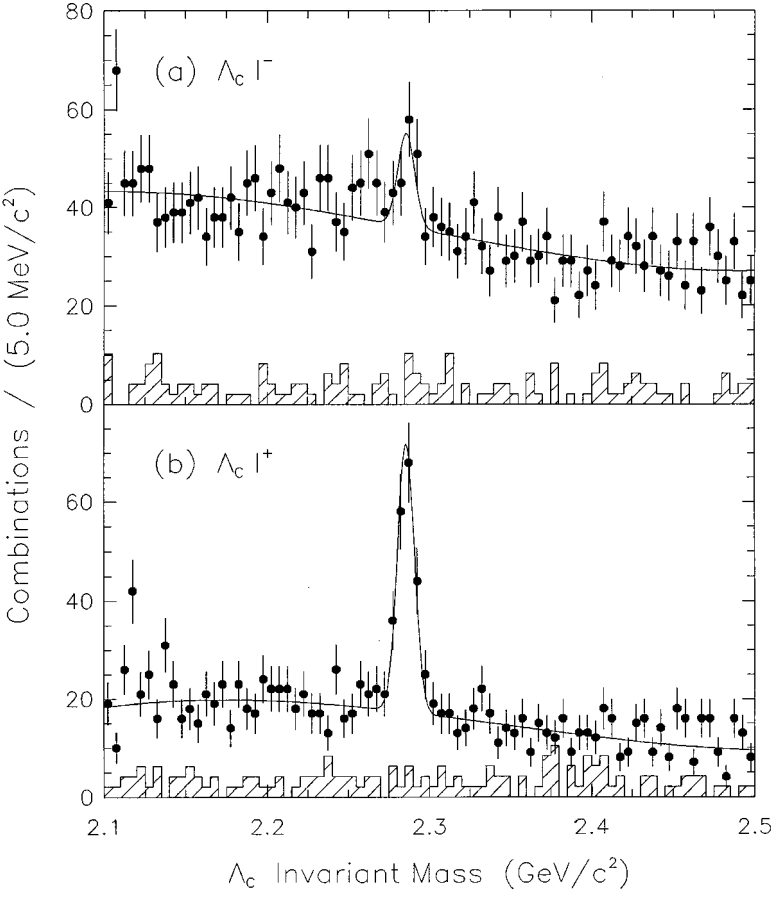

Figure 15 Λ_c-lepton correlation in B decay (CLEO II). (*a*) The $pK^-\pi^+$ invariant mass spectrum for $\Lambda_c^+ - \ell^-$ combinations. (*b*) The $pK^-\pi^+$ invariant mass spectrum for $\Lambda_c^+ - \ell^+$ combinations.

$B \to \Lambda_c^+ \bar{p} \ell^- \nu$ production having a missing mass consistent with a B decay. No significant signals were observed in these correlations (92). This indicates that the conventional and previously accepted picture of baryon production in B decay is incorrect.

A possible explanation of all the existing data requires the simultaneous presence of several production mechanisms. The internal spectator process $b \to c\bar{u}d$ followed by $u\bar{u}$ or $d\bar{d}$ quark popping is dominant. This leads to production of a high-mass excited anti-nucleon in conjunction with a charm baryon and accounts for the soft momentum spectrum of charm baryons produced in

B decay as well as the absence of $B \to \Lambda_c \bar{N} X \ell \nu$. The internal spectator process $b \to c\bar{c}s$ with quark popping as well as the internal spectator process $b \to c\bar{u}d$ with $s\bar{s}$ quark popping are also operative at the 10–20% level. The latter two mechanisms appear to account for the production of Ξ_c baryons in B decay.

5.4 *Charm Production in B Decay*

The measurements of inclusive decay rates can be used to test the parton level expectation that most B decays proceed via a $b \to c$ transition. If we neglect the small contributions from $b \to u$ and penguin transitions, we expect about 1.15 charm quarks to be produced per B decay. The additional 15% is due to the fact that the virtual W forms a $s\bar{c}$ quark pair with a probability of approximately 0.15. To verify this expectation, we use the experimental results listed in Table 8 and determine the charm yield, denoted n_c, to be

$$\begin{aligned} n_c = {} & \mathcal{B}(B \to D^0 X) + \mathcal{B}(B \to D^+ X) + \mathcal{B}(B \to D_s X) \\ & + \mathcal{B}(B \to \Lambda_c X) + \mathcal{B}\left(B \to \Xi_c^+ X\right) + \mathcal{B}\left(B \to \Xi_c^0 X\right) \\ & + 2 \times \mathcal{B}(B \to \psi X) + 2 \times \mathcal{B}(B \to \psi' X) + 2 \times \mathcal{B}(B \to \chi_{c1} X) \\ & + 2 \times \mathcal{B}(B \to \chi_{c2} X) + 2 \times \mathcal{B}(B \to \eta_c X \text{ (incl. other } c\bar{c})) \\ = {} & 1.15 \pm 0.05. \end{aligned}$$

The factor of 2 accounts for the two charm quarks produced in $b \to c\bar{c}s$ transitions. Wherever possible, the branching fractions for direct production are used. The contribution of $B \to \eta_c X$ and other charmonium states is generously taken to be at the CLEO 90% confidence level upper limit for the process $B \to \eta_c X$. This value of n_c is slightly larger than the value reported in the 1995 conferences due to the use of a smaller world average for the absolute branching fraction $\mathcal{B}(D^0 \to K^- \pi^+)$ (81).

Another interesting quantity is the fraction of B decays in which two charm quarks are produced, which is naively expected to be about 15%. This expectation can be compared to the sum of the experimental measurements

$$\begin{aligned} \mathcal{B}(B \to X_{c\bar{c}}) = {} & \mathcal{B}(B \to D_s X) + \mathcal{B}(B \to \psi X) + \mathcal{B}(B \to \psi' X) \\ & + \mathcal{B}(B \to \chi_{c1} X) + \mathcal{B}(B \to \chi_{c2} X) + \mathcal{B}(B \to \Xi_c X) \\ & + \mathcal{B}(B \to \eta_c X \text{ (incl. other } \bar{c})) \\ = {} & (15.8 \pm 2.8)\%, \end{aligned}$$

where the direct $B \to \psi$ and $B \to \chi_{c1}$ branching fraction have been used. The contribution from $B \to \Xi_c^0 X$ is reduced by 1/3 to take into account the fraction that is produced not by the $b \to c\bar{c}s$ subprocess but by $b \to c\bar{u}d + s\bar{s}$ quark popping. The measured value of $\mathcal{B}(B \to X_{c\bar{c}})$ is far below 30%.

The possibility of an additional contribution from $B \to D\bar{D}KX$ decays to the hadronic B width was suggested by Buchalla et al (95). These decays proceed via the quark level process $b \to \bar{c}cs$ with light quark popping at the upper $\bar{c}s$ vertex. Such decays give wrong-sign D-lepton correlations from the $\bar{D}$ mesons that hadronize, from the virtual W.

Note that such decays would increase the calculated $\mathcal{B}(b \to c\bar{c}s)$ but do not modify the determinations of n_c (the number of charm quarks produced per B decay).

Preliminary evidence for the presence of this decay mechanism has been presented by CLEO from the observation of $D - \ell^-$ correlation in $B\bar{B}$ events. An energetic lepton above 1.4 GeV is chosen in the same hemisphere as the D meson in order to tag the flavor of the other $\bar{B}$ meson. After subtracting backgrounds from mixing and lepton misidentification, $\Gamma(B \to DX)/\Gamma(B \to \bar{D}X) = 0.107 \pm 0.029 \pm 0.018$, which gives $\mathcal{B}(B \to DX) = 8.1 \pm 2.6\%$ for the branching fraction of the new mechanism. Attempts to reconstruct exclusive modes such as $B \to D\bar{D}K(^*)X$ are in progress (93).

With the addition of recent experimental results, the understanding of baryon production in B decay is improving. In contrast to meson production in B decay, $B \to$ baryon transitions proceed predominantly through the internal W-emission process $b \to c\bar{u}d$ followed by light quark pair popping. In a parton level calculation with diquark correlation taken into account, Palmer & Stech (94) have performed a calculation of the total rate for inclusive B decay to charm baryons. They find $\mathcal{B}(B \to \text{charm baryons}) \approx 6\%$. In order to compare this prediction with experimental data, we assume most B to charm baryon decays proceed through a Λ_c baryon but correct for the small fraction of Ξ_c baryons produced by $b \to c\bar{u}d$ transitions combined with $s\bar{s}$-popping. This gives

$$\begin{aligned}\mathcal{B}(B \to \text{charmed baryons}) &= \mathcal{B}(B \to \Lambda_c X) + 1/3 \times \mathcal{B}(B \to \Xi_c^0) \\ &= (7.1 \pm 1.6)\%.\end{aligned}$$

The experimental result for the charm yield per B decay is consistent with the naive expectation that 1.15 charm quarks are produced per b decay. However, it is not consistent with a number of proposals that suggest that 1.3 charm quarks should be produced per b decay. Such a high charm yield is required

by recent theoretical efforts that explain the discrepancy between theoretical calculations and experimental measurements of the inclusive semileptonic rate by an enhancement of the $b \to c\bar{c}s$ mechanism (see Section 7.8 for a more detailed discussion).

6. EXCLUSIVE HADRONIC *B* DECAY

The experimental branching ratios for B meson decay to exclusive final states containing D mesons are given in Tables 9 and 10.

Table 9 World average B^- branching fractions

Mode	Branching fraction (%)
$B^- \to D^0\pi^-$	$0.50 \pm 0.05 \pm 0.02$
$B^- \to D^0\rho^-$	$1.37 \pm 0.18 \pm 0.05$
$B^- \to D^0\pi^+\pi^-\pi^-$	$1.28 \pm 0.35 \pm 0.05$
$B^- \to D^{*0}\pi^-$	$0.52 \pm 0.08 \pm 0.02$
$B^- \to D^{*0}\rho^-$	$1.51 \pm 0.30 \pm 0.06$
$B^- \to D_J^{(*)0}\pi^-$	$0.13 \pm 0.05 \pm 0.01$
$B^- \to D^{*+}\pi^-\pi^-\pi^0$	$1.69 \pm 0.76 \pm 0.01$
$B^- \to D_J^{(*)0}\rho^-$	$0.33 \pm 0.21 \pm 0.01$
$B^- \to D^{*0}\pi^-\pi^-\pi^+$	$0.95 \pm 0.27 \pm 0.04$
$B^- \to D^{*0}a_1^-$	$1.89 \pm 0.53 \pm 0.08$
$B^- \to D^+\pi^-\pi^-$	< 0.14 (90% C.L.)
$B^- \to D^{*+}\pi^-\pi^-$	$0.20 \pm 0.07 \pm 0.01$
$B^- \to D^{**0}(2420)\pi^-$	$0.16 \pm 0.05 \pm 0.01$
$B^- \to D^{**0}(2420)\rho^-$	< 0.14 (90% C.L.)
$B^- \to D^{**0}(2460)\pi^-$	< 0.13 (90% C.L.)
$B^- \to D^{**0}(2460)\rho^-$	< 0.47 (90% C.L.)
$B^- \to D^0 D_s^-$	$1.36 \pm 0.28 \pm 0.33$
$B^- \to D^0 D_s^{*-}$	$0.94 \pm 0.31 \pm 0.23$
$B^- \to D^{*0} D_s^-$	$1.18 \pm 0.36 \pm 0.29$
$B^- \to D^{*0} D_s^{*-}$	$2.70 \pm 0.81 \pm 0.66$
$B^- \to \psi K^-$	0.102 ± 0.014
$B^- \to \psi' K^-$	0.070 ± 0.024
$B^- \to \psi K^{*-}$	0.174 ± 0.047
$B^- \to \psi' K^{*-}$	< 0.30 (90% C.L.)
$B^- \to \psi K^-\pi^+\pi^-$	0.140 ± 0.077
$B^- \to \psi' K^-\pi^+\pi^-$	0.207 ± 0.127
$B^- \to \chi_{c1} K^-$	0.104 ± 0.040
$B^- \to \chi_{c1} K^{*-}$	< 0.21 (90% C.L.)
$B^- \to \psi\pi^-$	0.0057 ± 0.0026
$B^- \to \psi\rho^-$	< 0.077 (90% C.L.)
$B^- \to \psi a_1^-$	< 0.120 (90% C.L.)

Table 10 World average $\bar{B}^0$ branching fractions

Mode	Branching fraction (%)
$\bar{B}^0 \to D^+\pi^-$	$0.31 \pm 0.04 \pm 0.02$
$\bar{B}^0 \to D^+\rho^-$	$0.84 \pm 0.16 \pm 0.07$
$\bar{B}^0 \to D^+\pi^-\pi^-\pi^+$	$0.83 \pm 0.24 \pm 0.07$
$\bar{B}^0 \to D^{*+}\pi^-$	$0.28 \pm 0.04 \pm 0.01$
$\bar{B}^0 \to D^{*+}\rho^-$	$0.73 \pm 0.15 \pm 0.03$
$\bar{B}^0 \to D^{*+}\pi^-\pi^-\pi^+$	$0.80 \pm 0.14 \pm 0.03$
$\bar{B}^0 \to D^{*+}a_1^-$	$1.27 \pm 0.30 \pm 0.05$
$\bar{B}^0 \to D^0\pi^+\pi^-$	< 0.17 (90% C.L.)
$\bar{B}^0 \to D^{**+}(2460)\pi^-$	< 0.22 (90% C.L.)
$\bar{B}^0 \to D^{**+}(2460)\rho^-$	< 0.49 (90% C.L.)
$\bar{B}^0 \to D^+D_s^-$	$0.74 \pm 0.22 \pm 0.18$
$\bar{B}^0 \to D^+D_s^{*-}$	$1.14 \pm 0.42 \pm 0.28$
$\bar{B}^0 \to D^{*+}D_s^-$	$0.94 \pm 0.24 \pm 0.23$
$\bar{B}^0 \to D^{*+}D_s^{*-}$	$2.00 \pm 0.54 \pm 0.49$
$\bar{B}^0 \to \psi K^0$	0.075 ± 0.021
$\bar{B}^0 \to \psi' K^0$	< 0.08 (90% C.L.)
$\bar{B}^0 \to \psi \bar{K}^{*0}$	0.153 ± 0.028
$\bar{B}^0 \to \psi' \bar{K}^{*0}$	0.151 ± 0.091
$\bar{B}^0 \to \psi K^-\pi^+$	0.117 ± 0.058
$\bar{B}^0 \to \psi' K^-\pi^+$	< 0.11 (90% C.L.)
$\bar{B}^0 \to \chi_{c1} K^0$	< 0.27 (90% C.L.)
$\bar{B}^0 \to \chi_{c1} \bar{K}^{*0}$	< 0.21 (90% C.L.)
$\bar{B}^0 \to \psi\pi^0$	< 0.006 (90% C.L.)
$\bar{B}^0 \to \psi\rho^0$	< 0.025 (90% C.L.)
$\bar{B}^0 \to \psi\omega^0$	< 0.027 (90% C.L.)

6.1 *Measurements of $D(n\pi)^-$ Final States*

To date, final states containing a D meson and one or two pions have been observed. To select $\bar{B} \to D\rho^-$ candidates, additional requirements are imposed on the $\pi^-\pi^0$ invariant mass and the ρ helicity angle in $\bar{B} \to D\pi^-\pi^0$ decays. By fitting the $\pi^-\pi^0$ mass spectrum and the helicity angle distribution, CLEO II finds that at least 97.5% of the $B \to D\pi^-\pi^0$ rate in the ρ mass region can be attributed to the decay $B \to D\rho^-$. [Two models are considered: non-resonant $B \to D\pi^-\pi^0$ and $B \to D^{**}(2460)\pi^-$. Both give very similar $\pi^-\pi^0$ mass spectra and comparable limits on the non-rho contamination in the signal region.]

6.2 *Measurements of $D^*(n\pi)^-$ Final States*

Final states containing a D^* meson and one, two, or three pions have also been observed. These include the $B \to D^*\pi^-$, $B \to D^*\rho^-$, and $B \to D^*a_1^-$ decay channels.

The B^- and $\bar{B}^0$ signals in the $D^*\pi$ and $D^*\rho$ decay channels from the CLEO II experiment are shown in Figure 16. It is found that $B \to D^*\pi^-\pi^0$ in the $\pi^-\pi^0$ mass region near the ρ meson is saturated by the decay $B \to D^*\rho^-$ (Figure 17) and a tight upper limit of $< 9\%$ at 90% C.L. is set on a possible nonresonant contribution. [CLEO II considers two models: (*a*) the $\pi^-\pi^0$ system, which is produced nonresonantly following a phase space distribution; or (*b*) the $D^{*+}\pi^-\pi^0$ system, which is produced from the decay $D^{**}\pi^-$. Both give similar limits on the non-ρ fraction.]

The CLEO II data also suggest that the signal in $B \to D^*\pi^-\pi^-\pi^+$ arises predominantly from $B \to D^*a_1^-$. Taking into account the $a_1 \to \pi^-\pi^-\pi^+$ branching fractions, it follows that $\mathcal{B}(B \to D^*a_1^-) = 2 \times \mathcal{B}(B \to D^*\pi^-\pi^-\pi^+)$. A fit to the $\pi^-\pi^-\pi^+$ mass distributions with contributions from $B \to D^{*+}a_1^-$ and a $B \to D^{*+}\pi^-\rho^0$ nonresonant background gives an upper limit of 13% on the nonresonant component in this decay.

The Cabibbo-suppressed decay modes such as $B \to DK$ should also be observed and studied in the near future. These modes, in particular, $B^+ \to D^0K^+$ and $B^+ \to \bar{D}^0K^+$ with $D^0 \to |f_{CP}\rangle$ (where $|f_{CP}\rangle$ denotes a CP

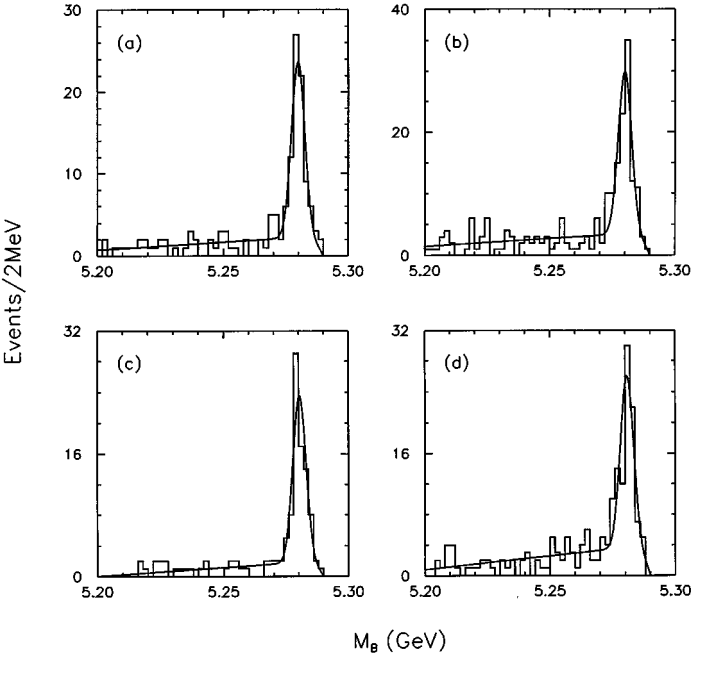

Figure 16 Beam-constrained mass distributions from CLEO II for (*a*) $B^- \to D^{*0}\pi^-$ decays, (*b*) $B^- \to D^{*0}\rho^-$ decays, (*c*) $\bar{B}^0 \to D^{*+}\pi^-$ decays, and (*d*) $\bar{B}^0 \to D^{*+}\rho^-$ decays.

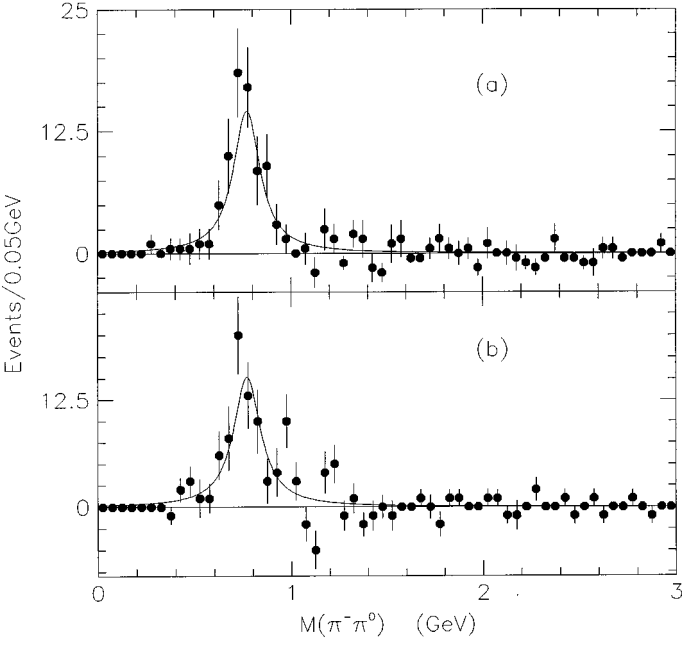

Figure 17 Resonant substructure for $B \to D^* \rho^-$ (CLEO II) for (*a*) the $\pi^0\pi^-$ invariant mass spectrum for $\bar{B}^0 \to D^{*+}\pi^0\pi^-$ and (*b*) the $\pi^0\pi^-$ invariant mass spectrum for $B^- \to D^{*0}\pi^0\pi^-$.

eigenstate), may be used at B factories to constrain one of the three angles of the unitary triangle.

6.3 *Polarization in $B \to D^{*+}\rho^-$ Decays*

By comparing the measured polarization in $\bar{B}^0 \to D^{*+}\rho^-$ with the expectation from the corresponding semileptonic B decay, a test of the factorization hypothesis can be performed (see Section 7.6.2). The polarization is obtained from the distributions of the helicity angles Θ_ρ and Θ_{D^*}. The D^{*+} helicity angle, Θ_{D^*}, is the angle between the D^0 direction in the D^{*+} rest frame and the D^{*+} direction in the rest frame of the B meson. After integration over χ, the angle between the normals to the D^{*+} and the ρ^- decay planes, the helicity angle distribution can be expressed as

$$\frac{d^2\Gamma}{d\cos\Theta_{D^*} d\cos\Theta_\rho} \propto \frac{1}{4}\sin^2\Theta_{D^*}\sin^2\Theta_\rho(|H_{+1}|^2 + |H_{-1}|^2) + \cos^2\Theta_{D^*}\cos^2\Theta_\rho|H_0|^2, \qquad 12.$$

where H_i are the amplitudes for the various possible D^* helicity states. The fraction of longitudinal polarization is defined by

$$\frac{\Gamma_L}{\Gamma} = \frac{|H_0|^2}{|H_{+1}|^2 + |H_{-1}|^2 + |H_0|^2}. \quad 13.$$

If Γ_L is large, both the D^{*+} and the ρ^- helicity angles will follow a $\cos^2\Theta$ distribution, whereas a large transverse polarization, Γ_T, gives a $\sin^2\Theta$ distribution for both helicity angles. An unbinned two-dimensional likelihood fit to the joint $(\cos\Theta_{D^*}, \cos\Theta_\rho)$ distribution gives

$$(\Gamma_L/\Gamma)_{\bar{B^0}\to D^{*+}\rho^-} = 93 \pm 5 \pm 5\%. \quad 14.$$

The same procedure has been applied to a sample of exclusively reconstructed $B^- \to D^{*0}\rho^-$ decays. While $\bar{B^0} \to D^{*+}\rho^-$ is an external spectator decay, $B^- \to D^{*0}\rho^-$ can proceed via both the external and the internal spectator mechanisms. The interference between the two amplitudes can modify the polarization (96). CLEO II finds (97)

$$(\Gamma_L/\Gamma)_{B^-\to D^{*0}\rho^-} = 84.2 \pm 5.1\%. \quad 15.$$

6.4 *Measurements of D^{**} Final States*

In addition to the production of D and D^* mesons, the charm quark and spectator antiquark can hadronize as a D^{**} meson. The $D^{**0}(2460)$ has been observed experimentally and identified as the $J^P = 2^+$ state, while the $D^{**0}(2420)$ has been identified as the 1^+ state. These states have full widths of approximately 20 MeV. Two other states, a 0^+ and another 1^+, are predicted but have not yet been observed, presumably because of their large intrinsic widths. There is evidence for D^{**} production in semileptonic B decays (98), and D^{**} mesons have also been seen in hadronic decays. However, early experiments did not have sufficient data to separate the two narrow D^{**} states and, hence, reported branching ratios only for the combination of the two (see Tables 9 and 10).

In order to search for D^{**} mesons from B decays, the final-states $B^- \to D^{*+}\pi^-\pi^-$ and $B^- \to D^{*+}\pi^-\pi^-\pi^0$ are studied. These decay modes are not expected to occur via a spectator diagram in which the c quark and the spectator antiquark form a D^* rather than a D^{**} meson. The D^{*+} is combined with a π^- to form a D^{**} candidate. CLEO II has also looked for D^{**} production in the channels $B^- \to D^+\pi^-\pi^-$ and $B^0 \to D^0\pi^-\pi^+$. Since $D^{**0}(2420) \to D\pi$ is forbidden, only the $D^{**0}(2460)$ is searched for in the $D\pi\pi$ final state.

CLEO II has reported a significant signal in the $D^{**0}(2420)\pi^-$ mode. ARGUS has also found evidence for $B \to D^{**}(2420)\pi^-$ using a partial reconstruction technique in which they observe a fast and slow pion from the D^{**} decay but do not reconstruct the D^0 meson (101).

Other final states with higher pion multiplicities should be systematically studied in the future.

6.5 *Exclusive Decays to D and D_s Mesons*

Another important class of modes are decays to two charm mesons. As shown in Figure 1*a*, the production of an isolated pair of charm mesons [$D_s^{(*)}$ and $D^{(*)}$] proceeds through a Cabibbo-favored spectator diagram in which the $s\bar{c}$ pair from the virtual W^- hadronizes into a D_s^- or a D_s^{*-} meson and the remaining spectator quark and the c quark form a $D^{(*)}$ meson. These modes have been observed by the CLEO 1.5, ARGUS, and CLEO II (79) experiments. B mesons are reconstructed in eight decay modes: $D_s^- D^+$, $D_s^- D^0$, $D_s^{*-} D^+$, $D_s^{*-} D^0$, $D_s^- D^{*+}$, $D_s^- D^{*0}$, $D_s^{*-} D^{*+}$, and $D_s^{*-} D^{*0}$. The sum of the branching fractions for the exclusive modes, averaged over B^- and $\bar{B}^0$ decays, is $5.50 \pm 0.81\%$. This can be compared to the branching fraction of the two-body component found in the fit to the inclusive D_s momentum spectrum of $4.9 \pm 1.3\%$. The error is dominated by the uncertainty in $\mathcal{B}(D_s \to \phi\pi)$. The remaining contribution to the inclusive production of D_s mesons must be due to the decay modes $B \to D_s^{**} D^{(*)}$, $B \to D_s^{(*)} D^{(*)}(n\pi)$, or $D_s^{(*)} D\pi$.

Partial reconstruction techniques have also been used to improve the size of the signals in $B \to D^{(*)} D_s^{(*)+}$. Larger samples not only reduce the statistical error in the branching ratio measurements, they also allow the polarization in $B \to D^* D_s^{*+}$ decays to be measured. Comparison of the yield in partially reconstructed and fully reconstructed $B \to D^* D_s^{(*)+}$ events gives a model-independent measurement of $\mathcal{B}(D_s \to \phi\pi^+)$, which sets the scale for the D_s branching fractions. Branching fractions and background levels for CP eigenstates such as $\bar{B}^0 \to D^{(*)+} D^{(*)-}$ will also be studied.

Since the internal spectator mechanism cannot contribute to the $B \to D^{(*)} D_s^{(*)}$ decay modes, in the absence of higher order processes, the B^- and $\bar{B}^0$ decay widths will be equal:

$$\frac{\Gamma\left(\bar{B}^0 \to D^{(*)} D_s^{(*)}\right)}{\Gamma\left(B^- \to D^{(*)} D_s^{(*)}\right)} = \frac{\mathcal{B}\left(\bar{B}^0 \to D^{(*)} D_s^{(*)}\right)}{\mathcal{B}\left(B^- \to D^{(*)} D_s^{(*)}\right)} \times \frac{\tau_{B^-}}{\tau_{\bar{B}^0}} = 1.$$

Using the world average for the lifetime ratio, we find

$$\frac{\Gamma\left(\bar{B}^0 \to D^{(*)} D_s^{(*)}\right)}{\Gamma\left(B^- \to D^{(*)} D_s^{(*)}\right)} = 0.78 \pm 0.23,$$

which is consistent with this expectation.

6.6 *Exclusive B Decay to Baryons*

The first exclusive $B \to$baryon decay has been observed by CLEO II (103). A small number of decays were reconstructed in the modes $\bar{B}^0 \to \Lambda_c^+ \bar{p}\pi^+\pi^-$ and

$\bar{B}^0 \to \Lambda_c^+ \bar{p}\pi^-$ corresponding to branching fractions of $0.162^{+0.019}_{-0.016} \pm 0.038 \pm 0.026\%$ and $0.63^{+0.023}_{-0.020} \pm 0.012 \pm 0.010\%$, respectively. In addition, CLEO II has set limits on other higher multiplicity exclusive modes with baryons in the final state.

6.7 *Color-Suppressed B decay*

6.7.1 EXCLUSIVE *B* DECAYS TO CHARMONIUM In B decays to $c\bar{c}$ mesons, the c-quark from the b decay combines with a $\bar{c}$-quark from the virtual W^- decay to form a charmonium state. This process is described by the color-suppressed diagram shown in Figure 1*b*. The branching fractions for these modes are listed in Tables 9 and 10.

The decay modes $\bar{B^0} \to \psi K^0$ and $\bar{B^0} \to \psi' K^0$ are of special interest since the final states are CP eigenstates. These decays are of great importance for the investigation of one of the three CP-violating angles accessible to study in B decays. It is also possible to use the decay $B^0 \to \psi K^{*0}$, $K^{*0} \to K^0\pi^0$, which has a somewhat higher branching ratio, but this final state consists of a mixture of CP eigenstates. It has even CP if the orbital angular momentum is $L = 0$ or $L = 2$ and odd CP if $L = 1$. If both CP states are present, the CP asymmetry will be diluted. A measurement of CP violation in this channel is only possible if one of the CP states dominates, or if a detailed moments analysis is performed (103). Measurements of the polarization in the decay $B^0 \to \psi K^{*0}$ can be used to determine the fractions of the two CP states.

Decay modes of this type have been reconstructed by CLEO 1.5, ARGUS, and CLEO II. The CDF collaboration (105) has also reported signals for $B \to \psi K^{*0}$ and $B \to \psi K^-$ and measurements of polarization in $B \to \psi K^*$ decays (107). Because of the large uncertainties associated with the b-quark production cross section at the Tevatron, the results are given as ratios of branching fractions,

$$\frac{\mathcal{B}(B^0 \to \psi K^0)}{\mathcal{B}(B^+ \to \psi K^+)} = 1.13 \pm 0.22 \pm 0.06\%$$

$$\frac{\mathcal{B}(B^0 \to \psi K^{*0})}{\mathcal{B}(B^+ \to \psi K^+)} = 1.33 \pm 0.27 \pm 0.11\%$$

$$\frac{\mathcal{B}(B^+ \to \psi K^{*+})}{\mathcal{B}(B^+ \to \psi K^+)} = 1.55 \pm 0.46 \pm 0.16\%.$$

Assuming equal production of B^+ and B^0 mesons, the measurements can be combined to determine the vector to pseudoscalar ratio in $B \to \psi$ decay

$$\frac{\mathcal{B}(B \to \psi K^*)}{\mathcal{B}(B \to \psi K)} = 1.32 \pm 0.23 \pm 0.16. \qquad 16.$$

Using the world average branching fractions from Tables 9 and 10 and combining B^- and $\bar{B}^0$ decays, we determine the sum of the exclusive two-body decays to $\mathcal{B}[B \to \psi\ K(K^*,\ \pi)] = 0.258 \pm 0.030\%$ and $\mathcal{B}[B \to \psi'\ K\ (K^*,\ \pi)] = 0.22 \pm 0.09\%$. Thus, about 1/4 of the inclusive rate for direct $B \to \psi$ production can be accounted for by exclusive modes. The experimental investigation of the remaining fraction is important, since any additional quasi two-body channel open to $B \to \psi$ transitions could be useful for future studies of CP violation. ψ mesons of lower momentum could originate from multibody final states or from two-body decays involving heavier $K^{(*)}$ resonances.

Evidence for the decay mode $B \to \chi_{c1}K$ has been reported by CLEO II (86, 100) and ARGUS (99). The average branching fraction is $\mathcal{B}(B^- \to \chi_c K^-) = (0.104 \pm 0.040)\%$. The CLEO II collaboration has also placed upper limits on $\chi_{c1}K^0$ and $\chi_{c1}K^*$ production in B decay.

Signals for Cabibbo-suppressed B decays with charmonium states have been found by CLEO II and CDF in the decay mode $B^+ \to \psi\pi^+$ (108, 110). [An updated value for $\mathcal{B}(B^0 \to \psi\pi)$ is given by Bishai (109).]

6.7.2 POLARIZATION IN $B \to \psi\, K^*$ The polarization in $B \to \psi K^*$ is studied by using the methods described for the $B^0 \to D^{*+}\rho^-$ polarization measurement in Section 6.3. After integration over the azimuthal angle between the ψ and the K^* decay planes, the angular distribution in $B \to \psi K^*$ decays can be written as

$$\frac{d^2\Gamma}{d\cos\Theta_\psi\, d\cos\Theta_{K^*}} \propto \frac{1}{4}\sin^2\Theta_{K^*}(1+\cos^2\Theta_\psi)(|H_{+1}|^2+|H_{-1}|^2) + \cos^2\Theta_{K^*}\sin^2\Theta_\psi|H_0|^2, \qquad 17.$$

where the K^* helicity angle Θ_{K^*} is the angle between the kaon direction in the K^* rest frame and the K^* direction in the B rest frame, Θ_ψ is the corresponding ψ helicity angle, and $H_{\pm1,0}$ are the helicity amplitudes. The fraction of longitudinal polarization in $B \to \psi K^*$ is determined by an unbinned fit to the ψ and K^* helicity angle distributions. The results obtained by the CLEO II, ARGUS, and CDF collaborations are given in Table 11 . The efficiency-corrected

Table 11 Longitudinal polarization of ψ mesons from $B \to \psi K^*$ decays

Experiment	Γ_L/Γ
CLEO II	$0.80 \pm 0.08 \pm 0.05$
ARGUS (109)	$0.97 \pm 0.16 \pm 0.15$
CDF (110)	$0.65 \pm 0.10 \pm 0.04$
Average	0.78 ± 0.07

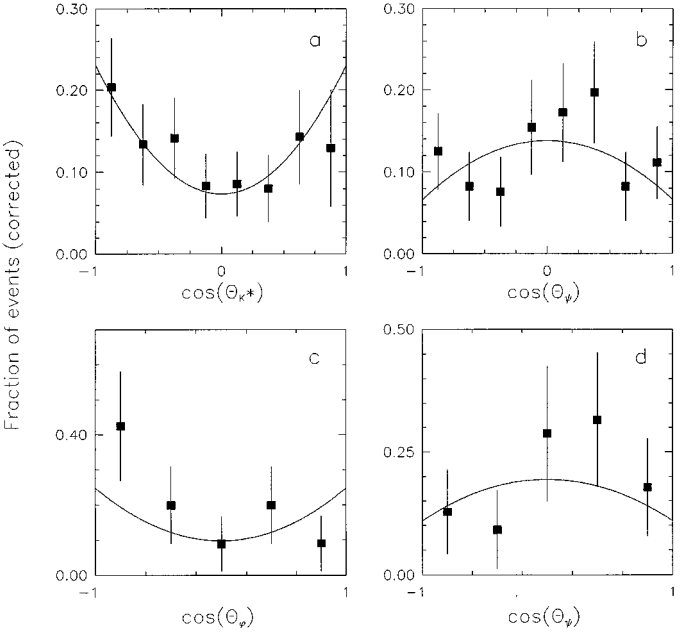

Figure 18 Distributions of the efficiency-corrected ψ and K^* helicity angles in reconstructed $B \to \psi K^*$ decays from CDF. The smooth curves are projections of the unbinned maximum likelihood fit described in the text (109).

distributions in each of the helicity angles $\cos\Theta_\psi$ and $\cos\Theta_{K^*}$ are shown in Figure 18. Assuming that the systematic errors from the various experiments are uncorrelated, these three results can be averaged to obtain

$$\frac{\Gamma_L}{\Gamma}(B \to \psi K^*) = 0.78 \pm 0.07. \qquad 18.$$

In addition, CDF has reported the first measurement of polarization for the $B_s \to \psi\phi$ mode,

$$\frac{\Gamma_L}{\Gamma}(B_s \to \psi\phi) = 0.56 \pm 0.21^{+0.02}_{-0.04}.$$

Although the decay mode $B \to \psi K^*$ may not be completely polarized, it is dominated by a single CP eigenstate and, therefore, will be useful for measurements of CP violation.

6.7.3 EXCLUSIVE DECAYS TO A $D^{0(*)}$ AND A NEUTRAL MESON B decays that can occur via an internal W-emission graph but that do not yield charmonium

mesons in the final state are expected to be suppressed relative to decays that occur via the external W-emission graph. For the internal graph, in the absence of gluons, the colors of the quarks from the virtual W must match the colors of the c-quark and the accompanying spectator antiquark. In this simple picture, one expects that the suppression factor should be $1/18$ in rate for decays involving π^0, ρ^0, and ω mesons. In heavy-quark decays, the effects of gluons cannot be neglected, and QCD-based calculations predict larger suppression factors on the order of $1/50$ (111). If color suppression is much less than expected, as is the case for some charm meson decays, then these B decay modes could also be useful for CP violation studies (112).

CLEO II has searched for color-suppressed decay modes of B mesons that contain a single D^0 or D^{*0} meson in the final state (these modes are also accessible via the W-exchange graph, which is expected to be small in B decay). [See Table 19 for the relevant modes. No signals were observed; however, the upper limits (14) on the branching ratios for color-suppressed modes are given.] These limits indicate that color suppression is present in B decay.

7. HADRONIC DECAYS: THEORETICAL INTERPRETATION

7.1 *The Effective Hamiltonian*

The Hamiltonian for weak hadronic charm (or beauty) decays is modified by gluon exchange between the quark lines in two ways. Hard gluon exchanges can be accounted for by perturbative methods and renormalization group techniques (113). There are also long distance or non–perturbative interactions are responsible for the binding of quarks inside the asymptotic hadron states. It is possible to separate the two regimes by means of the operator product expansion (114), which incorporates all long-range QCD effects into the hadronic matrix element of local four-quark operators (111). The effective Hamiltonian (115), for example in the case of the charm decays, can be expressed as

$$H_{eff} = \frac{G_F}{\sqrt{2}} V_{cs}^* V_{ud} \left[\frac{c_+ + c_-}{2} (\overline{u}d)(\overline{s}c) + \frac{c_+ - c_-}{2} (\overline{s}d)(\overline{u}c) \right], \qquad 19.$$

where Cabibbo-suppressed transitions and penguin diagrams are neglected. Here, $(\overline{q_i} q_j)$ denotes $\overline{q_i}\gamma^\mu(1-\gamma^5)q_j$, G_F is the Fermi coupling constant, and $c_\pm$ are the Wilson coefficients. Gluon exchange has the effect of generating the second term, which is an effective neutral current. Without QCD corrections, $c_+ = c_- = 1$ and the usual weak Hamiltonian is recovered. The Wilson coefficients $c_\pm(\mu)$ can be evaluated from QCD in the leading logarithmic approximation (111). There is a large uncertainty in the calculation from the

choice of the scale μ. The usual scale is taken to be $\mu \sim m_Q$, so that for the c-quark [$m_c = 1.5\,\text{GeV}$, $\Lambda^{(4)} = 234\,\text{MeV}$] and b-quark [$m_b = 5\,\text{GeV}$, $\Lambda^{(5)} = 200\,\text{MeV}$] we obtain,

$$\text{c-quark}: c_1 = \frac{c_+ + c_-}{2} = +1.25 \qquad c_2 = \frac{c_+ - c_-}{2} = -0.49 \qquad 20.$$

$$\text{b-quark}: c_1 = \frac{c_+ + c_-}{2} = +1.12 \qquad c_2 = \frac{c_+ - c_-}{2} = -0.27.$$

7.2 *Factorization*

The hypothesis that the decay amplitude can be expressed as the product of two single current matrix elements is called factorization. This hypothesis is taken by analogy to semileptonic decays where the amplitude can be decomposed into a leptonic and a hadronic current.

A qualitative justification for the factorization hypothesis based on color transparency was suggested by Bjorken (117). For example, in a B^- decay, a $\bar{u}d$ pair, which is produced as a color singlet from the virtual W^-, could travel fast enough to leave the interaction region without influencing the second hadron formed from the c-quark and the spectator antiquark. Buras et al (118) show that factorization is valid in the limit $1/N_c \to 0$ and have considered leading $1/N_c$ corrections to this limit. Dugan & Grinstein (116) have suggested that factorization follows from perturbative QCD in certain kinematic regions. It is expected that the factorization hypothesis will be more reliable in B hadronic decays than in the equivalent D hadronic decays because of the larger energy transfers.

There are several phenomenological models of the nonleptonic two-body decays of heavy flavors (119). The model of Bauer, Stech & Wirbel (BSW) is widely used (120). In addition to factorization, the BSW model uses hadronic currents instead of quark currents and allows the coefficients a_1, a_2 of the products of currents to be free parameters determined by experimental data. The effective Hamiltonian becomes

$$H = \frac{G_F}{\sqrt{2}} V_{cs}^* V_{ud} [a_1 (\bar{u}d)_H (\bar{s}c)_H + a_2 (\bar{s}d)_H (\bar{u}c)_H]. \qquad 21.$$

The relation between a_1, a_2 and the QCD coefficients c_1, c_2 is

$$\begin{aligned} a_1 &= c_1 + \xi c_2 \\ a_2 &= c_2 + \xi c_1, \end{aligned} \qquad 22.$$

where the factor $\xi (= 1/N_c)$ is the color-matching factor.

Three classes of decay can be distinguished: decays determined by a_1 (class I), e.g. $D^0 \to K^- \pi^+$ (Figure 1*a*); decays determined by a_2 (class II), e.g. $D^0 \to \overline{K^0} \pi^0$ (Figure 1*b*); and those where both the a_1 and a_2 contributions are

present and interfere (class III), e.g. the decay $D^+ \to \overline{K^0}\pi^+$. In this model, the rate for any exclusive two-body decay can be calculated once the parameters a_1 and a_2 are given.

For example, the amplitude for the decay $D^0 \to K^-\pi^+$ (neglecting the exchange diagram term) is given by

$$A = \frac{G_F}{\sqrt{2}} V_{cs}^* V_{ud} a_1 \langle \pi^+ | (\bar{u}d)_H | 0 \rangle \langle K^- | (\bar{s}c)_H | D^0 \rangle, \qquad 23.$$

where the first matrix element is the amplitude for creating a pion from the vacuum via the axial current, proportional to the pion decay constant f_π; the second term is the matrix element for the transition $D^0 \to K^-$ that can be expressed in terms of form factors extracted from the data on semileptonic decays (6).

7.3 *Final-State Interactions*

FSI can dramatically modify observed decay rates. These interactions occur in a space-time region where the final-state particles have already been formed by the combined action of weak and strong forces but are still strongly interacting while recoiling from each other (10). The relation between the decay amplitudes A_i, corresponding to final-state i, and the bare amplitude A_j^0 (without FSI) is

$$A_i = \sum_j S_{ij}^{1/2} A_j^0, \qquad 24.$$

where S denotes the strong interaction S-matrix for hadron-hadron scattering. As a result, there is mixing between channels that have the same quantum numbers and relative phases will be induced. It is worthwhile to note that, in general, the final-state i might not be directly accessible through weak-decay diagrams. For example, the observed rate for a decay mode that is small in a short-distance quark level calculation can be dramatically enhanced by rescattering from modes with larger branching fractions. The factorization approximation can only be used to determine the bare decay amplitudes A_j^0. One way to eliminate the uncertainties associated with the S-matrix is to sum over all decay channels with the same conserved quantum numbers. From Equation 24 and the unitarity of the S-matrix, we have

$$\sum_i |A_i|^2 = \sum_j |A_j^0|^2; \qquad 25.$$

that is, the sum of related decay rates remains unaffected by FSI.

It is customary to distinguish elastic and inelastic FSI. For example, for two coupled channels, Equation 24 gives

$$\begin{pmatrix} A_1 \\ A_2 \end{pmatrix} = \begin{pmatrix} \eta e^{2i\delta_1} & i\sqrt{1-\eta^2}\, e^{i(\delta_1+\delta_2)} \\ i\sqrt{1-\eta^2}\, e^{i(\delta_1+\delta_2)} & \eta e^{2i\delta_2} \end{pmatrix} \begin{pmatrix} A_1^0 \\ A_2^0 \end{pmatrix}_{\text{bare}}, \qquad 26.$$

where δ_1, δ_2 are the strong interaction phase shifts and η is the elasticity parameter (120, 121). Inelastic FSI ($\eta < 1$) alter the observed amplitudes compared with the factorization predictions. It should be noted that elastic FSI ($\eta = 1$) may also change the observed width of coupled channels by modifying the interference between two isospin amplitudes.

7.4 *Heavy-Quark Effective Theory*

It has recently been appreciated that there is a symmetry of QCD that is useful in understanding systems containing one heavy quark. This symmetry arises when the quark becomes sufficiently heavy to make its mass irrelevant to the nonperturbative dynamics of the light quarks. This allows the heavy quark degrees of freedom to be treated in isolation from the the light quark degrees of freedom. This is analogous to the canonical treatment of a hydrogen atom, in which the spin and other properties of the nucleus can be neglected. The behavior and structure of the atom are determined by the electron degrees of freedom. Heavy-quark effective theory (HQET) was developed by Isgur & Wise (122), who define a single universal form factor, $\xi(v \cdot v')$, known as the Isgur-Wise function. In this function, v and v' are the four-vector velocities of the initial and final-state heavy quarks. In the heavy-quark limit, all the form factors for hadronic matrix elements such as $B \to D^*$ and $B \to D$ can be related to this single function. The value of this function can be determined from a measurement of the $B \to D^* \ell \nu$ rate as a function of q^2 (122). The theory also provides a framework for systematic calculations of corrections to the heavy-quark limit.

The evaluation of amplitudes for hadronic decays requires not only the assumption of factorization, but hadronic form factors and meson decay constants. Based on HQET, many of the hadronic form factors for $b \to c$ transitions can be calculated in an essentially model-independent way. This has been done by several groups (111, 123). The comparison of these theoretical predictions with the experimental results can be used to test the range of validity of HQET and the extent to which $1/M_Q$ corrections to the heavy-quark symmetry are needed. It is not yet clear whether HQET can also be correctly applied to the calculation of form factors for charm quark decays.

7.5 *FSI in Charm Decay*

The presence of FSI often complicates the comparison between experimental data and theoretical predictions. In charm decay, FSI are particularly problematic because there are several resonances that contribute in the mass region. From the measurements now available, it is possible to disentangle these contributions.

An isospin analysis gives quantitative results about the FSI. For example, consider the decays $D^0 \to \pi^-\pi^+$, $D^0 \to \pi^0\pi^0$, and $D^+ \to \pi^0\pi^+$, which repre-

sent all possible two-body $D \to \pi\pi$ transitions. The amplitudes for these final states can be expressed in terms of amplitudes for the isospin 0 and 2 eigenstates.

The isospin decomposition gives (124)

$$\begin{aligned} A(D^0 \to \pi^-\pi^+) &= \frac{1}{\sqrt{3}}(\sqrt{2}A_0 + A_2) \\ A(D^0 \to \pi^0\pi^0) &= \frac{1}{\sqrt{3}}(-A_0 + \sqrt{2}A_2) \\ A(D^+ \to \pi^0\pi^+) &= \sqrt{3/2}A_2, \end{aligned} \qquad 27.$$

where $A_I = A_I\, e^{i\delta_i}$ is the complex amplitude for isospin I and δ is the phase shift from FSI.

These expressions lead to the following phase-independent relations:

$$|A(D^0 \to \pi^-\pi^+)|^2 + |A(D^0 \to \pi^0\pi^0)|^2 = |A_0|^2 + |A_2|^2$$

$$|A(D^+ \to \pi^0\pi^+)|^2 = \frac{3}{2}|A_2|^2. \qquad 28.$$

Using the D branching fractions from this review, we have calculated world averages for phase shifts and isospin amplitudes. The results in Table 12 show that several phase shifts between different isospin amplitudes are close to 90°, indicating large contributions from FSI. Moreover, the lower isospin amplitudes are always larger than the higher ones.

If inelastic FSI can be neglected, it is possible to extract branching fractions corrected for FSI (120). The prescription consists in adding the isospin amplitudes with zero phase shift.

In Tables 13, 14, and 15, branching fractions for a number of Cabibbo-favored and Cabibbo-suppressed decays are compared to predictions of the BSW model using updated values for a_1 and a_2. The values in parentheses are BSW model predictions corrected for isospin phase shifts (taken from Table 12) due to FSI. These corrections generally improve the agreement with the data. However,

Table 12 Isospin amplitudes and phase shifts for hadronic D decay modes[a]

Decay mode	Ratio of isospin amplitudes	$\delta = \delta_I - \delta_{I'}$
$K\pi$	$\lvert A_{1/2}\rvert/\lvert A_{3/2}\rvert = 4.12 \pm 0.40$	$88^\circ \pm 8^\circ$
$K^*\pi$	$\lvert A_{1/2}\rvert/\lvert A_{3/2}\rvert = 5.23 \pm 0.59$	$90^\circ \pm 16^\circ$
$K\rho$	$\lvert A_{1/2}\rvert/\lvert A_{3/2}\rvert = 3.22 \pm 0.64$	$10^\circ \pm 47^\circ$
$K^*\rho$	$\lvert A_{1/2}\rvert/\lvert A_{3/2}\rvert = 4.93 \pm 1.95$	$33^\circ \pm 57^\circ$
KK	$\lvert A_1\rvert/\lvert A_0\rvert = 0.58 \pm 0.12$	$47^\circ \pm 13^\circ$
$\pi\pi$	$\lvert A_2\rvert/\lvert A_0\rvert = 0.63 \pm 0.13$	$81^\circ \pm 10^\circ$

[a]Calculated using the isospin decomposition and updated branching fraction.

Table 13 Comparisons of measured branching fractions for Cabibbo-favored D decays to predictions from the BSW model[a]

Decay mode	Branching fraction (%) (18)	BSW model (%)
$D^0 \to K^-\pi^+$	3.76 ± 0.15	5.0 (3.8)
$D^0 \to \overline{K^0}\pi^0$	1.99 ± 0.26	0.8 (2.0)
$D^0 \to \overline{K^0}\eta^0$	0.74 ± 0.16	0.3
$D^0 \to \overline{K^0}\rho^0$	1.10 ± 0.17	0.3 (0.9)
$D^0 \to K^-\rho^+$	9.8 ± 1.2	8.7 (8.1)
$D^0 \to \overline{K^0}\omega$	1.7 ± 0.5	0.3
$D^0 \to K^{*-}\pi^+$	5.1 ± 0.6	2.6 (2.3)
$D^0 \to \overline{K^{*0}}\pi^0$	2.7 ± 0.5	1.0 (1.2)
$D^0 \to K^{*-}\rho^+$	5.9 ± 2.4	17.1 (15.3)
$D^0 \to \overline{K^{*0}}\rho^0$	1.4 ± 0.3	1.9 (3.6)
$D^+ \to \overline{K^0}\pi^+$	2.44 ± 0.43	2.5 (2.5)
$D^+ \to \overline{K^0}\rho^+$	7.3 ± 2.5	11.9 (11.9)
$D^+ \to \overline{K^{*0}}\pi^+$	2.1 ± 0.4	0.1 (0.1)
$D^+ \to \overline{K^{*0}}\rho^+$	2.2 ± 1.5	12.3 (12.3)
$D^+ \to \overline{K^0}a_1^+$	7.9 ± 2.0	3.2

[a]The values in parentheses take into account isospin phase shifts.

some serious discrepancies still remain in the decays to vector particles such as K^* and ρ. These discrepancies could be due to either an incorrect determination of these form factors or to mixing between $\overline{K}\rho$ and $K^\star\pi$ due to inelastic FSI.

While the BSW model agrees reasonably well with the experimental measurements of branching fractions for two-body decays of D^0 and D^+, it fails to predict the observed pattern of D_s^+ decays. For example, the ratio of hadronic branching fractions $\Gamma(D_s \to \eta\pi^+)/\Gamma(D_s \to \eta'\pi^+) = 0.39 \pm 0.13$ (14) is considerably different from the corresponding semileptonic ratio $\Gamma(D_s \to \eta\ell^+\nu)/\Gamma(D_s \to \eta'\ell^+\nu) = 2.45 \pm 0.94$ (125). These two ratios are expected to be nearly equal if factorization holds. A possible explanation

Table 14 Measurements of branching fractions for Cabibbo-favored D_s decays compared to predictions from the BSW model

Decay mode	Branching fraction (%) (18)	BSW model (%)
$D_s^+ \to \phi\pi^+$	3.6 ± 0.9	2.7
$D_s^+ \to \overline{K^0}K^+$	3.6 ± 1.1	1.5
$D_s^+ \to \eta\pi^+$	1.9 ± 0.6	2.8
$D_s^+ \to \eta\rho^+$	10.3 ± 3.2	5.2
$D_s^+ \to \eta'\pi^+$	5.0 ± 1.9	1.6
$D_s^+ \to \overline{K^{*0}}K^+$	3.4 ± 0.9	1.8
$D_s^+ \to K^{*+}\overline{K^0}$	4.3 ± 1.4	0.7
$D_s^+ \to \phi\rho^+$	6.7 ± 2.3	16.8

Table 15 Measurements of branching fractions for Cabibbo-suppressed D decays to predictions from the BSW model[a]

Decay Mode	Branching fraction (%) (18)	BSW model (%)
$D^0 \to \pi^-\pi^+$	0.15 ± 0.01	0.26 (0.18)
$D^0 \to \pi^0\pi^0$	0.08 ± 0.02	0.03 (0.10)
$D^0 \to K^-K^+$	0.43 ± 0.03	0.38 (0.30)
$D^0 \to \overline{K^0}K^0$	0.11 ± 0.05	0. (0.08)
$D^0 \to K^{*+}K^-$	0.31 ± 0.08	0.37
$D^0 \to K^{*-}K^+$	0.18 ± 0.10	0.14
$D^0 \to \phi\rho^0$	0.18 ± 0.05	0.08
$D^+ \to \pi^+\pi^0$	0.25 ± 0.07	0.10 (0.10)
$D^+ \to \overline{K^0}K^+$	0.68 ± 0.19	0.97 (0.97)
$D^+ \to \overline{K^{*0}}K^+$	0.50 ± 0.10 0.37	
$D^+ \to \phi\pi^+$	0.66 ± 0.08	0.26
$D^+ \to \overline{K^{*0}}K^{*+}$	2.6 ± 1.1 1.91	

[a]The values in parentheses take into account isospin phase shifts.

could be the interference between spectator and annihilation diagrams (126); a relatively small annihilation amplitude could have a large effect via an interference term. Alternately, there could be a gluonium component in the η' meson that is responsible for the enhancement of the hadronic modes.

Another puzzling problem is the anomalous value of the ratio of the Cabibbo-suppressed decay of D^0 into K^+K^- and $\pi^+\pi^-$ (14):

$$\frac{\Gamma(D^0 \to K^-K^+)}{\Gamma(D^0 \to \pi^-\pi^+)} = 2.85 \pm 0.20. \qquad 29.$$

Models predict a substantially lower number, ~ 1.4, from SU(3) breaking in the decay constants. The suggestion that penguin contributions could explain such a high value (127) seems to be ruled out by a recent calculation (128). FSI seem to be responsible for the sizeable branching fraction $\mathcal{B}(D^0 \to K^0\overline{K}^0)$ as the quark level contributions from two W-exchange diagrams are small. A better way to look at this problem would be to consider the ratio (129)

$$\frac{\Gamma(D^0 \to K^-K^+) + \Gamma(D^0 \to K^0\overline{K}^0)}{\Gamma(D^0 \to \pi^-\pi^+) + \Gamma(D^0 \to \pi^0\pi^0)} = 2.3 \pm 0.4. \qquad 30.$$

This ratio should not be affected by elastic FSI because the sum of D^0 decay modes is independent of strong interaction phases. The measured value is still above the expected level of SU(3) breaking (1.4). Inelastic FSI may explain this ratio (121, 128). A recent calculation that takes into account both non–spectator diagrams and rescattering effects can also accommodate this result (130).

Inelastic FSI are probably responsible for the decay mode $D^0 \to \phi\overline{K}^0$, which is observed at the level of $0.8 \pm 0.1\%$. Initially, this decay mode was called the smoking gun for W-exchange in charm decay, since it cannot occur at the quark level in any other way. However, Donoghue noted that the large rate for the $\phi\overline{K}^0$ channel could be the result of rescattering from other decay modes such as $\overline{K}^{*0}\eta$ (131). This explanation requires that the branching fraction for $D^0 \to \overline{K}^{*0}\eta$ be large enough O(2%) to allow for significant rescattering. The observed value, $\Gamma(D^0 \to \overline{K}^{*0}\eta) = 1.7 \pm 0.5\%$, supports this interpretation. In this sense, the decay $D^0 \to \phi\overline{K}^0$ should now be considered the smoking gun for inelastic FSI in charm decay.

Observation of the decay $D^+ \to \phi K^+$ was reported by the E691 collaboration (132) with a branching ratio $\mathcal{B}(D^+ \to \phi K^+)/\mathcal{B}(D^+ \to \phi\pi^+) = 5.8^{+3.2}_{-2.6} \pm 0.7\%$. This decay mode is quite unusual and intriguing. At the quark level, it is doubly Cabibbo-suppressed and requires annihilation. Rescattering may contribute, but the rescattering must proceed from an initial state that is doubly Cabibbo-suppressed. Observation of a similar nonresonant decay $D^+ \to K^+K^-\pi^+$ was reported by the WA82 collaboration (133). These signals are not confirmed by E687, which finds (134) $\mathcal{B}(D^+ \to \phi K^+)/\mathcal{B}(D^+ \to \phi\pi^+) < 2.1\%$ at the 90% confidence level and $\mathcal{B}(D^+ \to K^+K^-K^+)/\mathcal{B}(D^+ \to K^-\pi^+\pi^+) < 2.5\%$ at the 90% confidence level, which are marginally consistent with the original observations.

7.6 *Tests of the Factorization Hypothesis*

7.6.1 TESTS OF FACTORIZATION WITH BRANCHING FRACTIONS The factorization hypothesis can be tested by comparing hadronic exclusive decays to the corresponding semileptonic mode. These tests can be performed for exclusive hadronic decays of either D or B mesons (135).

As an example, we consider the specific case of $\bar{B}^0 \to D^{*+}\pi^-$. The amplitude for this reaction is

$$A = \frac{G_F}{\sqrt{2}} V_{cb}V_{ud}^* c_1 \langle \pi^-|(\bar{d}u)|0\rangle \langle D^{*+}|(\bar{c}b)|\bar{B}^0\rangle. \qquad 31.$$

The CKM factor $|V_{ud}|$ arises from the $W^- \to \bar{u}d$ vertex. The hadronic current that creates the π^- from the vacuum is related to the pion decay constant, f_π, by

$$\langle \pi^-(p)|(\bar{d}u)|0\rangle = -if_\pi p_\mu. \qquad 32.$$

The other hadron current can be determined from the semileptonic decay $\bar{B}^0 \to D^{*+}\ell^-\bar{\nu}_\ell$. Here, the amplitude is the product of a lepton current and the hadron current that we seek to insert in Equation 32.

Factorization can be tested experimentally by verifying the relation

$$\frac{\Gamma(\bar{B^0} \to D^{*+}\pi^-)}{\frac{d\Gamma}{dq^2}(B^0 \to D^{*+}\ell^-\bar{\nu_l})|_{q^2=m_\pi^2}} = 6\pi^2 c_1^2 f_\pi^2 |V_{ud}|^2. \quad 33.$$

Here, q^2 is the four-momentum transfer from the B meson to the D^* meson. Since q^2 is also the mass squared of the lepton-neutrino system, by setting $q^2 = m_\pi^2 = 0.019\ GeV^2$ we are requiring that the lepton-neutrino system have the same kinematic properties as does the pion in the hadronic decay. For the coefficient c_1, we use the value 1.12 ± 0.1 at $\mu = m_b$, deduced from perturbative QCD for the factorization tests involving hadronic B decays (the error is due to the uncertainty in the scale at which to evaluate the Wilson coefficient). The error in c_1 reflects the uncertainty in the mass scale at which the coefficient c_1 should be evaluated. In the original test of Equation 33, Bortoletto & Stone (136) found that the equation was satisfied for $c_1 = 1$. In the following discussion, we denote the left-hand side of Equation 33 by $R_{\rm exp}$ and the right-hand side by $R_{\rm theo}$.

We now consider the channels $D^0 \to K^-\pi^+$ and $D^0 \to K^{*-}\pi^+$, which are examples of $P \to PP$ and $P \to VP$ decay modes, respectively. The semileptonic modes that should be compared are $D \to K\ell\nu$ and $D \to K^*\ell\nu$, respectively. An updated value for a_1 is used in place of c_1 in the factorization test, while the semileptonic quantities are extracted from a recent review (6). In the following, each form factor is assumed to have a pole form for the q^2 dependence, with $M_p = 2.1\ \text{GeV}/c^2$ for the vector and $M_p = 2.5\ \text{GeV}/c^2$ for the axial vector. The other ingredients for the factorization test are collected in Table 16.

We emphasize that the branching fraction with elastic FSI removed is the quantity that should be compared to the semileptonic rate for a factorization test. Therefore, we correct the measured branching fractions using the values of the isospin amplitudes and phase shifts from Table 12. For example, the $D^0 \to K^-\pi^+$ branching fraction without elastic FSI is $\Gamma(D^0 \to K^-\pi^+)_{\text{no FSI}} = (1.3 \pm 0.1) \times \Gamma(D^0 \to K^-\pi^+)_{\text{measured}}$. The results of factorization tests for charm decays are given in Table 17.

There is excellent agreement for the pseudoscalar decay mode, while we note a serious discrepancy for the vector mode. On the other hand, we have already observed that models based on factorization give a poor description of the observed rates for charm decay modes involving vector particles, such as K^* and ρ.

An alternative way to test factorization has been proposed by Kamal & Pham (137). The main feature of their proposal is to compare quantities that are independent of the strong interaction phases (see for example Equation 29),

Table 16 Ingredients for factorization tests

$f_\pi = 131.74 \pm 0.15$ MeV
$f_\rho = 215 \pm 4$ MeV
$f_{a_1} = 205 \pm 16$ MeV
$V_{ud}\,(14) = 0.9744 \pm 0.0010$

Charm	Bottom
$a_1 = 1.10 \pm 0.03$	$\lvert c_1\rvert = 1.12 \pm 0.1$
$f_+^{DK}(0) = 0.76 \pm 0.03$	$\frac{d\mathcal{B}}{dq^2}(B \to D^* \ell\nu)\lvert_{q^2=m_\pi^2} = (0.237 \pm 0.026) \times 10^{-2}$ GeV^{-2}
$A_1^{DK^*}(0) = 0.56 \pm 0.04$	$\frac{d\mathcal{B}}{dq^2}(B \to D^* \ell\nu)\lvert_{q^2=m_\rho^2} = (0.250 \pm 0.030) \times 10^{-2}$ GeV^{-2}
$A_2^{DK^*}(0) = 0.39 \pm 0.08$	$\frac{d\mathcal{B}}{dq^2}(B \to D^* \ell\nu)\lvert_{q^2=m_{a_1}^2} = (0.335 \pm 0.033) \times 10^{-2}$ GeV^{-2}
$V^{DK^*}(0) = 1.1 \pm 0.2$	$\frac{d\mathcal{B}}{dq^2}(B \to D^* \ell\nu)\lvert_{q^2=m_{D_s}^2} = (0.483 \pm 0.033) \times 10^{-2}$ GeV^{-2}
$\frac{d\mathcal{B}}{dq^2}(D \to K \ell^+\nu)\lvert_{q^2=m_\pi^2} = 9.90 \pm 0.78 \times 10^{10} s^{-1}$ GeV^{-2}	$\frac{d\mathcal{B}}{dq^2}(B \to D^* \ell\nu)\lvert_{q^2=m_{D_s^*}^2} = (0.507 \pm 0.035) \times 10^{-2}$ GeV^{-2}
$\frac{d\mathcal{B}}{dq^2}(D \to K^* \ell^+\nu)\lvert_{q^2=m_\pi^2} = 4.38 \pm 0.98 \times 10^{10}$ s^{-1} GeV^{-2}	

Table 17 Test of factorization in hadronic and semileptonic decay rates

		R_{exp} (GeV^2)	R_{theo} (GeV^2)
Charm	$D^0 \to K^-\pi^+$	1.19 ± 0.14	1.18 ± 0.03
	$D^0 \to K^{*-}\pi^+$	3.09 ± 0.82	1.18 ± 0.03
Bottom	$\bar{B}^0 \to D^{*+}\pi^-$	1.14 ± 0.21	1.22 ± 0.15
	$\bar{B}^0 \to D^{*+}\rho^-$	2.80 ± 0.69	3.26 ± 0.42
	$\bar{B}^0 \to D^{*+}a_1^-$	3.6 ± 0.9	3.0 ± 0.50

focusing on the isospin amplitudes instead of the decay amplitudes. The breakdown of factorization in channels involving vector particles is attributed to an inelastic coupling between $\overline{K}\rho$ and $\overline{K}^*\pi$ channels in the I = 3/2 state, which could feed the $\overline{K}^*\pi$ final state at the expense of the $\overline{K}\rho$ channel.

The large samples of reconstructed hadronic B decays have been used to obtain precise measurements of branching fractions, as discussed in Section 6. These results can also be used to test the factorization hypothesis. The factorization tests can be extended to B decays by using the modes $B^0 \to D^{*+}X^-$ decays, e.g. $X = \pi^-$, $X^- = \rho^-$, or a_1^-.

To obtain numerical predictions for R_{theo}, we must interpolate the observed differential q^2 distribution (since the form factor for $B \to D^*\ell\nu$ is slowly varying, the width of the ρ^- meson does not significantly modify the result.) for $B \to D^*\ell\ \nu$ to $q^2 = m_\pi^2$, m_ρ^2, and $m_{a_1}^2$, respectively. Until this distribution is measured more precisely, we have to use theoretical models to perform this interpolation. The differences between the extrapolations using models for $B \to D^*\ell\ \nu$ are small, on the order of 10–20%. The measurement of this differential distribution recently published by CLEO II can be combined with the earlier results from the ARGUS and CLEO 1.5 experiments (136, 138). The values of $d\Gamma/dq^2(B \to D^*\ell\nu)$ used for the factorization test are given in Table 16. Using the information listed in Table 16, we obtain from Equation 33 the results (which are similar for $D^*\rho$) given in Table 17.

At the present level of precision, there is good agreement between the experimental results and the expectation from factorization for hadronic B decays in the q^2 range $0 < q^2 < m_{a_1}^2$. Note that it is possible that factorization will be a poorer approximation for decays with smaller energy release or larger q^2. Factorization tests can be extended to higher q^2 using $B \to D^* D_s^{(*)}$ decays, as is discussed in Section 7.6.3.

7.6.2 FACTORIZATION AND ANGULAR CORRELATIONS More subtle tests of the factorization hypothesis can be performed by examining the polarization in B (or D) meson decays into two vector mesons (139). Again, the underlying

principle is to compare the hadronic decays to the appropriate semileptonic decays evaluated at a fixed value in q^2. For instance, the ratio of longitudinal to transverse polarization (Γ_L/Γ_T) in $B^0 \to D^{*+}\rho^-$ should be equal to the corresponding ratio for $B \to D^*\ell\nu$ evaluated at $q^2 = m_\rho{}^2 = 0.6\ \mathrm{GeV}^2$.

$$\frac{\Gamma_L}{\Gamma_T}(\bar{B}^0 \to D^{*+}\rho^-) = \frac{\Gamma_L}{\Gamma_T}(B \to D^*\ell\nu)|_{q^2=m_\rho^2}. \qquad 34.$$

The advantage of this method is that it is not affected by QCD corrections (139).

For $B \to D^*\ell\nu$ decay (or $D \to K^*\ell\nu$), longitudinal polarization dominates at low q^2, whereas near $q^2 = q^2_{\max}$ transverse polarization dominates. There is a simple physical argument for the behavior of the form factors near these two kinematic limits. Near $q^2 = q^2_{\max}$, the D^* is almost at rest and its small velocity is uncorrelated with the D^* spin, so all three D^* helicities are equally likely and we expect $\Gamma_T/\Gamma_L = 2$. At $q^2 = 0$, the D^* has the maximum possible momentum, while the lepton and neutrino are collinear and travel in the direction opposite to the D^*. The lepton and neutrino helicities are aligned to give $S_z = 0$, so near $q^2 = 0$ longitudinal polarization is dominant.

Factorization breaks down in the charm sector as a result of the presence of FSI. From MARK III results (145) on the decay mode $D^0 \to K^{*0}\rho^-$, and the measured form factors for the semileptonic decay mode, we can evaluate Equation 34 for this vector-vector decay mode:

$$\begin{aligned} \frac{\Gamma_L}{\Gamma_T}(D^0 \to K^{*+}\rho^-) \qquad &= 0.90 \pm 0.65 \\ \frac{\Gamma_L}{\Gamma_T}(D^0 \to K^*\ell\nu)|_{q^2=m_\rho^2} &= 0.78 \pm 0.07. \end{aligned} \qquad 35.$$

This result supports the factorization hypothesis with large errors. The observation of large transverse polarization and a D-wave component in the color-suppressed decay $D^0 \to K^{*0}\rho^0$ indicates the presence of large nonfactorizable contributions (146, 147). In the future, polarization in the vector-vector mode $D_s^+ \to \phi\rho^+$ will also be measured.

For $B^0 \to D^{*+}\rho^-$, we expect 88% longitudinal polarization from the argument described above (141). Similar results have been obtained by Neubert (142), Rieckert (143), and Kramer et al (144). Using the measured q^2 distribution for $B \to D^*\ell\nu$, Neubert (141) calculated the transverse and longitudinal polarization in $B \to D^*\ell\nu$ decays. Using his result, we find Γ_L/Γ to be 85% at $q^2 = m_\rho{}^2 = 0.6$. The agreement between these predictions and the experimental result (see Section 6.3)

$$\Gamma_L/\Gamma \ = \ 93 \pm 5 \pm 5\% \qquad 36.$$

supports the factorization hypothesis in hadronic B meson decay for q^2 values up to m_ρ^2.

The strength of FSI in B decay can be determined by performing an isospin analysis of related decay channels such as $B^- \to D^0\pi^-$, $\bar{B}^0 \to D^0\pi^0$, and $\bar{B}^0 \to D^+\pi^-$, as was done for the $D \to K\pi$ and $D \to K^*\pi$ systems. At the present level of experimental precision and in contrast to D decay, there is no evidence for non-zero isospin phase shifts in B decay. From a maximum likelihood fit to the observed branching fractions, Yamamoto found that $\cos\delta^* > 0.82$ at the 90% confidence level, where δ^* is the phase shift for the $B \to D\pi$ system and comparable constraints, and $\cos\delta^* > 0.57(0.92)$ for the $B \to D^*\pi$ ($B \to D\rho$) isospin multiplets (148). In B (and D) decays to two-vector mesons, such as $B \to D^*\rho$, the presence of FSI could also be probed by studying the angle χ between the D^* and ρ decay planes. FSI would cause a phase shift between the helicity amplitudes and break the symmetry of the χ distribution. The presence of FSI would lead to a angular distribution proportional to $\sin\chi$ or $\sin 2\chi$ (149).

Until the D_s decay constant, f_{D_s}, is measured more precisely in $D_s \to \mu\nu$, tests of the factorization hypothesis based on branching fractions cannot be applied to $B \to D^*D_s$ decays. As data samples increase, it will become possible to measure the polarization in $\bar{B}^0 \to D^{*+}D_s^{*-}$ decay modes and to investigate whether factorization is still valid at $q^2 = m_{D_s}^2$.

7.6.3 APPLICATIONS OF FACTORIZATION If factorization holds, hadronic B decays can be used to extract information about semileptonic decays. For example, we can determine the poorly measured rate $B \to D^{**}(2420)\ \ell\ \nu$ from the branching ratio of $B \to D^{**}(2420)\pi$. By assuming that the rate for $B \to D^{**}(2420)\pi$ is related to $d\Gamma/dq^2(B \to D^{**}(2420)\ell\nu)$ evaluated at $q^2 = m_\pi^2$. Using the model of Colangelo et al (123) to determine the shape of the form factors, we obtain the ratio

$$\frac{\Gamma(B \to D^{**}(2420)\ \ell\ \nu)}{\Gamma(B \to D^{**}(2420)\pi)} = 3.2.$$

Combining this with the experimental result $\mathcal{B}[B^- \to D^{**0}(2420)\pi^-] = 0.16 \pm 0.05\,\%$ (Table 9), we predict $\mathcal{B}(B \to D^{**}(2420)\ell\nu) = 0.51 \pm 0.16\%$. This is not inconsistent with the average of recent direct measurements (8) $\mathcal{B}[B \to D^{**}\ (2420)\ell\nu] = 1.17 \pm 0.24\%$.

A second application of factorization is the determination of f_{D_s} using the decays $B \to D^*D_s$. The rate for $B^0 \to D^{*+}D_s$ is related to the differential rate for $B^0 \to D^{*+}\ell^-\nu$ at $q^2 = m_{D_s}^2$ if factorization continues to be valid at larger values of q^2:

$$\frac{\Gamma(\bar{B}^0 \to D^{*+}D_s^-)}{\frac{d\Gamma}{dq^2}(B^0 \to D^{*+}\ell^-\nu)|_{q^2=m_{D_s}^2}} = 6\pi^2\delta\, c_1^2 f_{D_s}^2 |V_{cs}|^2. \qquad 37.$$

The factor $\delta = 0.37$ accounts for the different form factors that enter in $B \to D^* D_s$ and $B \to D^* \ell \nu$ (111).

Using the value listed in Table 16 for $d\Gamma/dq^2(B \to D^* \ell \nu)$ at $q^2 = m^2_{D_s}$ and the average branching ratio for $\mathcal{B}(B \to D^* D_s^-) = 1.02 \pm 0.27\%$, we obtain

$$f_{D_s} = (277 \pm 77)\sqrt{3.6\%/\mathcal{B}(D_s \to \phi\pi^+)}\ \text{MeV},$$

and with $\mathcal{B}(B \to D^* D_s^{*-}) = 2.23 \pm 0.60\%$, we find ($\delta = 1$)

$$f_{D_s^*} = (243 \pm 70)\sqrt{3.6\%/B(D_s \to \phi\pi^+)}\ \text{MeV}.$$

This result can be compared to the value

$$f_{D_s} = (288 \pm 30 \pm 30 \pm 24)\sqrt{\mathcal{B}(D_s \to \phi\pi^+)/3.6\%}\ \text{MeV}$$

that was obtained from a direct measurement of $D_s \to \mu\nu$ decays in continuum charm events (150). Both values of f_{D_s} are entirely consistent with theoretical predictions that are in the range $f_{D_s} = 200$–290 MeV (151). If both the $D_s^+ \to \phi\pi^+$ branching fraction and f_{D_s} are measured more precisely, then measurements of the branching ratios of $B \to D^* D_s$ decays can be used to test factorization in B decay at $q^2 = m^2_{D_s}$. As noted earlier, it will also be possible to test factorization in this q^2 range by measuring Γ_L/Γ in $B \to D^* D_s^*$ decays.

7.6.4 FACTORIZATION IN COLOR-SUPPRESSED DECAY It is not obvious whether the factorization hypothesis will be satisfied in decays that proceed via internal W-emission, e.g $B \to \psi K^{(*)}$. Two observables have been compared to phenomenological models based on the factorization hypothesis: the ratio of vector to pseudoscalar modes, and the polarization in $B \to \psi K^*$ decays.

Using the results listed in Tables 9 and 10, we can determine the ratio of vector to pseudoscalar meson production

$$\frac{\mathcal{B}(B \to \psi K^*)}{\mathcal{B}(B \to \psi K)} = 1.69 \pm 0.33. \qquad 38.$$

Combined with the CDF measurement (Equation 17), we obtain

$$\frac{\mathcal{B}(B \to \psi K^*)}{\mathcal{B}(B \to \psi K)} = 1.47 \pm 0.21. \qquad 39.$$

This quantity can be calculated using factorization and the ratio of the $B \to K^*$ and $B \to K$ form factors. The revised BSW model of Neubert et al (111) predicts a value of 1.61 for this ratio, which is close to the experimental result. Another test is the corresponding ratio for ψ' decays

$$\frac{\mathcal{B}(B \to \psi' K^*)}{\mathcal{B}(B \to \psi' K)} = 2.1 \pm 1.5. \qquad 40.$$

This measurement can be compared to the revised BSW model, which predicts 1.85 for this ratio. Gourdin et al (152) argue that the ratio $\mathcal{B}(B \to \eta_c K^*)/\mathcal{B}(B \to \eta_c K)$ would provide a good test of the factorization hypothesis in internal spectator decays. However, it will require a significantly larger data sample than is available at present before this ratio can be measured with sufficient precision. Other ratios of decay rates in modes with charmonium mesons may also be used to test factorization (153).

The experimental results on ψK^* polarization can be compared to the theoretical predictions of Kramer & Palmer (154), which depend on the assumption of factorization and on the unmeasured $B \to K^*$ form factor. Using the BSW model to estimate the form factors, they find $\Gamma_L/\Gamma = 0.57$. Using HQET to extrapolate from the E691 measurements of the $D \to K^*$ form factor, they obtain $\Gamma_L/\Gamma = 0.73$. Gourdin et al and Aleksan et al have noted that there is no set of experimental or theoretical form factors that can simultaneously reproduce the measured values of Γ_L/Γ and $\mathcal{B}(B \to \psi K^*)/\mathcal{B}(B \to \psi K)$ (155, 156). They conclude that there is either a fundamental problem in heavy to light form factors or a breakdown of factorization for this class of decay modes. Kamal & Santra have suggested that all the measured observables in exclusive $B \to \psi$ can be accommodated with a single nonfactorizable amplitude (157).

CLEO finds evidence at the 2.5 standard deviation level for $B \to \chi_{c2}$ transitions at a branching ratio of $0.25 \pm 0.10 \pm 0.03\%$. If confirmed, this would indicate the presence of either nonfactorizable color octet contributions that are neglected in the usual treatment of hadronic B decays or higher order processes $O(\alpha_s^2)$ in $b \to c\bar{c}s$ decays (81).

7.7 *Determination of the Color-Suppressed Amplitude*

7.7.1 COLOR SUPPRESSION IN B AND D DECAY In the decays of charm mesons, the effect of color suppression is obscured by the effects of FSI or reduced by nonfactorizable effects. The nonfactorizable contribution arises from the soft gluon exchange between color currents (146). Table 18 gives ratios of several charm meson decay modes with approximately equal phase space factors where the mode in the numerator is color-suppressed while the mode in the denominator is an external spectator decay. With the exception of the decay $D^0 \to \bar{K}^0\rho^0$, it is clear that the color-suppressed decays do not have significantly smaller branching ratios.

The data on charm decays supports the *new factorization* scheme (118), that is $N_c \to \infty$ in Equation 33. This scheme gives values of $a_1 \sim 1.25$ and $a_2 \sim -0.49$ for nonleptonic charm decays. Assuming that the values of the coefficients can be extrapolated from $\mu = m_c^2$ to $\mu = m_b^2$, taking into account the evolution of the strong coupling constant α_s, we obtain the predictions $a_1 \sim 1.12$ and $a_2 \sim -0.27$ for B decays.

Table 18 Measured ratios of decay rates for color-suppressed and external spectator diagrams

Ratio	Branching ratio (18)
$\Gamma(D^0 \to \pi^0\pi^0)/\Gamma(D^0 \to \pi^-\pi^+)$	0.56 ± 0.15
$\Gamma(D^0 \to \overline{K^0}\pi^0)/\Gamma(D^0 \to K^-\pi^+)$	0.53 ± 0.07
$\Gamma(D^0 \to \overline{K^0}\rho^0)/\Gamma(D^0 \to K^-\rho^+)$	0.11 ± 0.02
$\Gamma(D^0 \to \overline{K^{*0}}\pi^0)/\Gamma(D^0 \to K^{*-}\pi^+)$	0.53 ± 0.11
$\Gamma\left(D_s^+ \to \overline{K^{*0}}K^+\right)/\Gamma\left(D_s^+ \to \phi\pi^+\right)$	0.95 ± 0.10
$\Gamma\left(D_s^+ \to \overline{K^0}K^+\right)/\Gamma\left(D_s^+ \to \phi\pi^+\right)$	1.01 ± 0.16

The smaller magnitude of a_2 means that, in contrast to the charm sector, one expects to find a more consistent pattern of color suppression in B meson decays.

In Section 6.7.3, we obtained upper limits for color-suppressed B decays with a D^0 or D^{*0} meson in the final state. In Table 19, these results are compared to the predictions of the BSW and the RI models.

In contrast to charm decay, color suppression seems to be operative in hadronic decays of B mesons. The limits on the color-suppressed modes with $D^{0(*)}$ and neutral mesons are still above the level expected by the two models, but we can already exclude a prediction by Terasaki (158) that $\mathcal{B}(\bar{B}^0 \to D^0\pi^0) \approx 1.8\mathcal{B}(\bar{B}^0 \to D^+\pi^-)$. To date, the only color-suppressed B meson decay modes that have been observed are final states that contain charmonium mesons, e.g. $B \to \psi K$ and $B \to \psi K^*$. (The branching ratio for the modes $B \to \psi K$ and $B \to \psi K^*$ can be accommodated by the value $\xi \sim 0$ while $\xi \sim 1/3$ gives a branching ratio that is about a factor of 4 too low.)

Table 19 Measured and predicted branching fractions of color-suppressed B decays

Decay Mode	U.L. (%)	BSW (%)	$\mathcal{B}$ (BSW)	RI model (%)
$\bar{B}^0 \to D^0\pi^0$	< 0.048	0.012	$0.20a_2^2(f_D/220\text{ MeV})^2$	0.0013–0.0018
$\bar{B}^0 \to D^0\rho^0$	< 0.055	0.008	$0.14a_2^2(f_D/220\text{ MeV})^2$	0.00044
$\bar{B}^0 \to D^0\eta$	< 0.068	0.006	$0.11a_2^2(f_D/220\text{ MeV})^2$	
$\bar{B}^0 \to D^0\eta'$	< 0.086	0.002	$0.03a_2^2(f_D/220\text{ MeV})^2$	
$\bar{B}^0 \to D^0\omega$	< 0.063	0.008	$0.14a_2^2(f_D/220\text{ MeV})^2$	
$\bar{B}^0 \to D^{*0}\pi^0$	< 0.097	0.012	$0.21a_2^2(f_{D_*}/220\text{ MeV})^2$	0.0013–0.0018
$\bar{B}^0 \to D^{*0}\rho^0$	< 0.117	0.013	$0.22a_2^2(f_{D_*}/220\text{ MeV})^2$	0.0013–0.0018
$\bar{B}^0 \to D^{*0}\eta$	< 0.069	0.007	$0.12a_2^2(f_{D_*}/220\text{ MeV})^2$	
$\bar{B}^0 \to D^{*0}\eta'$	< 0.27	0.002	$0.03a_2^2(f_{D_*}/220\text{ MeV})^2$	
$\bar{B}^0 \to D^{*0}\omega$	< 0.21	0.013	$0.22a_2^2(f_{D_*}/220\text{ MeV})^2$	

7.7.2 DETERMINATION OF $|a_1|$, $|a_2|$ AND THE RELATIVE SIGN OF (a_2/a_1) We have determined the free parameters a_1 and a_2 of the BSW model for D decays taking into account the isospin phase shifts due to FSI. Using updated world averages for the branching fraction of the decay $D \to K\pi$, where no inelastic effects are expected, gives

$$a_1 = +\,1.10 \pm 0.03 \qquad 41.$$

$$a_2 = -\,0.50 \pm 0.03.$$

A comparison with the QCD Wilson coefficients (see Equation 21) shows that $a_1 \simeq c_1$ and $a_2 \simeq c_2$, that is $\xi \sim 0$. This result is anticipated in the $1/N_c$ expansion by Buras et al (118) and implies that quarks belonging to different color singlet currents do not easily combine to form a single meson (159).

If instead we use the perturbative QCD result, Equation 23 with $N_c = 3$, we obtain the following values of a_1 and a_2.

$$\text{c-quark:} \quad a_1 = +\,1.08 \qquad a_2 = -\,0.07; \qquad 42.$$

$$\text{b-quark:} \quad a_1 = +\,1.03 \qquad a_2 = +\,0.11.$$

The value of a_2 from the QCD calculation is inconsistent with the experimental results for hadronic charm decay. This discrepancy suggests that nonfactorizable contributions and FSI play an important role. Nonperturbative soft gluon effects become more important in decays with smaller energy release, allowing for FSI. This may explain why a_2 is class-dependent in charm decay, whereas it appears to be fairly stable in B decays (146).

Kamal et al (160) [see also Cheng (161)] recently argued that a_1 and a_2 (in the factorized amplitude) should be replaced by the effective and unitarized parameters $a_1^{\mathrm{U,eff}}$ and $a_2^{\mathrm{U,eff}}$. These quantities receive contributions from annihilation and nonfactorizable processes as well as from FSI. Since these effective parameters are process-dependent, factorization tests (comparing hadronic to semileptonic rate) should be used as a tool to determine the moduli of these quantities (160). In this way, much of the predictive power of the phenomenological models (based on factorization) is lost, because the a_1 and a_2 parameters are now dependent on the particular decay channel.

In the BSW model (111), the branching fractions of the $\bar{B}^0$ normalization modes are proportional to a_1^2 while the branching fractions of the $B \to \psi$ decay modes depend only on a_2^2. A fit to the branching ratios for the B decay modes $B^0 \to D^+\pi^-$, $D^+\rho^-$, $D^{*+}\pi^-$, and $D^{*+}\rho^-$ using the model of Neubert et al yields

$$|a_1| = 1.07 \pm 0.04 \pm 0.06, \qquad 43.$$

and a fit to the modes with ψ mesons in the final state gives

$$|a_2| = 0.23 \pm 0.01 \pm 0.01. \quad 44.$$

The first error on $|a_1|$ and $|a_2|$ includes the uncertainties from the charm or charmonium branching ratios, the experimental systematics associated with detection efficiencies, and background subtractions, as well as the statistical errors from the branching ratios. The second error quoted is the uncertainty due to the B meson production fractions and lifetimes. We assumed that the ratio of B^+B^- and $B^0\bar{B}^0$ production at the $\Upsilon(4S)$ is one (10) and assigned an uncertainty of 10% to it.

The magnitude of the amplitude for external spectator processes, $|a_1|$, can also be determined from $B \to D^{(*)}D_s^{(*)}$ decays. Since these transitions are not subject to interference with the internal spectator amplitude, we can combine B^- and $\bar{B}^0$ decays to reduce the statistical error. Using the average branching fractions given in Tables 9 and 10, we obtain

$$|a_1|_{DD_s} = 0.98 \pm 0.06 \pm 0.04. \quad 45.$$

It is interesting to note that this value of $|a_1|$ agrees with the result of the fit to the $B \to D^{(*)}\pi$ and $B \to D^{(*)}\rho$ modes (see Equation 44). In general, $|a_1|$ could be different for exclusive $b \to c\bar{u}d$ and $\underline{b} \to c\bar{c}s$ processes.

By comparing branching ratios of B^- and B^0 decay modes, it is possible to determine the sign of a_2 relative to a_1. The BSW model (111) predicts the following ratios:

$$R_1 = \frac{\mathcal{B}(B^- \to D^0\pi^-)}{\mathcal{B}(B^0 \to D^+\pi^-)} = (1 + 1.23a_2/a_1)^2; \quad 46.$$

$$R_2 = \frac{\mathcal{B}(B^- \to D^0\rho^-)}{\mathcal{B}(B^0 \to D^+\rho^-)} = (1 + 0.66a_2/a_1)^2; \quad 47.$$

$$R_3 = \frac{\mathcal{B}(B^- \to D^{*0}\pi^-)}{\mathcal{B}(B^0 \to D^{*+}\pi^-)} = (1 + 1.29a_2/a_1)^2; \quad 48.$$

$$R_4 = \frac{\mathcal{B}(B^- \to D^{*0}\rho^-)}{\mathcal{B}(B^0 \to D^{*+}\rho^-)} \approx (1 + 0.75a_2/a_1)^2. \quad 49.$$

Table 20 shows a comparison between the experimental results and the two allowed solutions in the BSW model. The systematic errors due to detection efficiencies partly cancel each other out. In the ratios R_3 and R_4, the D meson branching ratio uncertainties do not contribute to the systematic error.

A least-squares fit to the ratios R_1 to R_3 gives

$$a_2/a_1 = 0.26 \pm 0.07 \pm 0.05, \quad 50.$$

Table 20 B^- to $\bar{B}^0$ branching ratios to determine the sign of a_2/a_1[a]

Ratio	$a_2/a_1 = -0.23$	$a_2/a_1 = 0.23$	Experiment	RI model
R_1	0.51	1.64	1.60 ± 0.30	1.20–1.28
R_2	0.72	1.33	1.61 ± 0.39	1.09–1.12
R_3	0.49	1.68	1.85 ± 0.40	1.19–1.27
R_4	0.68	1.37	2.10 ± 0.61	1.10–1.36

[a]The magnitude of a_2/a_1 is the value in the BSW model that agrees with our result for $B \to 4$ modes.

where we have ignored uncertainties in the theoretical predictions. R_4 is not included in the fit since the model prediction in this case is not thought to be reliable (V Rieckert, private communication). (The result of a fit including R_4 is not significantly different. We find in this case $a_2/a_1 = 0.282 \pm 0.07 \pm 0.06$.)

The second error is due to the uncertainty in the B meson production fractions and lifetimes that enter into the determination of a_1/a_2 in the combination $(f_+\tau_+/f_0\tau_0)$. As this ratio increases, the value of a_2/a_1 decreases. The allowed range of $(f_+\tau_+/f_0\tau_0)$ excludes a negative value of a_2/a_1.

Other uncertainties in the magnitude[2] of f_D, f_{D^*} and in the hadronic form factors can change the magnitude of a_2/a_1 but not its sign. The numerical factors that multiply a_2/a_1 include the ratios of $B \to \pi(B \to \rho)$ to $B \to D$ $(B \to D^*)$ form factors, as well as the ratios of the meson decay constants. We assume values of 220 MeV for f_D and f_{D^*} (162). To investigate the model dependence of the result, we have recalculated $|a_1|$, $|a_2|$, and a_2/a_1 in the model of Deandrea et al. We find $|a_1| = 1.00 \pm 0.04 \pm 0.06$, $|a_2| = 0.24 \pm 0.01 \pm 0.01$, and $a_2/a_1 = 0.25 \pm 0.07 \pm 0.05$, consistent with the results discussed above. A different set of $B \to \pi$ form factors can be calculated using QCD sum rules. By using the form factors determined by Belyaev et al (163) and by Ball (164), a_2/a_1 changes by 0.04. Kamal & Pham have also considered the effect of uncertainties in form factors, the effects of FSI, and annihilation terms. They conclude that these may change the magnitude of a_2/a_1 but not its sign (165). Systematic uncertainties in the ratio of D branching fractions could also modify its magnitude.

The magnitude of a_2 determined from this fit to the ratio of B^- and B^0 modes is consistent with the value of a_2 determined from the fit to the $B \to \psi$ decay modes. The sign of a_2 disagrees with the theoretical extrapolation from the fit to charm meson decays using the BSW model. [In the fits of Neubert et al (111), the CLEO 1.5 data favor a positive sign while the ARGUS data prefer a negative sign.] It also disagrees with the expectation from the $1/N_c$ rule (166,

[2]We considered variations of f_D between 120 and 320 MeV; for $f_D = 320$ MeV, we find $a_2/a_1 = 0.18$.

167). The result may be consistent with the expectation of perturbative QCD (168).

7.8 *The Sign of a_2/a_1 and the Anomalous Semileptonic Branching Ratio*

The observation that the coefficients a_1 and a_2 have the same relative sign in B^+ decay came as a surprise since destructive interference was observed in hadronic charm decay. Although constructive interference has been observed in all the B^+ modes studied so far these comprise only a small fraction of the total hadronic rate. If the constructive interference observed in B^+ decay is present at the same level in the remainder of hadronic B^+ decays, then we would expect a lifetime ratio $\tau_{B^+}/\tau_{B^0} \sim 0.83$ unless there is a large compensating contribution from W-exchange to B^0 decay (169). It is also possible that there is no interference in higher multiplicity B decays that have not yet been reconstructed. It, therefore, is important to measure a_1 and a_2 for a large variety of decay modes.

It is intriguing that a_1 determined from $B \to D^{(*)}\pi$, $D^{(*)}\rho$ modes agrees well with the value of a_1 extracted from $B \to DD_s$ decays. The observation of color-suppressed decays such as $\bar{B}^0 \to D^0\pi^0$ would give another measure of $|a_2|$, complementary to that obtained from $B \to$ charmonium decays .

Keum (96) has suggested that the relative sign of a_1 and a_2 could be determined from a measurement of the polarization in $B^- \to D^{*0}\rho^-$ decays. For $a_2/a_1 > 0$, the amount of longitudinal polarization should be less than 88%, while for $a_2/a_1 < 0$, the converse will hold. At the present level of precision, both possibilities are consistent with the data on polarization.

The experimentally measured semileptonic branching ratio is determined to be $(10.35 \pm 0.17 \pm 0.35)\%$ in the model-independent dilepton analysis (8). Comparable, but more precise, rates are also obtained from the analysis of the single lepton spectrum. These measurements are significantly below the theoretical lower bound $\mathcal{B}_{sl} > 12.5\%$ from QCD calculations within the parton model (170).

It is possible to understand the origin of the theoretical limit in a simple way. In the absence of QCD corrections, the virtual W emitted by the b quark can decay into either a lepton-antineutrino pair, a $\bar{u} - d$ quark pair, or a $\bar{c} - s$ quark pair. For the decay into a quark pair, there are three possible color states that are equally probable. In addition, corrections must be made for the reduction in phase space in the $W \to \tau\nu$ and $W \to \bar{c}s$ decays. Then the semileptonic fraction, $\mathcal{B}_{SL}$, is given by

$$\mathcal{B}_{SL} = \frac{f_c}{5f_c + 3f_{\bar{c}s} + f_{c\tau}}. \qquad 51.$$

Using the phase space factors, $f_c = 0.45$, $f_{\bar{c}s} \approx f_{c\tau} = 0.12$ gives $\mathcal{B}_{SL} = 16.5\%$. QCD corrections modify the hadronic contributions to the width and give $\mathcal{B}_{SL} = 14.3\%$. The theoretical lower limit of 12.5% is obtained by varying the quark masses and QCD scale to their lower limits.

Several explanations of this discrepancy, awaiting experimental confirmation have been proposed.

1. There might be an increased $b \to c\bar{c}s$ component of the B meson hadronic width (170, 94, 171). However, recent experimental data rule out the mechanism suggested by Dunietz et al (171) as a major contributor to $B \to$ baryon decays.

2. Higher order contributions might reduce the theoretical expectation, or the assumption of duality may not hold for b quark decay (172). The former has been advocated by Bagan et al, who find results consistent with the experimental result (173, 174) but who also predict $N_c = 1.28 \pm 0.08$ for the number of charm quarks produced per b decay, again due to higher order enhancements of the $b \to c\bar{c}s$ channel (174).

3. Constructive interference in B^- decays would reduce the theoretical expectation for the semileptonic branching ratio. A small contribution from W exchange to $\bar{B}^0$ decays would keep the lifetime ratio close to unity and satisfy the experimental constraints on this quantity (169).

4. There could also be a large contribution to the inclusive rate that has not been measured. It has been suggested by Palmer & Stech (94) that $b \to c\bar{c}s$ followed by $c\bar{c} \to$ gluons, which in turn hadronize into a final state with no charm, has a large branching ratio. The charm content for this mechanism would not be properly taken into account.

5. It is possible that the rate for the hadronic penguin diagram $b \to sg$ is larger than expected (176). This possibility will lead to significant production of high-multiplicity charmless final states, which are quite difficult to distinguish experimentally.

Increasing the $b \to c\bar{c}s$ component would increase the average number of c-quarks produced per b-quark decay and would lead to another interesting problem: The predicted number of charm quarks per b decay would increase to 1.3 while the current experimental world average for this number is 1.15 ± 0.05 (see Section 5.4). Moreover, $\mathcal{B}(b \to c\bar{c}s) = 15.8 \pm 2.8\%$, which is far below 30%.

With the recent observation of $B \to D\bar{D}KX$ transitions, the branching fraction for $(b \to c\bar{c}s)$ has increased from $15.8 \pm 2.8\%$, to $23.9 \pm 3.8\%$, which is now consistent with the QCD calculations of Ball et al. However,

the new source of $b \to c\bar{c}s$ decays does not modify the charm yield and was already included in the determination of n_c. This suggests that the problem of reconciling the semileptonic branching fraction and n_c has not yet been completely resolved.

The data are not yet sufficiently precise to convincingly rule out the possibility of a larger charm yield. In addition, there are several possible systematic experimental flaws in the computation of the yield of charm quarks. The charm meson absolute branching fractions can contribute a systematic uncertainty, although the errors from this source have been significantly reduced by the precise determinations of $\mathcal{B}(D^0 \to K^-\pi^+)$ (11) and $\mathcal{B}(D^+ \to K^-\pi^+\pi^+)$. The effect of a small change in the branching fractions for charm meson is demonstrated by the following example: Decreasing $\mathcal{B}(D^0 \to K^-\pi^+)$ and $\mathcal{B}(D^+ \to K^-\pi^+\pi^+)$ by 7% increases the total charm yield in B decay to $125 \pm 6\%$ (CLEO II measurements). Note that the value for n_c reported here is slightly higher than the value given at the 1995 conferences due to the smaller world average for the absolute branching fraction $\mathcal{B}(D^0 \to K^-\pi^+)$ used in this review. The absolute branching fraction scales for the D_s meson and Λ_c baryons are still quite uncertain. Since the inclusive branching ratios to these particles are small, a substantial change to the branching ratio scale would be required to significantly modify the charm yield.

A systematic study of inclusive hadronic B decays to mesons and baryons and more precise measurements of charm meson absolute branching fractions will be required to resolve this problem.

8. CONCLUSIONS

Significant progress in the physics of B and D mesons has been made in the last several years.

Fixed-target experiments with silicon vertex detectors such as E691 and E687 have led to precise measurements of charm meson and baryon lifetimes. The observed hierarchy of lifetimes can be compared to theoretical models and is used to assess the size of non–spectator effects. The D^+/D^0 lifetime difference is attributed to constructive interference in D^+ decays. This conclusion is supported by the observation of destructive interference in many exclusive D^+ decay modes.

There has also been rapid progress in the measurement of lifetimes of b-flavored hadrons from the LEP experiments, SLD, and CDF. These results now clearly show that to a good approximation $\tau_{B^+} \approx \tau_{B^0} \approx \tau_{B_s}$ while the Λ_b lifetime is significantly shorter. The small value of $\tau(\Lambda_b)$ is unexpected and cannot be easily accommodated in most theoretical frameworks given the observed size of non–spectator effects in charm decay (50, 51).

The fixed-target experiments and CLEO have reported many new measurements of hadronic charm decay modes. There are now sufficiently precise data to isolate the effects of FSI, and to solve for the isospin amplitudes and relative phases in a number of quasi two-body decay modes. Unambiguous evidence for DCSD in D^+ decay has been observed. There is no compelling evidence for W-exchange or W-annihilation in charm meson decay from measurements of either hadronic decays or the lifetimes. Charm baryon decay shows strong evidence for W-exchange contributions. In this case, however, there is no helicity suppression. Comparison of the observed rates for hadronic charm meson decays and models based on factorization show a number of discrepancies in D^0, D^+, and D_s decays. The most dramatic of these are in exclusive D_s decays to final states with η and η' mesons. These discrepancies may indicate the breakdown of factorization in hadronic charm decay.

Results from CLEO II have significantly changed our understanding of hadronic B decay. A complete experimental picture of inclusive B decay is now emerging. The problem of simultaneously accomodating the value of n_c and the B semileptonic branching fraction remains. The data and measurements of exclusive hadronic branching fractions are now of sufficient quality to perform nontrivial tests of the factorization hypothesis, including comparisons of rates for $\bar{B}^0 \to D^{*+}X^-$ (where $X^- = \pi^-$, ρ^-, or a_1^-) with rates for $D^{*+}\ell^-\bar{\nu}$ at $q^2 = M_X^2$, as well as comparisons of the polarizations in $\bar{B}^0 \to D^{*+}\rho^-$ with $\bar{B}^0 \to D^{*+}\ell^-\bar{\nu}_\ell$. In all cases, the factorization hypothesis is consistent with the data at the present level of experimental precision and for $q^2 < m_{a_1}^2$, in contrast to the situation in charm decay. No evidence for FSI is observed in B decay. Limits on the strong interaction phase shift in $B \to D\pi$, $B \to D\rho$ have been obtained.

Improved measurements of branching ratios of two-body decays with a ψ meson in the final state have been reported from ARGUS, CDF, and CLEO II. The decay $B \to \psi K^*$ is polarized with $\Gamma_L/\Gamma = (78 \pm 7)\%$. Therefore, this mode will be useful for measuring CP violation. However, it is difficult to simultaneously accommodate these results on polarization and the ratio of $\mathcal{B}(B \to \psi K^*)/\mathcal{B}(B \to \psi K)$ branching fractions in models that assume factorization.

Color suppression appears to operate in hadronic B decays in contrast to charm decays. There is no experimental evidence for (color-suppressed) decays of neutral B mesons to a charm meson and light neutral hadron in the final state. The most stringent limit, $\mathcal{B}(B^0 \to D^0\pi^0)/\mathcal{B}(B^0 \to D^+\pi^-) < 0.07$ from CLEO II, is still above the level where these color-suppressed B decays are expected in most models. The observation of $B \to \psi$ modes shows that color-suppressed decays are present. The appearance of many internal spectator

decays at levels comparable to external spectator decays in the charm sector may be due to FSI.

Using results on exclusive $B \to \psi$ decays from CLEO 1.5, CLEO II, and ARGUS, we obtain values of the BSW parameter $|a_2| = 0.23 \pm 0.01 \pm 0.01$. We also report a new value for the BSW parameter $|a_1| = 1.03 \pm 0.04 \pm 0.06$. By comparing the rates for B^- and $\bar{B}^0$ modes, it is been shown that the sign of a_2/a_1 is positive, in dramatic contrast to what is found in charm decays. It is difficult to reconcile this result with the near equality of the B^+/B^0 meson lifetimes unless the pattern is significantly different for higher multiplicity decay modes or unless there is a large W-exchange contribution to B^0 decay.

In the next few years, the samples of reconstructed charm particles should increase by a factor of 10 as E791 complete their data analysis and as FOCUS, the upgrade of the E687 experiment, SELEX, and CLEO III begin taking data. These large charm samples will allow for more sensitive searches for $D^0 - \bar{D}^0$ mixing, rare decays, and CP violation, and for a systematic investigation of charm baryons and their lifetimes.

Large samples of reconstructed hadronic B decays will be obtained in the next few years by CLEO II/CLEO III as a result of further improvements in the luminosity of CESR and upgrades of the detector. There will also be significant increases in the size of data samples available from the CDF experiment. Accurate tests of the factorization hypothesis over the full q^2 range will become feasible. The large tagged sample at CLEO can be used to study inclusive properties of B^+ and B^0 decays. Measurements of additional decays to final states with charmonium mesons will be performed and other color-suppressed decays will be observed.

The ultimate goal of the study of heavy-flavor mesons is to measure the large CP asymmetries predicted by the standard model in decay modes such as $\bar{B}^0 \to \psi K^0$, $\bar{B} \to \pi^+\pi^-$, and $B^- \to D^0 K^-$. In order to throughly test the consistency of the standard model's description of CP violation in these decays at future facilities, the mechanisms that operate in hadronic decays of heavy quarks must be well understood. This review shows that rapid progress is being made in this program.

ACKNOWLEDGMENTS

We thank our colleagues from the CLEO, E687, E691, E791, ARGUS, CDF, SLD, ALEPH, OPAL, DELPHI, and L3 experiments for their contributions to the work discussed in this review. We thank the US Department of Energy, the Italian Istituto Nazionale di Fisica Nucleare, the University of Hawaii, and The Ohio State University for their unwavering support.

Literature Cited

1. Aubert JJ, et al. *Phys. Rev. Lett.* 33:1404 (1974); Augustin JE, et al. *Phys. Rev. Lett.* 33:1406 (1974)
2. Glashow S, Illiopoulos J, Maiani, L. *Phys. Rev. D* 2:1285 (1970)
3. Herb SW, et al. *Phys. Rev. Lett.* 39:252 (1977)
4. Abe F, et al (CDF Collaboration). *Phys. Rev. Lett.* 74:2626 (1995); Abachi S, et al (D0 Collaboration). *Phys. Rev. Lett.* 74:2632 (1995)
5. Cabibbo N. *Phys. Rev. Lett.* 10:531 (1963); Kobayashi M, Maskawa T. *Prog. Theor. Phys.* 49:652 (1979)
6. Burchat P, Richman JD. *Rev. Mod. Phys.* 67:893 (1995)
7. Witherell MS. *AIP Conf. Proc.* 302:198 (1993)
8. Browder TE, Honscheid K. In *Progress in Nuclear and Particle Physics*, ed. K Faessler, 35:81–220 (1995)
9. Kaplan DM. IIT-HEP-95/7, hep-ex/9512002
10. Barish B, et al (CLEO Collaboration). *Phys. Rev. D* 51:1014 (1995)
11. Akerib D, et al (CLEO Collaboration). *Phys. Rev. Lett.* 71:3070 (1993); Decamp D, et al (ALEPH Collaboration). *Phys. Lett.* B266:218 (1991); Albrecht H, et al (ARGUS Collaboration). *Phys. Lett.* B340:125 (1995)
12. Bergfeld T, et al (CLEO Collaboration). *Phys. Lett.* B373:334 (1996)
13. Albrecht H, et al (ARGUS Collaboration). *Z. Phys. C* 56:7 (1992)
14. Montanet L, et al. *Phys. Rev. D* 50:1173 (1994)
15. Bai JZ, et al (BES Collaboration). *Phys. Rev. D* 52:3781 (1995)
16. Artuso M, et al (CLEO Collaboration). Cornell preprint CLNS-95-1387
17. Gronberg J, et al (CLEO Collaboration). *Phys. Rev. Lett.* 75:3232 (1995)
18. Kubota Y, et al. Preprint CLNS-95-1363 (1995)
19. Guberina B, et al. *Z. Phys. C* 33:297 (1986)
20. Voloshin MB, Shifman MA. *Sov. Phys. JETP* 64(4):698 (1986); Blok B, Shifman MA. *3rd Worksh. Tau-Charm Factory, Marbella, June* (1993)
21. Fernandez E, et al (MAC Collaboration). *Phys. Rev. Lett.* 51:1022 (1983)
22. Lockyer NS, et al (MARK II Collaboration). *Phys. Rev. Lett.* 51:1316 (1983)
23. Bigi II, et al. *Contribution to B Decays*, ed. S Stone. Singapore: World Sci. (1994); CERN-TH-7132/94 (1994)
24. Frabetti PL, et al (E687 Collaboration). *Nucl. Instrum. Methods A* 320:519 (1992)
25. Frabetti PL, et al (E687 Collaboration). *Phys. Lett.* B357:678 (1995)
26. Forty R. In *Proc. XIV Int. Conf. Phys. Collision, Tallahassee*, (1994)
27. Adamovich MI, et al (WA89 Collaboration). *Phys. Lett.* B358:151 (1995)
28. Frabetti PL, et al (E687 Collaboration). *Phys. Rev. Lett.* 70:1381 (1993); ibid. 70:1755 (1993); ibid. 70:2058 (1993); ibid. 71:827 (1993); *Phys. Lett.* B323:459 (1994)
29. Malvezzi S. In *Proc. 6th Int. Symp. Heavy Flavor Phys., Pisa, Italy, 6–9 June* (1995)
30. Bigi II, Uraltsev NG. *Z. Phys. C* 62:623 (1994)
31. Sharma V. *B Decays*, ed. S. Stone. Singapore: World Sci. (1994)
32. Kroll IJ. In *Proc. 17th Int. Lepton-Photon Conf., Beijing, China* (1995)
33. CDF Collaboration, EPS0217. Presented at the Brussels Europhys. Conf. Beijing Lepton-Photon Conf. (1995)
34. Abe F, et al (CDF Collaboration). *Phys. Rev. Lett.* 72:3456 (1994)
35. Abe F, et al (CDF Collaboration). *Phys. Rev. Lett.* 74:4988 (1995)
36. ALEPH Collaboration, EPS0412. Presented at the Brussels Europhys. Conf. Beijing Lepton-Photon Conf. (1995)
37. ALEPH Collaboration, EPS0402. Presented at the Brussels Europhys. Conf. Beijing Lepton-Photon Conf. (1995)
38. ALEPH Collaboration, EPS0411. Presented at the Brussels Europhys. Conf. Beijing Lepton-Photon Conf. (1995)
39. ALEPH Collaboration, EPS0406. Presented at the Brussels Europhys. Conf. Beijing Lepton-Photon Conf. (1995)
40. OPAL Collaboration, EPS0412. Presented at the Brussels Europhys. Conf. Beijing Lepton-Photon Conf. (1995)
41. OPAL Collaboration, EPS0402. Presented at the Brussels Europhys. Conf. Beijing Lepton-Photon Conf. (1995)
42. OPAL Collaboration, EPS0411. Presented at the Brussels Europhys. Conf. Beijing Lepton-Photon Conf. (1995)
43. DELPHI Collaboration, EPS0412. Presented at the Brussels Europhys. Conf. Beijing Lepton-Photon Conf. (1995)
44. DELPHI Collaboration, EPS0402. Presented at the Brussels Europhys. Conf. Beijing Lepton-Photon Conf. (1995)
45. DELPHI Collaboration, EPS0411. Pre-

sented at the Brussels Europhys. Conf. Beijing Lepton-Photon Conf. (1995)
46. DELPHI Collaboration. CERN-PPE/95-29 (1995)
47. SLD Collaboration, EPS0254 and EPS0256. Presented at the Brussels Europhys. Conf. Beijing Lepton-Photon Conf. (1995)
48. Athanas M, et al (CLEO Collaboration). *Phys. Rev. Lett.* 73:393 (1994)
49. Browder TE, Pakvasa S. *Phys. Rev. D* 52:3123 (1995)
50. Neubert M, Sachrajda CT. CERN-TH/96-19.
51. Rosner J. Preprint CERN-TH-96/24, EFI-96-03, hep-ph/9602265, submitted for publication
52. Frabetti PL, et al. *Phys. Lett.* B359:403 (1995)
53. M. Purohit et al. In *Proc. 1994 DPF Conf., Alburquerque, New Mexico* (1994)
54. Bigi I. In *Proc. Tau-Charm Factory Worksh.* (1989)
55. Burdman GI. In *Proc. CHARM2000 Workshop, FERMILAB-Conf-94/190, 75* (1994)
56. Anjos JC, et al (E691 Collaboration). *Phys. Rev. Lett.* 60:1239 (1988)
57. Cinabro D, et al (CLEO Collaboration). *Phys. Rev. Lett.* 72:1406 (1994)
58. Frabetti PL, et al (E687 Collaboration). *Phys. Lett.* B351:591 (1995)
59. Wiss J. In *Proc. 6th Int. Symp. Heavy Flavor Phys., Pisa, Italy, 6–9 June* (1995)
60. Montanet L, et al. *Phys. Rev. D* 50:1670 (1994)
61. Moroni L. In *Proc. 15th Int. Conf. Phys. Collision, Cracow, Poland, 8–10 June* (1995)
62. Anselmino M, et al. Preprint CBPF-NF-45-95
63. Anjos JC, et al (E691 Collaboration). *Phys. Lett.* B223:267 (1989)
64. Albrecht H, et al (ARGUS Collaboration). *Phys. Lett.* B288:367 (1992); Frabetti PL, et al (E687 Collaboration). *Phys. Lett.* B300:190 (1993); ibid. *Phys. Lett.* B338:106 (1994)
65. Alexander JP, et al (CLEO Collaboration). Preprint CLNS-95-1343 (1995)
66. Frabetti PL, et al (E687 Collaboration). *Phys. Lett.* B314:477 (1993)
67. Datta A. hep-ph/9504428; Korner JG, Kramer G. *Z. Phys. C* 55:659 (1992); Cheng H, Tseng B. *Phys. Rev. D* 46:1042 (1992); Kamal AN, Xu Q. *Phys. Rev. D* 46:3836 (1992); Kaur G, Khanna M. *Phys. Rev. D* 44:182 (1991)
68. Ammar R, et al (CLEO Collaboration). *Phys. Rev. Lett.* 74:3534 (1995)
69. Albrecht H, et al (ARGUS Collaboration). *Phys. Lett.* B342:397 (1995)
70. Avery P, et al (CLEO Collaboration). *Phys. Rev. Lett.* 71:2391 (1993)
71. Gittelman B, Stone S. CLNS 87/81; Ito M. PhD thesis. Cornell Univ. (1989)
72. Albrecht H, et al (ARGUS Collaboration). *Z. Phys. C* 54:13 (1992)
73. Abe F, et al (CDF Collaboration). *Phys. Rev. Lett.* 69:3704 (1992)
74. Alam MS, et al (CLEO Collaboration). *Phys. Rev. Lett.* 58:1814 (1987); Crawford G, et al (CLEO Collaboration). *Phys. Rev. D* 45:572 (1992)
75. Albrecht H, et al (ARGUS Collaboration). *Z. Phys. C* 62:371 (1994); DESY 93-084 (1993); *Z. Phys. C* 58:191 (1993); ibid. 58:199 (1993)
76. Dunietz I. Fermilab preprint FERMILAB-PUB-94-163-T.
77. Albrecht H, et al (ARGUS Collaboration). *Z. Phys. C* 52:353 (1991); ibid. 54:1 (1992)
78. Bortoletto D, et al (CLEO Collaboration). *Phys. Rev. D* 45:21 (1992); *Phys. Rev. Lett.* 64:2117 (1990)
79. Wirbel M, Wu Y-L. *Phys. Lett.* B288:430 (1989)
80. Bergfeld T, et al (CLEO Collaboration). PRD 53:4734 (1996)
81. Browder TE. hep-ex/9602009, presented at the Proc. 1995 Brussels Europhys. Conf., Brussels, Belgium (1995)
82. Balest R, et al (CLEO Collaboration). *Phys. Rev. D* 52:2661 (1995); Schrenk S. *Inclusive decays of B mesons to charmonium*. PhD thesis. Univ. Minn, Minneapolis. 196 pp. (1994)
83. Bodwin GT, Braaten E, Yuan TC, Lepage GP. *Phys. Rev. D* 46:R3703 (1992)
84. Kühn JH, Nussinov S, Rückl R. *Z. Phys. C* 5:117 (1980)
85. Albrecht H, et al (ARGUS Collaboration). *Phys. Lett.* B277:209 (1992)
86. Kubota Y, et al (CLEO Collaboration). Submitted for publication
87. Albrecht H, et al (ARGUS Collaboration). *Z. Phys. C* 56:1 (1992); ibid. *Z. Phys. C* 42:519 (1989); ibid. *Phys. Lett.* B210:263 (1988)
88. Crawford G, et al (CLEO Collaboration). *Phys. Rev. D* 45:752 (1992)
89. Procario M, et al (CLEO Collaboration). *Phys. Rev. Lett.* 73:1472 (1994)
90. Cinabro D, et al (CLEO Collaboration). CLEO CONF 94-8; Davis REP. In *Proc. ICHEP Conf.* (1994)
91. Dunietz I, Cooper PS, Falk AF, Wise M. PRL 73, 1075 (1994)

92. Cinabro D, et al (CLEO Collaboration). CLEO CONF 94-8; Baringer P. In *Proc. 1994 Meet. Div. Particles Fields, Albuquerque, New Mexico* (1994)
93. Kwon Y. *Moriond Worksh. Electroweak Interactions, Moriond* (1996)
94. Palmer WF, Stech B. *Phys. Rev. D* 48:4174 (1993)
95. Buchalla G, Dunietz I, Yamamoto H. *Phys. Lett.* B364:188 (1995)
96. Keum YY. *Phys. Lett.* B348:247 (1995)
97. Honscheid K. Presented at the Proc. Pisa Heavy Flavor Physics Conf. (1995)
98. Henderson S, et al (CLEO Collaboration). *Phys. Rev. D* 45:2212 (1992)
99. Albrecht H, et al (ARGUS Collaboration). *Z. Phys. C* 48:543 (1990)
100. Alam MS, et al (CLEO II Collaboration). *Phys. Rev. D* 50:43 (1994)
101. Albrecht H, et al (ARGUS Collaboration). DESY preprint DESY-94-069; Krieger P. Presented at the Proc. McGill Heavy Flavor Physics Conf. (1993)
102. Bortoletto D, et al (CLEO Collaboration). *Phys. Rev. Lett.* 64:2117 (1990)
103. Kubota Y, et al (CLEO Collaboration). CLEO CONF 94-13; Davis EP. In *Proc. of the Conf.* In press; Fu X, et al (CLEO Collaboration). Preprint CLNS 96/1397, submitted for publication
104. Dunietz I, et al. *Phys. Rev. D* 43:2193 (1991)
105. Abe F, et al (CDF Collaboration). *Phys. Rev. Lett.* 76:2015 (1996)
106. Albrecht H, et al (ARGUS Collaboration). *Phys. Lett.* B340:217 (1994)
107. Abe F, et al (CDF Collaboration). *Phys. Rev. Lett.* 75:3068 (1995)
108. Alexander JP, et al (CLEO Collaboration). *Phys. Lett.* B341:435 (1995)
109. Bishai M, et al (CLEO Collaboration). CLNS 95/1379
110. Abe F, et al (CDF Collaboration). FERMILAB-CONF-95/224-E
111. Neubert M, Rieckert V, Xu QP, Stech B. In *Heavy Flavors*, ed. AJ Buras, H Lindner. Singapor: World Sci. (1992)
112. Dunietz I, Snyder A. *Phys. Rev. D* 43:1593 (1991)
113. Altarelli G, Maiani L. *Phys. Lett.* B52:351 (1974); Gaillard MK, Lee BW. *Phys. Rev. Lett.* 33:108 (1974)
114. Wilson KG. *Phys. Rev.* 179:1499 (1969)
115. Gilman FG, Wise MB. *Phys. Rev. D* 20:2392 (1979)
116. Dugan MJ, Grinstein B. *Phys. Lett.* B255:583 (1991)
117. Bjorken J. *Nucl. Phys. B* 11(Proc. Suppl.):325 (1989)
118. Buras AJ, Gerard GM, Rückl R. *Nucl. Phys. B* 16:268 (1986)
119. Bedaque P, Das A, Mathur VS. *Phys. Rev. D* 49:269 (1994); Blok BY, Shifman MA. *Sov. J. Nucl. Phys.* 45:522 (1987); Buccella F, et al. *Phys. Rev. D* 51:3478 (1995); Chau LL, Cheng HY. *Phys. Rev. D* 36:137 (1987); Gibilisco M, Preparata G. *Phys. Rev. D* 47:4949 (1993)
120. Bauer M, Stech B, Wirbel M, *Z. Phys. C* 29:637 (1985); ibid. 34:103 (1987); ibid. 42:671 (1989)
121. Czarnecki A, et al. *Z. Phys. C* 54:411 (1992)
122. Isgur N, Wise MB. *Phys. Lett.* B232:113 (1989); ibid. B237:527 (1990)
123. Colangelo P, Nardulli G, Paver N. *Phys. Lett.* B293:207 (1992); Colangelo P, De Fazio F, Nardulli G. *Phys. Lett.* B303:152 (1993)
124. Gronau M, London D. *Phys. Rev. Lett.* 65:3381 (1990); Lipkin HJ, et al. *Phys. Rev. D* 44:1454 (1991)
125. Battle M, et al (CLEO Collaboration). Cornell Univ. Rep. No. CLEO-CONF-94-18
126. Lipkin HJ. *Phys. Lett.* B254:247 (1991)
127. Sanda A. *Phys. Rev. D* 22:2814 (1980)
128. Kamal AN, Pham TN. *Phys. Rev. D* 50:R1832 (1994)
129. Bigi I. In *Adv. Study Conf. Heavy Flavors, Pavia* (1993)
130. Buccella F, et al. *Phys. Rev. D* 51:3478 (1995)
131. Donoghue JF. *Phys. Rev. D* 33:1516 (1986)
132. Anjos JC, et al (E691 Collaboration). *Phys. Rev. Lett.* 69:2892 (1992)
133. Adamovich M, et al (WA82 Collaboration). *Phys. Lett.* B305:177 (1993)
134. Frabetti PL, et al (E687 Collaboration). *Phys. Lett.* B363:259 (1993)
135. Stone S. In *Heavy Flavors*, ed. AJ Buras, M Lindner. Singapore: World Sci. (1992)
136. Bortoletto D, Stone S. *Phys. Rev. Lett.* 65:2951 (1990)
137. Kamal AN, Pham TN. *Phys. Rev. D* 50:6849 (1994)
138. Browder TE, Honscheid K, Playfer S. In *B Mesons*, ed. S Stone. Singapore: World Sci. 2nd ed. (1994)
139. Korner J, Goldstein G. *Phys. Lett.* B89B:105 (1979)
140. Lepage, P. Private communication; Rieckert V. *Phys. Rev. D* 47:3053 (1993)
141. Rosner JL. *Phys. Rev. D* 42:3732 (1990)
142. Neubert M. *Phys. Lett.* B264:455 (1991)
143. Rieckert V. *Phys. Rev. D* 47:3053 (1993); Rieckert V. *Hadronische Zerfälle von B Mesonen*. Thesis. Univ. Heidelberg. 136 pp. (1994)

144. Kramer G, Mannel T, Palmer WF. *Z. Phys. C* 55:497 (1992)
145. Coffman D, et al (Mark III Collaboration). *Phys. Rev. D* 45:2196 (1992)
146. Cheng HY. Preprint IP-ASTP-04-95, hep-ph/9503219 (1995)
147. DeJongh DF. PhD thesis. Calif. Inst. Technol., Pasadena (1990)
148. Yamamoto H. Harvard preprint HUTP-94/A006
149. Yamamoto H. In *Proc. Snowmass Conf. B Phys. Hadron Colliders* (1996)
150. Gibaut D, et al (CLEO Collaboration). CLEO CONF 95-22, EPS0184; Acosta D, et al (CLEO Collaboration). *Phys. Rev. D* 49:5690 (1994); Aoki S, et al (WA75 Collaboration). *Prog. Theor. Phys.* 89:131 (1993); Bai JZ, et al (BES Collaboration).*Phys. Rev. Lett.* 74:4599 (1995)
151. Martinelli G. CERN-TH-95-116
152. Gourdin M, Keum YY, Pham XY. Univ. Paris preprint, PAR-LPTHE-94-32, hep-ph/9409221
153. Pham XY, Keum YY. Univ. Paris preprint PAR/LPTHE/95-01, hep-ph/95-01257; Preprint PAR/LPTHE/94-44, hep-ph/9501360
154. Kramer G, Palmer WF. *Phys. Lett.* B279:181 (1992)
155. Gourdin M, Kamal AN, Pham XY. *Phys. Rev. Lett.* 73:3355 (1994)
156. Aleksan R, et al. Orsay preprint LPTHE-Orsay 94/15, DAPNIA/SPP/94-24
157. Kamal AN, Santra AB. Univ. Alberta preprint, Alberta Thy-31-94
158. Terasaki K. *Phys. Rev. D* 47:5177 (1993)
159. Bauer M, Stech B. *Phys. Lett.* B152:380 (1985)
160. Kamal AN. Preprint Alberta-Thy-01-96, hep-ph/9601213 (1996)
161. Cheng HY. Preprint IP-ASTP-14-95, hep-ph/9506340 (1995)
162. Rosner JL. In *Proc. TASI-90, Boulder*, pp. 91–224 (1990)
163. Belyaev V, Khodjamirian A, Rückl R. *Z. Phys. C* 60:349 (1993)
164. Ball P. *Phys. Rev. D* 48:3190 (1993)
165. Kamal AN, Pham TN. *Phys. Rev. D* 50:395 (1994)
166. Blok B, Shifman M. *Nucl. Phys. B* 389:534 (1993)
167. Halperin I. *Phys. Lett.* B349:548 (1995)
168. Buras AJ. *Nucl. Phys.* B434:606 (1995)
169. Honscheid K, Schubert KR, Waldi R. *Z. Phys. C* 63:117 (1994)
170. Bigi I, Blok B, Shifman MA, Vainshtein AI. *Phys. Lett.* B323:408 (1994)
171. Dunietz I, Cooper PS, Falk AF, Wise M. *Phys. Rev. Lett.* 73:1075 (1994)
172. Falk AF. Johns Hopkins Univ. preprint JHU-TIPAC-940016, hep-ph/9410312; In *Proc. John Hopkins Worksh. Current Prob. Particle Theory, Florence, Italy* (1994)
173. Bagan E, Ball P, Braun VM, Gosdzinsky P. *Nucl. Phys.* B432:3 (1994)
174. Bagan E, Ball P, Braun VM, Gosdzinsky P. *Phys. Lett.* B342:362 (1995); *Phys. Lett.* B374:363 (1996) (Erratum)
175. Falk AF, Wise MB, Dunietz I. Preprint hep/ph-940534, CALT-68-1933
176. Kagan AL. *Phys. Rev. D* 51:6196 (1995)

Annual Review of Nuclear and Particle Science
Volume 46, 1996

CONTENTS